De novo Design of Bioinspired Peptide based Molecular Constructs

A thesis submitted in partial fulfilment of the requirements for the degree of

DOCTOR OF PHILOSOPHY

by

VIVEK PRAKASH

Department of Biosciences and Bioengineering
Indian Institute of Technology Guwahati
Guwahati-781039, India

April 2022

Dedicated

To

My Family

De novo Design of Bioinspired Peptide based Molecular Constructs

A thesis submitted in partial fulfilment of the requirements for the degree of

DOCTOR OF PHILOSOPHY

by

VIVEK PRAKASH

Department of Biosciences and Bioengineering
Indian Institute of Technology Guwahati
Guwahati-781039, India

April 2022

Indian Institute of Technology Guwahati
Department of Biosciences and Bioengineering

DECLARATION

I do hereby declare that the research findings of this thesis are the result of research work carried out by me in the Department of Biosciences and Bioengineering, Indian Institute of Technology Guwahati, Guwahati, India, under the supervision of Prof. Vibin Ramakrishnan.

As per the general norms of reporting research findings, I take full responsibility for the data represented. Acknowledgments have been made wherever the research findings of other researchers have been cited in this thesis.

Vivek Prakash

Date: 29.04.2022 Vivek Prakash

Indian Institute of Technology Guwahati

Department of Biosciences and Bioengineering

CERTIFICATE

It is certified that the work described in this thesis entitled "***De novo* Design of Bioinspired Peptide based Molecular Constructs**" by Mr.Vivek Prakash for the award of the degree of Doctor of Philosophy is an authentic record of the results obtained from the research work carried out under my supervision in the Department of Biosciences and Bioengineering, Indian Institute of Technology Guwahati, India. To the best of my knowledge, no part of this work has been submitted elsewhere for the award of any degree.

Prof. Vibin Ramakrishnan

(Thesis Supervisor)

Date: 29.04.2022

Place: IIT Guwahati

Acknowledgments

I would like to place my deep sense of gratitude and sincere thanks to my Ph.D. thesis supervisor, Prof. Vibin Ramakrishnan, for giving me an opportunity to work in the Molecular Informatics and Design Laboratory (MID). His guidance, constant support, critical reviews have been a driving force to explore the different areas of research in my doctoral research. I thank him for giving me the freedom to think and execute ideas independently.

I would like to thank my doctoral committee members, Prof. Vishal Trivedi, Dr. Nitin Chaudhary, and Dr. Sachin Kumar, for their valuable suggestions and insightful comments during progress seminars. I would also like to thank all faculty members and technical staffs who extended their support when required.

I am grateful to Departmental Central Instrument Facility BSBE, for providing various facilities to carry out my experiments efficiently. I acknowledge the Central Instrument Facility and Centre of Nanotechnology, for allowing me to operate the ITC and FESEM, respectively, as an operator.

I extend my gratitude to Dr. R. Anandalakshmi, Associate professor, Department of Chemical Engineering, and her students Abhishek Roy and Dr. K. Dharmalingam, for helping me with the rheological studies. I am grateful to Dr. Narayanasamy Selvaraju, Assistant professor, Department of BSBE, and his lab members for assisting in heavy metal removal experiments. I extend my gratitude to Prof Kanagraj, Professor, Department of Chemical Engineering, and his student Arnab for helping in the Ball-mill experiment.

My profound gratitude goes to my seniors and colleagues of MID and BCL lab Dr. Sajitha, Dr. Ruchika, Dr. Gaurav Jerath, Dr. Gaurav Pandey, Dr. Prakash, Dr. Karabi, Dr. Debika, Sravani, Anshuman, Vinay, Jahnu, Yvonne, Feba, Kalpana, Amay, for their immense help and suggestions throughout my Ph.D. tenure. My earnest thank goes to my batch mates and friends Smita, Darshana, Angshu, Manish, Shweta, Deepti, Dr. Ram, Dr. Puja, Anil, Aman, Rajveer, Saurabh, Shahab, Vibhav, Naveen, Akash, Ramiz, Tarun for their incredible support and encouragement.

I am in debt to my parents and siblings Dr. Shweta, Dr. Shivam, Prateek, brother-in-law Anshuman Mitra, and sister-in-law Anju for their blessing and unconditional support. This would not have been possible without their sacrifices, support, and constant motivation.

Vivek Prakash

Table of contents

List of Figures

List of Tables

List of Abbreviations

AFM	Atomic Force Microscopy
AR-SAMD	Automated Repetitive Simulated Annealing by Molecular Dynamics
ATR	Attenuated total reflection
AzAla	β-(1-azulenyl)-L-alanine
CD	Circular Dichroism Spectroscopy
CFU	Colony forming unit
DIPEA	N, Ndiisopropylethylamine
DLS	Dynamic Light Scattering
DSC	Differential Scanning Calorimetry
EDX	Energy Dispersive X-Ray Spectroscopy
FESEM	Field Emission Scanning Electron Microscope
FETEM	Field Emission Transmission Electron Microscope
FF	Diphenylalanine
Fmoc	Fluorenylmethyloxycarbonyl
FTIR	Fourier transform infrared spectroscopy
G'	Storage modulus
G"	Loss modulus
HBTU	2-(1H-benzotriazol-1- yl)-1,1,3,3-tetramethyluronium hexafluorophosphate
HFIP	Hexafluoroisopropanol
HOBt	Hydroxybenztriazole
HP	Hair powder
HPLC	High Performance Liquide Chromatography

LVE	Linear viscoelastic region
MALDI-TOF	Matrix Assisted Laser Desorption Ionization-Time of Flight
MD	Molecular Dynamics
PH	Pulverized hair
PL	Photoluminescence Emission
PLE	Photoluminescence Excitation
QC	Quantum confinement
QDs	Quantum dots
RH	Raw Hair
SAMD	Simulated Annealing Molecular Dynamics
SPPS	Solid-phase peptide synthesis
ThT	Thioflavin T
TIPS	Triisopropyl silane
Trp	Tryptophan

Abstract

Molecular self-assembly is a powerful tool for the generation of functional nanostructures in a bottom-up fabrication. Electrostatic interactions, hydrophobic interactions, hydrogen bonding and π-π stacking interactions, together contribute to the stability of a supramolecular assembly. Peptides have drawn significant attention to be used as basic building blocks for such hierarchical assemblies, due to their simple structure, relative chemical and physical stability, diversity in sequences and shapes, and the feasibility to synthesize in fairly large quantities. Diversification of chain stereochemistry offers tremendous increase in the peptide and protein design space. The use of D-amino acids in the peptide sequence can possibly help in accessing the otherwise "forbidden" region of the Ramachandran map for the generation of novel functional peptide sequences composed of L and D amino acids. In this thesis, we have de novo designed different sets of peptide molecules for four different application fronts. In the first project, we have designed a 30 amino acid long artificial blue fluorescent protein by impregnating an unnatural amino acid in the hydrophobic core of an altogether novel fold, which gives blue fluorescence.

Phenylalanine dipeptide (FF) has an intrinsic ability to form supramolecular nanostructures. We have designed syndiotactic hexamer peptide $(Ff)_3$-OH, which folds into a gramicidin helical architecture, facilitating an extended phenylalanine network forming quantum confinement. In the third project, we have synthesized Fmoc conjugated ultra-short peptide hydrogels, with interesting self-healing property, which make them potential candidates for tissue engineering and drug delivery. The antimicrobial property of the synthesized peptide hydrogel has been verified against Gram-positive and Gram-negative bacteria.

The aromatic π-π stacking involves interactions of aromatic rings, resulting in the formation of stable nanostructures. Triphenyl group (trityl radical) possessing three-phenyl rings, self-assemble through aromatic π-π stacking interactions, can form an interesting crystalline organic nano-flower. In the last project, we have explored the possibility of using 1,2 bis(tritylthio) ethane crystal, for removing heavy metals in water. As an extension of this objective, we fabricated a cost-effective, water purification system using pulverized human hair for heavy metal removal.

1

Introduction

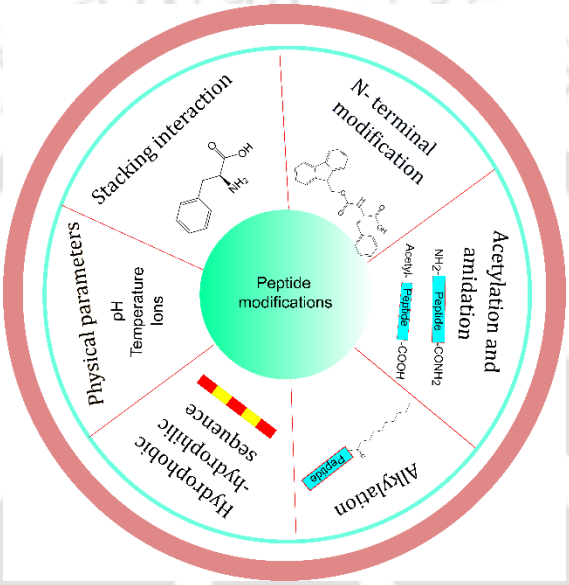

Although the first report of non-covalent interaction was proposed by Johannes Diderik van der Waals in 1873, proper description of non-covalent chemistry was proposed by Jean-Marie Lehn, who coined the term 'Supramolecular Chemistry.' While traditional chemistry explains strong covalent bonding, supramolecular chemistry deals with weak non-covalent interactions, and intermolecular forces between molecules. Over the years, the self-assembly of peptides and other biomolecules have been studied extensively towards the development of novel synthetic biomaterials. In this thesis, we exploit the possibilities of peptide supramolecular chemistry, to fabricate biomaterials for different application fronts such as fluorescent mini proteins, quantum dots, hydrogels, antimicrobials, and water remediation.

1.1 Introduction

Bioinspired materials are synthetic materials whose structure, properties, or function, mimic natural materials or living matter.[1] Biomimetics, inspired by the biological structures and functions, focussed on emulating biological systems using synthetic or biomolecules by diverse approaches. The capability of biomolecules to self-assemble into highly ordered structure, opens up a new option to study the complex natural systems. Molecular self-assembly is defined as organizing molecules into a stable and well-defined structure spontaneously, through non-covalent interactions.[2] It is a robust technique for the synthesis of functional nanostructures through a bottom-up fabrication method.[3] Top-down approaches are concerned with the protein engineering and modifications of already existing proteins. In contrast, the bottom-up approach allows for complete design and control over the size, shape, folding, and assembly of the targets [4] (Figure 1.1). Therefore, it opens up an extended range of architectural spaces in the biomolecular design.

Supramolecular chemistry is an interdisciplinary field referring to the physical, chemical, and biological aspects of molecular assemblies having more complexity than their respective individual molecules.[5] Inspired by nature, chemists have attempted to explore the supramolecular self-assembly for various studies such as; (i) studying the complex molecular structure and self-assembly process, (ii) designing the nature-inspired functional self-assembled molecules mimicking complex structure, and (iii) creating the novel biomaterials capable of novel biological functions. Self-assembly is a spontaneous process of organizing chaotic molecules into ordered structures due to intramolecular or intermolecular interactions. The self-assembly process is controlled by the balance of attractive or repulsive forces within and between molecules. In most cases, a thermodynamically stable structure is formed through enthalpic and entropic interactions that involve the basic assembling units, and the reacting solvent molecules.[6] Electrostatic interactions, hydrophobic interactions, hydrogen bonding, π-π stacking, etc. together make sure that the molecules are at the stable global energy minimum.[7]

Many fluorescent proteins are reported for imaging and spectroscopic measurements to facilitate the study of wide range of biochemical and physiological processes, and interactions between molecules.

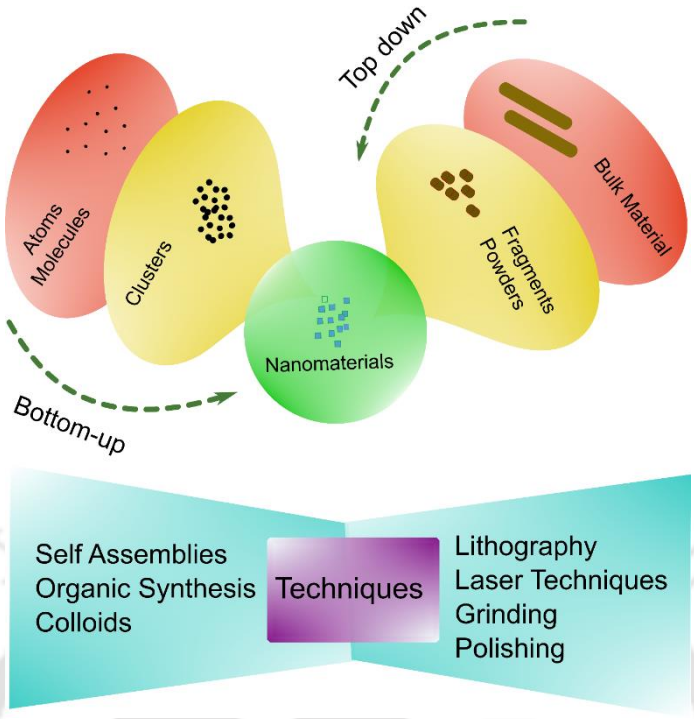

Figure 1.1 Top-down and Bottom- up approach of nanomaterial fabrications

However, in the application where a small fluorescent reporter molecule is required, the choice of fluorophores is limited. Continuous efforts have been devoted to the development of amino acid based fluorophores having large fluorescence quantum yield, fluorescence lifetime, good photostability, and emission spectrum in the visible region. In recent years, the design and study of mini-proteins (specifically polypeptide chain < 40 amino acids) that adopt a defined structure has been explored.[8] Mini-proteins may provide the new route of studies related to protein stability, structure, and function. In addition, mini-proteins are useful scaffolds for templating functional domains, for example, those involved in protein–protein interactions, catalysis, and biomolecular binding, leading to potential applications in biotechnology and medicine. Many mini-proteins reported are fragments of larger globular proteins and have been subjected to iterative redesign and optimization to increase stability and impart function. Trp-cage, a 20- residue miniprotein from extendin-4, is reported to fold in 4μs.[9] Owing to its small size and wealth of experimental data now available, the Trp-cage has become a standard for experimental and

computational mini-protein folding. Some other examples of mini-proteins are TrpPlexus,[10] Villin Headpiece,[11] and PPα.[12]

The use of organic materials to replace the common metallic and semiconductor materials in the micro- and nano-industries has attracted much interest during the past decade. One of the most studied bio-organic groups in this context, is that of proteins and peptides.[13] On account of their low toxicity and high translational values, peptide nanostructures have great potential in biological and biomedical applications. Peptide engineered with appropriate amino acids to bind with inorganic semiconductors as peptide-quantum dots conjugates have been an active field of research in the areas of imaging probes, drug delivery, and antimicrobial agents.[14] The incorporation of cell-penetrating peptides on the surface of QDs has allowed the translocation of quantum dots for intracellular imaging applications.[15] However, because of the use of transition elements mainly, peptide-conjugated QDs have limitations such as toxicity, low bioavailability, and photobleaching. An alternative to the peptide conjugated quantum dots are peptide molecules showing intrinsic QDs property. Diphenylalanine-based peptide has been reported to form self-assemblies with distinct optical,[16] ferroelectrical,[17] and piezoelectrical,[18] properties. The morphology of the formed nanostructures can be modified by substituting amino acids, covalent conjugation, or co-assembled with external molecules. Li and co-workers have been reported the tryptophan based cyclic dipeptide, which self-assembled into a quantum-confined structure with distinct optical properties. Diphenylalanine molecule in the presence of methanol has been reported to form nanocrystalline structures with a diameter of 2.1 nm.[19] They found that the peptide assemblies have the characteristic optical properties of quantum dots.

Peptide hydrogels are formed by molecular self-assembly in water with or without the intervention of cofactors. Compared to traditional cross-linked polymeric hydrogels, peptide-based hydrogels are stimulus-responsive, can be modified easily for tailor made applications, and generally do not require additional cross-linking. Ultrashort peptides have been demonstrated to be efficient low molecular weight supramolecular hydrogelators as they confer excellent propensity of unidirectional amide H-bonding. Bioinspired peptide based hydrogel has been studied extensively for different application fronts such as drug delivery, regenerative medicine, and cell culture. The self-assembled peptide can work as both hydrogelator and the active drug itself. Hydrogel implants aid the healing of traumatic and chronic

wounds by providing them a hydrated environment, suitable for the function of the affected cells. However, these implants provide the microenvironment suitable not only for the host cells but, also for microorganism growth. Infection results in the compromised tissue regeneration at the implanted sites. Peptide hydrogels having inherent antimicrobial properties are the alternatives to these hydrogel implants. Traditionally, antimicrobial agents are either entrapped in hydrogels or drug delivery vehicles, or covalently attached to polymeric scaffolds. Peptides having inherent antimicrobial property was first reported by Schneider and co-workers.[20] They have designed a self-assembling peptide hydrogel scaffolds MAX1, whose surface has broad-spectrum antimicrobial activity against Gram-positive and Gram-negative bacteria. Zhang and co-workers have reported pH-induced peptide hydrogel, PAF26, having antimicrobial activity. [21] In recent years, study on Fmoc based peptide hydrogels have gained momentum due to their effect on aromatic stacking, leading to increased cross-linking and hydrogel formation. Fmoc protected peptide (Fmoc-F) was reported to form hydrogels with antimicrobial property against Gram-positive bacteria, including methicillin-resistant Staphylococcus aureus (MRSA).[22] At low concentrations, where Fmoc-F does not form micelles, it inhibits bacterial growth by entering the cell and reducing the glutathione levels. However, Fmoc-F triggers oxidative and osmotic stress at higher concentrations and alters the membrane permeabilization, which kills Gram-positive bacteria.

In this thesis, de novo peptide design catering to four distinct application fronts has been presented. The overall design strategy has been applied to the generation of short fluorescent 'mini proteins', peptide based quantum confinements and ultrashort peptide hydrogels with antimicrobial activity.

2

Bioinspired Functional Molecular Constructs

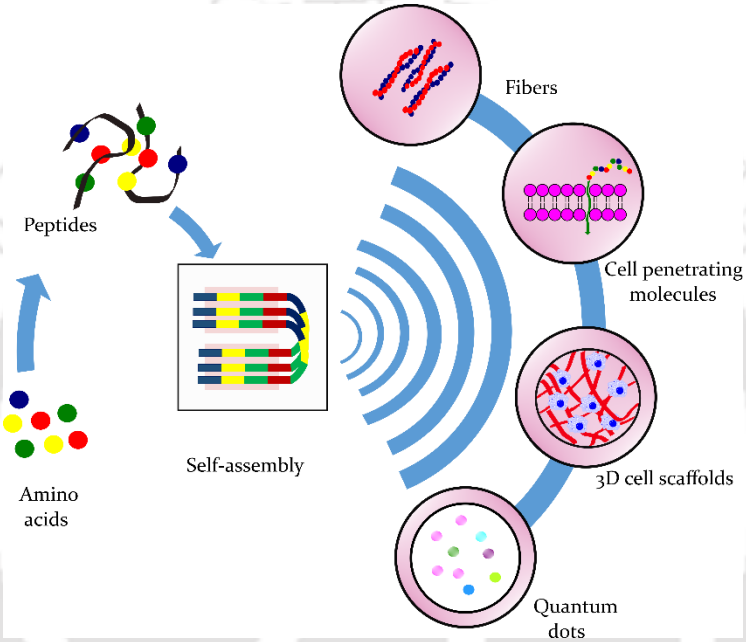

Bioinspired molecular design is a non-traditional problem solving approach which often results in uniquely engineered solutions for complex practical problems. From a materials perspective, biology offers a substantial source of novel approaches capable of inspiring innovation in every aspect of materials, including fabrication, design, and functionality. Consequently, significant efforts have been devoted to fabricating the bioinspired materials with wide range of applications. This chapter provides a comprehensive review of the recent advancements in the generation of peptide based bioinspired functional molecular constructs.

2.1 Introduction

Supramolecular chemistry is an interdisciplinary field referring to the physical, chemical, and biological aspects of molecular assemblies having more complexity than their respective individual molecules.[5] According to Nobel laureate Lehn, supramolecular chemistry refers to the domain of chemistry beyond the realm of the normal molecules.[23] Supramolecular chemistry of biomolecules and bioinspired molecules has attracted tremendous interest due to their acknowledged importance in constructing novel functional materials and in revealing the mechanisms of birth and evolution of natural living organisms. Bioinspired materials are synthetic materials whose structure, properties or function mimic natural materials or living matter.[1] Molecular self-assembly is a spontaneous organization of molecules into a stable and well-defined structure under equilibrium conditions through non-covalent interactions.[2] It is a powerful tool in the synthesis of functional nanostructures as a bottom-up fabrication approach.[3] Top-down approaches are concerned with the protein engineering and modifications of already existing proteins, whereas the bottom-up approach allows for complete design and control over size, shape, folding, and assembly of the targets. [4]

Self-assembly is a spontaneous process of organising molecules into ordered structures resulting from intramolecular and intermolecular interactions. The self-assembly process is controlled by the balance of attractive or repulsive forces within and between molecules. In most cases, a thermodynamically stable structure is formed through enthalpic and entropic interactions that involve the basic assembling units and the reacting solvent molecules.[6] Electrostatic interactions, hydrophobic interactions, hydrogen bonding, and π-π stacking together contribute to the overall stability of the assembly.[7]

The self-assembly process results in the generation of many biological molecules, such as DNA double helix, protein's secondary and tertiary structures, and cell membrane formation after phospholipid assembly.[24] Peptides have drawn significant attention for self-assembly due to their simple structure, relative chemical and physical stability, diversity in sequences and shapes, and the feasibility of synthesizing them in large amounts. In addition, peptides are known as useful building blocks for creating self-assembled nanomaterials due to their intrinsic biocompatibility and biodegradability.

This chapter focuses on the de novo design of peptide-based systems that are directed towards the self-assembly of biomaterials (specifically fibrous biomaterials and hydrogels), and discrete nanoscale objects.

2.2 Peptide based functional materials

A good peptide design strategy starts with identifying potential bioactive candidates, then optimizing the sequence to improve the molecules' stability and reactivity**.** Several points should be considered during peptide design such as peptide length, solubility, cross-linking, and stability. Traditionally peptide originates from native protein sequences. The native sequences can be modified or conjugated with other molecule to increase stability, and activity. Random or site specific modification can also be implemented to increase the specificity of peptides towards the target.[25] These strategies, often based on the deep learning algorithms,[26] intensifies the hope to generate new *de novo* designed peptides with targeted applications.

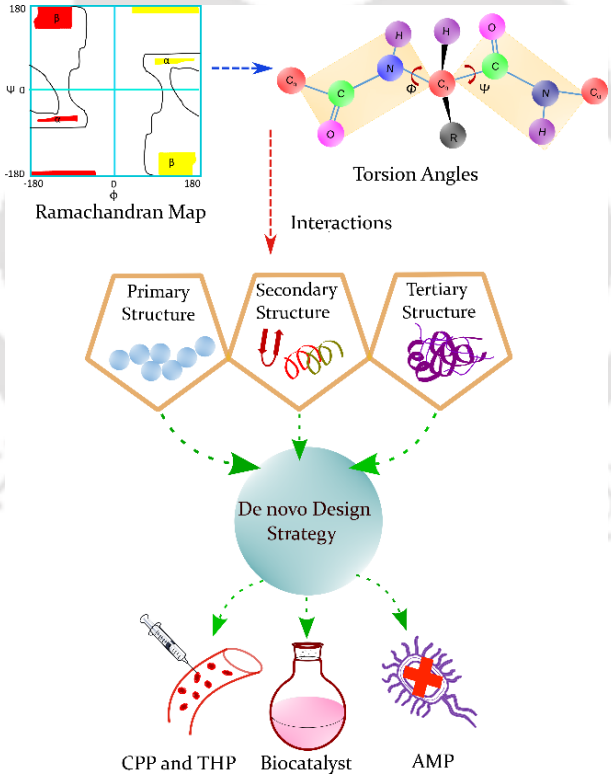

Figure 2.1 Schematic representation of Ramachandran map and torsion angles leading to the formation of different structural organization of peptides.

Diversification of chain stereochemistry offers tremendous increase in peptide or protein design space.[27] Tacticity refers to the stereochemical sequence of successive chiral centers in a polymer.[28] Peptides and proteins are polymers of amino acids with an immutable main chain and variable side- chain. The C-alpha carbon in the amino acid is the stereo-center in the peptide main chain. The allowed region in the Ramachandran map for L-amino acid is restricted owing to the stearic hindrance of different side chains. This restriction limits the protein folding space accessible on the Ramachandran map to design the new peptide sequences. The use of D-amino acids in the peptide sequence assists in accessing the "forbidden" region of the Ramachandran map for new peptide sequences composed of L and D amino acids (Figure 2.1). An isotactic polypeptide sequence is characterized by amino acids having L-or D-stereochemistry. A syndiotactic sequence has a stereo-regular arrangement with alternate L- and D-amino acids (or vice versa) in succession, whereas a heterotactic polymer is a random distribution of L- and D-amino acids in a sequence. Syndiotacticity in polypeptide was reported in Gramicidin A, an antibacterial peptide.[29] The alternating L and D amino acids in Gramicidin A leads to the formation of $\pi_{(L,D)}$ helical structure. This helix is thermodynamically more stable than the isotactic alpha helix with (i, to i+5) hydrogen bonding pattern. Therefore the syndiotactic backbone in Gramicidin A leads to the formation of stable $\pi_{(L,D)}$ helices. This design template, in theory, would provide the necessary template for designing peptides with tailored properties such as charge distribution, and structural amphipathicity. Using stereochemically constrained unnatural amino acids, it is possible to stabilize secondary structures or design new conformations.[30]

2.2.1 Fluorescent Peptide: Synthetic peptides are popular choices as targeting molecules for bio-imaging or diagnostic applications. Unfortunately, broad utilization of linear, naturally occurring peptides is severely limited by their (a) inherent flexibility which often lowers targeting capability, (b) charged N- and C-terminal groups which inhibit cell permeation, and (c) sensitivity to proteolytic degradation.[31] Efforts to obviate these drawbacks have led to a wide range of molecular design strategies in peptidomimetics with improved properties.[32] One approach is to design structures that incorporate amino acids with unnatural side chains or opposite chirality, or alternatively use an unnatural polymer backbone.[33] By doing so, different strategies have been applied to design the peptide based fluorophore for various applications such as cancer therapeutics,[34] chemical detections,[35] and heavy metal detections.[36]

A key decision in the development of a new fluorescent peptide probe is determining the optimal sensing mechanism. It has to be considered that of the 20 natural amino acids, only Tyrosine (Tyr) and Tryptophan (Trp) display significant emission, and among them, only the Trp fluorescence is sensitive to its immediate environment.[37] For this reason, the introduction of extrinsic fluorophores to the peptide probe is usually necessary, in order to obtain a good fluorescence. Moreover, Trp suffers from strong photobleaching, and its excitation and emission are masked by the strong background typical of biological media. Therefore, applications that require measuring fluorescence in complex mixtures will demand the introduction of extrinsic fluorophores with long-wavelength excitation and emission. Except for peptide-functionalized fluorescent platforms, selected peptides could also be self-assembled into fluorescent nano-architectures without introducing organic dyes. Inspired by the fluorescence mechanism in natural fluorescent proteins, Zhang and co-workers have reported Trp-Phe dipeptide nanoparticles (DNPs) that shifted the intrinsic peptide fluorescence from ultraviolet to the visible range.[38] Similar to natural fluorescent proteins, DNPs were prepared through self-assembly with Zn2+, which shifted peptide's intrinsic fluorescent signal from the ultraviolet to the visible range. Narrow emission bandwidth in visible range and remarkable photostability of DNPs were observed, which could be an effective agent for fluorescent biomedical imaging. Subsequently, Li and co-workers have reported the quantum confined self-assembly of aromatic cyclic dipeptides cyclo-Phe-Trp and cyclo-Trp-Trp.[39] The cyclic dippetides were designed as Quantum dots (QDs) to self-assemble into quantum-confined nanostructures which

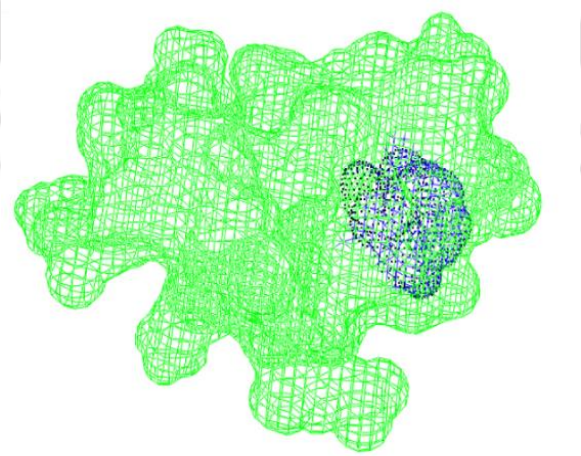

Figure 2.2 Surface mesh model of BP02 mini-protein. Blue colour represents β-(1-azulenyl)-L-alanine

dimerized to form nano strucutres. The emission of QDs can be tuned from the visible region to the NIR region (420–820 nm) by modulating self-assembly. Ramakrishnan and co-workers have designed a heterochiral *de novo* minimal fluorescent protein that can be selectively excited at 342 nm.[40] β-(1-azulenyl)-L-alanine, an unnatural amino acid was impregnated into the hydrophobic core of a heterotactic protein scaffold, which gives emission in visible region (Figure 2.2).

2.2.2 Antimicrobial peptides (AMPs): The emergence of drug-resistant bacteria has restricted the use of many conventional antibiotics, leading to the new research to develop antibiotics, specifically AMPs, which generally target the bacterial cell membranes, possibly decreasing the risk of resistance.[41] AMPs are typically 20-50 residues and generally tend to adopt a highly amphiphilic structure. The electrostatic interactions between the positively charged AMPs and the negatively charged phospholipid layer provide an initial mode of interaction, whereas hydrophobic interactions allow the peptides to penetrate the cell membrane, in some cases leading to depolarization of the bacterial membrane and cell death (Figure 2.3).[42] Although natural peptides are excellent candidates as antimicrobial agents, they have limitations as well, such as reduced bioavailability, protease mediated degradation, and instability in pH environment.[43] To counter these limitations, tailor-made approach to design the AMPs have increased in recent decades. Altering peptide chirality by insertion of D-amino acids has resisted degradation of peptides with increased half-life. Many studies have reported the de novo design of AMPs, mimicking natural AMPs.[44, 45,46]

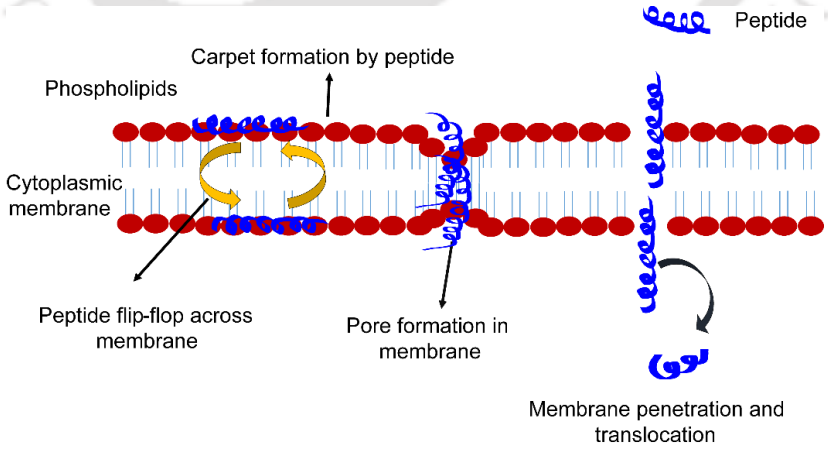

Figure 2.3 Schematic representation of the mechanism of Antimicrobial peptides

2.2.3 Cell Penetrating (CPP) and Tumor homing peptide (THP): The most crucial factor in successful drug development is insuring that the drug molecule interacts with the target efficiently. Several drug delivery strategies have been proposed to increase the bioavailability of the drugs, such as electroporation, liposomal formulation, and micro injection. However, each of these has its limitations, mainly in terms of toxicity and therapeutic feasibility.

Peptide molecules can be an alternative delivery strategy that can translocate the cytoplasmic membrane.[47] Majority of cell penetrating peptides (CPPs) reported to date have been identified or developed from natural protein sources of different origins and mainly have L-amino acids. The incorporation of D- amino acids in CPP sequences increased peptide stability in biological fluids, but often have lower cellular uptake than poly L- amino acid CPP sequences.[48] However, the use of D-Proline in CPP sequences provides the much needed proteolytic stability. Ramakrishnan and co-workers have designed a series of 12-mer peptides to address the instability issues of the CPPs, by reverse engineering the syndiotactic backbone.[49] The synthesized peptides were stable in both human plasma and bovine serum.

Poor penetration of antitumor drugs in the extravascular tumor tissue is often a major factor limiting the efficacy of cancer treatments. Tumor homing peptides (THPs) can be used to deliver drugs into tumors.[50] THPs are the molecules that have been engineered for targeted drug delivery in various cancer types. Receptor mediated interactions of THPs favours high specificity, and low cross reactivity in recognition of cancer cells due to the presence of frequently occurring peptide motifs such as RGD,[51] and NGR.[50] RGD is the most studied THP motif which targets integrins, over-expressed on tumor blood vessels.

2.2.4 De novo designed Biocatalysts: The efficiency and selectivity of enzymes have encouraged the researchers to find out the approaches to design the catalysts for the reactions not found in nature, or to come up with the new approach for catalyzing the reactions already known, with better performance. The computational approach is prominently successful in this effort owing to the high complexity of protein structures and our limited understanding of the protein structure-function relationships.[52] Computational *de novo* design relies on placing the designed catalytic active sites into the existing scaffolds. The idea behind this is that enzymes enhance chemical reactions by lowering of activation energy, by designed

active site.[53] The *de novo* design of enzymes has been supported by the computational tools such as DEZYMER,[54] ORBIT,[55] and ROSETTA.[56]

The main drawback of many enzymes are their size as they are either large polypeptide or fragments of proteins. As even short peptides can catalyse many chemical reactions,[57] it seems logical that their subsequent improvement can yield incredibly efficient enzymes. The supramolecular self-assembly of peptides yield an array of nanostructures such as amyloid fibers,[58] hydrogels,[59] and coil-coiled bundles.[60] Synthetic modifications of the peptide such as N and C-terminus modification, introduction of unnatural amino acids, and aromatic π-π stacking, provide additional opportunity to tune the large variety of supramolecular structures including twisted ribbons,[61] collagen mimicking peptides,[62] and nanobelts.[63] In one of the earliest attempts Benner and co-workers have rationally designed a 14-mer alpha-helical peptide, which converts oxaloacetate to pyruvate.[64] Baltzer and co-workers have designed KO-42, a 42-residue polypeptide, that folded into a helix-loop-helix hairpin motif.[65] KO-42 peptide catalyzes hydrolysis of p-nitrophenyl esters. Further, they introduced aldimine binding sites into KO-42 peptide to catalyze the conversion of aldimine into ketamine, emulating the biosynthesis of amino acids. The resulting catalysts bound the aldimines and catalyzed conversion of aldimine into ketamine three times faster than imidazole.[66] Inoue described that the aggregation of a peptide-based catalyst notably improved the stereoselectivity of the asymmetric addition of hydrogen cyanide to m-phenoxybenzaldehyde.[67] Recently, Das and co-workers have developed KLVFF based nanotube peptide catalysts and demonstrated catalysis of aldol and retro-aldol condensation reactions.[68]

2.2.4.1 Proline based supramolecular catalyst: The extensive work suggests great promise for the proline based self-assembled peptide as a potential catalyst.[69] It was first reported in early the 1970s that amino acids, such as proline, could catalyze asymmetric aldol cyclizations.[70] Clark and co-workers designed minimal peptide pro-nap, by tagging proline to amido naphthyridine (Nap), and provided a library of asymmetric assemblies capable of enamine catalysis.[71] Miravet and co-workers have designed Pro-Val dipeptide hydrogel for enamine based catalysis.[72] The formed hydrogel showed dual catalytic behaviour as free molecules and as aggregates. In the solution phase dipeptides behave as moderately active and stereo-selective L-Pro based organo-catalysts participating in the aldol reaction, whereas in the gel phase, they turned into basic catalytic residues inactive in the aldol reaction, but active in the non-

stereospecific deprotonation of the aldol product.[73] Recently, Hamley and co-workers developed a series of proline-based amyloid peptides and lipopeptides which form several nanostructures and show excellent catalytic activity and high selectivity for aldol reactions.[74]

2.2.4.2 Histidine based supramolecular catalyst: Much attention has been given to develop self-assembling catalysts for hydrolytic reactions. A single amino acid histidine (His) on its own is capable of promoting hydrolysis, although the catalytic efficiency is very low. However, incorporation of His into self-assembling structures has emerged as a powerful strategy for creating artificial hydrolases (Figure 2.4). Guller and Stupp have demonstrated the hydrolysis of para-nitrophenyl acetate (PNPA) on the surface of nanofibers formed by the assembly of peptide amphiphiles.[75] They have incorporated the two histidine residues in the peptide amphiphiles.

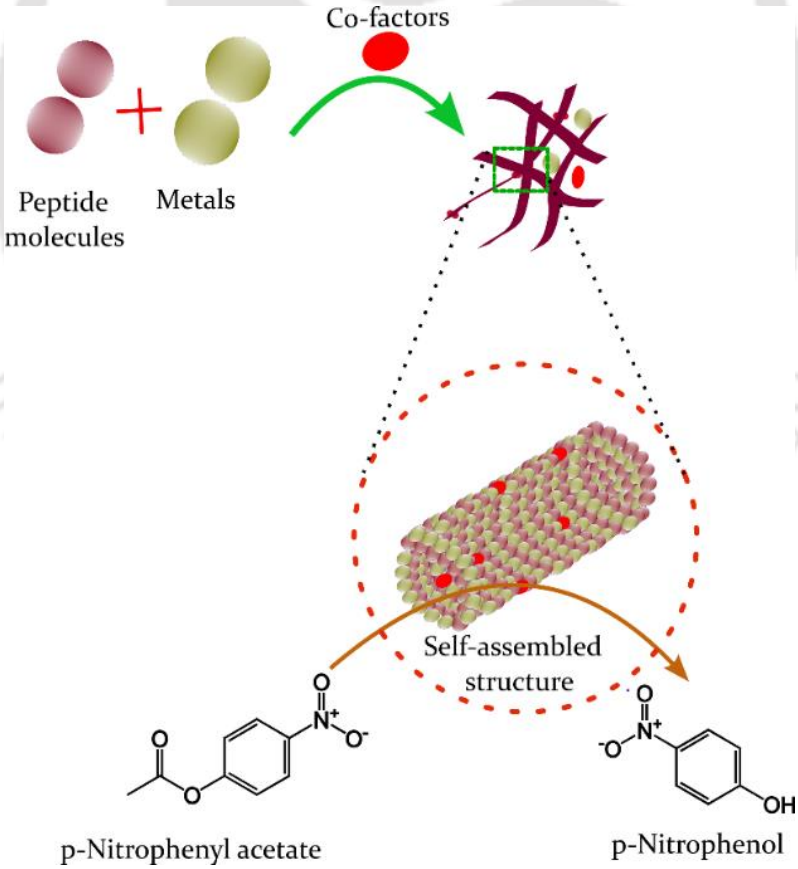

Figure 2.4 Schematic representation of Ester hydrolysis by self-assembled nanostructures

The resulting nabofiber hydrolyzed the PNPA, while non-fibrils structure showed poor catalytic activity. Leu and co-workers have synthesized the short amphiphilic peptide Fmoc-FFH-$CONH_2$, which self assembles to form nanotube and hydrolyzed PNPA.[76] The synthesized peptide catalyst followed typical kinetics behaviour of natural enzymes with catalytic efficiency 519-fold higher than the one without catalysts. Further, Zhimin He and co-workers formed the catalytic Ser/His/Asp triad by mixing the varying ratio of Fmoc-FFH-$CONH_2$ with Fmoc-FFS-$CONH_2$ and Fmoc-FFD-$CONH_2$ peptide. At the optimal ratio of 40:1:1 (Fmoc-FFH-$CONH_2$:Fmoc-FFS-$CONH_2$:Fmoc-FFD-$CONH_2$) catalytic efficiency was observed to be 2-fold higher than the activity of the fibrils formed by Fmoc-FFH-$CONH_2$.[77] Dejugnat and co-workers have designed lipopeptides by joining tripeptides with lipophilic molecules which catalyzed the hydrolysis of PNPA upon self-assembly.[78] They concluded that the lipopeptides are more efficient catalysts as monomers than in aggregates, showing that a subtle balance of the hydrophobic part could be used to orient it towards activated hydrolysis or rather protection of the substrate.

2.2.4.3 Peptide catalyst with metal ions: Metal ions are ubiquitous in nature, playing structural or catalytic roles in nearly half of all proteins. They play a key role in regulating the activity of proteins both at allosteric and at catalytic sites. Natural amino acids comprise several functional groups in the side arms which act as binding sites for metal ions.[79] This can occur for peptides of amino acids without coordinating side chains, such as alanine or phenylalanine, or with coordinating side chains, such as His or cysteine.[80] Kaplan and DeGrado developed a heterotetrameric coiled-coil 'DFtet' peptide which self-assembled to bind to two Fe (II) in active sites. The structure of DFet comprised of two different "A" and "B" subunits, which help in binding with iron.[81] The resulting co-assembly with iron catalyzes oxidation of 4-aminophenol to the corresponding quinone. Serpell and co-workers have designed the peptides that form an amyloid-like architecture and reveal their capability to mimic carbonic anhydrase.[82] These amyloid fibril structures can bind the metal ion Zn^{2+} by a three-dimensional arrangement of His residues created by the amyloid architecture. The peptide catalyzed the PNPA molecules in the presence of Zn^{2+} ion. Laungani and co-workers have designed C- and N-terminal phosphane-functionalized peptides to bind noble metals (Pt/Rh).[83] Upon mixing, the peptides and appropriate metal salts form β-sheet assemblies that can do asymmetric hydroformylation of styrene with quantitative yield and excellent regioselectivity but modest enantioselectivity.

2.2.5 Peptide Based Smart Materials: With the technological advancement in imaging, peptides have recently been considered for their potential use as biomaterials. Researchers are now exploring the ability of peptide-based biomaterials to respond to external cues; this responsiveness has been collectively referred as 'smart behaviour.'[84] Responsiveness can be defined either at the structural or at the functional level.[84] For structural smartness, assemblies built from α-helical units tend to be more readily reversible than structures dominated by β-strand units. This difference arises principally from the relative importance of hydrogen bonding and hydrophobic contributions to structural stability.

The ability of peptides and proteins to change the conformations in response to the external stimuli such as pH, temperature, and the presence of specific small molecules is ubiquitous in nature. This property of peptide have been exploited to engineer several stimulus responsive systems with potential applications in biomaterials, nano-devices, biosensors, bio-separations, tissue engineering and drug delivery. This section will highlight some recent advances in the field of self-assembling peptides used in biomaterials design. Emphasis will be placed on work that either implicitly or explicitly incorporates concepts of smartness.

2.2.5.1 Stimulus responsive materials: Several peptide based systems have been designed to respond various stimuli. In a work, temperature dependent 12 and 16 residue peptide were designed. [85] At the temperature more than 70°C, the designed peptides showed conformational change from β-sheet formation to an α-helical structure. With cooling, these peptides retained the a-helix structure, and took several weeks at room temperature to partially return to the β-sheet form. Peptides whose bulk behaviour can be controlled by metal ions have also been successfully engineered.[86]

An emerging area of interest in the field of stimulus responsive peptides is the concept of enzyme-responsive peptides. Gao and co-workers have designed an enzyme-responsive zwitter ionic peptide coating capable of responding to matrix metalloproteinase-9 (MMP-9) which is overexpressed in tumor microenvironment.[87] The repetitive pentameric sequence of peptide VPGVG is one of the most studied stimulus-responsive peptide which is naturally found in the polymeric elastin-like polypeptide (ELP) of the mammalian elastin protein.[88] The physiochemical properties of ELP can be altered by mutating fourth residue of this sequence. The highly multimeric form of peptides (20-300 pentameric repeats), induces a

sharp reversible hydrophilic- hydrophobic phase transition in ELP, that is triggered by changes in pH, temperature, or ionic strength. Below transition temperature, the ELP exists in an extended state and is soluble in water, while at above transition temperature, the ELP collapses into an ordered b-spiral that aggregates and precipitates out of solution.[88] The stimulus responsive properties of ELPs fused to appropriate peptides or proteins have been used for remediation of toxic metals,[89] and targeted drug delivery.[90]

2.2.5.2 Molecular Shuttles: The inherent restrictions in rotational and translational freedom imposed on the components of mechanically-interlocked molecules make them particularly attractive architectures for precisely controlling the positioning of functional units or substituents with the possibility of switching their relative separation and orientation.[91] Such control has been elegantly demonstrated through π-donor-acceptor interactions in the "molecular shuttles,"[91] metal ion co-ordination in the catenates,[92] and in pseudorotaxanes, prepared by Sauvage and co-workers.[93] Molecular shuttles are rotaxanes in which the macrocycles are translocated from one binding site ("station") on the thread to the second station in response to the external stimuli (e.g., chemical fuels, light, pH, or temperature) that invert the initial relative affinity of each of the sites for the macrocycle.[94] Some of the most advanced synthetic molecular machines described to date are based on the molecular shuttle concept.[95] Gariepy and co-workers have designed loligomers, a peptide-based intracellular vehicles, that can penetrate cells and self-localize into distinct cellular compartments.[96] The loligomers were able to transfer the gene into mammalian cells, which was a non-viral gene delivery system.[96] As it is well-known that ion transport is essential for maintaining normal cell function and biological processes, Tian and co-workers have designed an artificial molecular shuttle which operates in lipid Bilayers for ion transport.[97] Recently, peptide based molecular shuttle system is explored for applications such as gene therapy,[98] and drug delivery.[99]

2.2.5.3 Metal Organic Frameworks (MOFs): MOFs have been used extensively for different application such as gas storage,[100] catalysis,[101] and chemical separation.[102] The incorporation of biomolecules as organic linkers in MOF synthesis makes them one of the most exciting and rapidly growing areas of modern chemistry research. Ferry G and co-workers first reported the loading and release kinetics of the analgesic drug, ibuprofen from the first MOF family, MIL-100 and MIL-101.[103] Both MIL structures are composed of trivalent metal centers with carboxylic bridging ligands and possess large pores

with large surface areas. Several theoretical and experimental researches demonstrated the potential application of MOFs as an ideal drug delivery system for various therapeutic drugs.[104] Zhang and co-workers have reported the RGD peptide functionalized MIL-101 for targeted release of the drug doxorubicin with effective cancer cell inhibition and reduced side effect.[105] Jimenez and co-workers have reported the use of a MOF to load, protect, and deliver small interfering ribonucleic acids (siRNAs) by avoiding enzymatic degradation.[106] They have encapsulated the siRNAs in the MOF with KALA peptide and ammonium chloride, to evade the endosomal retention and ensure that gene knockdown is efficacious.

Surface functionalization of MOFs are important for biomedical application because this interface controls the stability of the framework, the rate of drug release, cell uptake, and the overall biological response.[107] Short peptides functionalized MOFs have been used as electrochemical devices, and biosensors.[108]

2.2.5.4 Peptide Based Vaccines: Classical whole organism vaccines may have several pitfalls such as the potential risk of inducing autoimmune and allergic responses.[109] The "peptide vaccines" containing only epitopes capable of inducing positive, desirable T cell and B cell mediated immune response may be a substitute for this.[110] Since epitopes are the antigenic determinants within larger proteins, these peptides are considered sufficient to activate the appropriate cellular and humoral responses, while eliminating allergenic and reactogenic responses.[111] Peptide based vaccines are built of defined, small-peptide antigens engineered to induce the desired immune response. Several factors should be considered in formulating an effective peptide vaccine including inclusion of a universal T helper epitope, and the necessity to mimic the structure of the parent antigen to generate high-affinity antibodies.[112] On the other hand, owing to the relatively small size of peptides, they are often weakly immunogenic by themselves and therefore require carrier molecules, to add chemical stability and adjuvant for the induction of a robust immune response.[113] There are many peptide vaccines under development, such as vaccine for human immunodeficiency virus,[114] malaria,[115] and anticancer vaccine.[116]

2.3. *De novo* designed peptide nano-assemblies

Peptides self-assemble into different nanostructures, playing crucial role in fabricating hierarchical architectures that have good biocompatibility and functionalities.[117] On the basis of their chemical structure peptides, can be classified as linear,[118] cyclic,[119] and branched.[120] Some self-assembled nanostructure is summarized in Figure 2.5.

2.3.1 Nanotubes: Among the notable supramolecular self-assembly, peptide nanotube is a well-studied architecture with diversified applications. Alternating D-octapeptide and L-octapeptide, upon cyclization, have been shown to stack through hydrogen bonding to form a nanotubular assembly.[121] One of the most well studied building blocks for supramolecular structures is diphenylalanine (FF) peptide. The nanotube formed by FF molecules have shown remarkable rigidity along with various physical and chemical functions such as semiconductivity,[122] luminescence,[123] and piezoelectricity.[124]

2.3.2 Nanosheets: Surfactant like peptide were known to form nanotubes,[125] but Castelletto and co-workers first reported the nanosheet formation with surfactant like peptide, A_6R.[126] Further, they have reported the RFL_4FR peptide aggregates into ultrathin flat sheets because of β-sheet assemblies.[127] Liu and co-workers have first reported the amyloid like nanosheets formed by the KLVFFAK segment.[128] They have also shown its application as retroviral transduction.

2.3.3 Cyclic Peptides: Cyclic peptides have promising potential applications in biologicals and materials.[129] Rationally designed cyclic peptides with flat conformations can self-assemble into tubular nanostructures mainly stabilized by inter-cycle hydrogen bonding.[121] Generally, when the assembly of cyclic peptides occurs in solution, which can be triggered by cooling the solution, they can stack into nanotubes that, in turn, organize into a compact crystal structure.[130] Cyclic peptide based molecular construct have been utilized as enzyme inhibitors,[131] gene delivery,[132] organic electronics,[133] and antibacterial agents.[134]

2.3.4 Nanofibers: Among the various constructs of self-assembly, nanofibers are considered to be the most promising structure with various applications. Fibrous structures have a large length to diameter ratio. Hierarchical architectures with self-assembled peptide nanofibers may be constructed through

entanglement and non-covalent binding between peptide nanofibers. Self-assembled fibrous materials have a broad range of biomedical application such as scaffold for 3D cell culture, biofilm,[58] and tissue engineering.[135] Factors promoting the nanofiber formation are aromatic stacking, metal-π interaction, and hydrogen bonding.[136] It has been observed that the high content of β-strand could enhance the rigidity of nanofibers.[137] pH also modulates the mechanical property of nanofibers. Dong and co-workers have investigated the effect of pH on peptide sequence SSSSFAFAC.[138] At pH 2, this peptide formed amyloid like fibres with relativelyhigher amount of ordered random coil (38%), and β-sheets (37%), but no α-helices, while more flexible fibrils that are rich in α-helices were formed at pH 7. Furthermore, they confirmed that a high amount of ordered β-sheets contributed to improve the rigidity of the formed fibrils.[138]

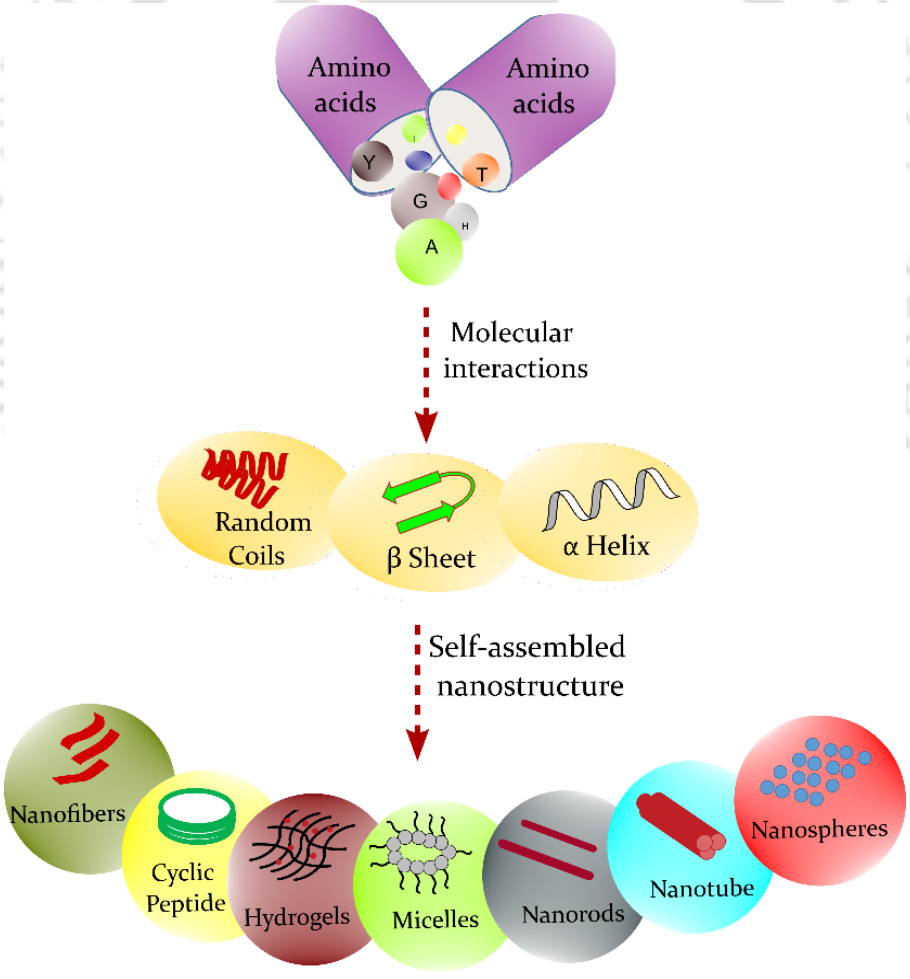

Figure 2.5 Peptide based self -assembled nanostructures

2.3.5 Hydrogels: Peptide-based hydrogels are a class of soft materials that typically have three-dimensional (3D) fibrous networks cross-linked through physical or chemical bonding. They are characterized by their high-water content, microporous structure, tuneable mechanical stability, good biocompatibility, and elasticity.[139] In addition, hydrogels are readily decorated or functionalized through side-chain modifications to realize specific applications.[140] The main factor responsible for the gelation is aromatic π-π interaction, which also increases the hydrogen bonding and other non-bonding interactions in water, usually lead to supramolecular hydrogels.

2.3.5.1 Single amino acid based Hydrogels: There are several reports on hydrogels formed by dipeptides and tripeptides with different N-terminally conjugated aromatic groups. However, a single amino acid containing hydrogel is relatively less reported.[141] Nilsson and co-workers have reported that halogenation of the phenyl side chain of Fmoc-Phe resulted in rapid self-assembly, and hydrogelation relative to Fmoc–Phe or Fmoc-Tyr.[142] Hydrogels formed from the self-assembly of Fmoc-F_5-Phe-OH or monohalogenated derivatives were mechanically rigid, but unstable in solvent.[143] To increase the stability of the designed peptide, they have conjugated it with polyethylene glycol. Banerjee and co-workers have reported pyrene conjugated phenylalanine derivate superhydrogel with minimum gelation concentration less than 0.1% w/v, showing thixotropic property.[144] Thakur and co-workers have reported the Fmoc-Phe hydrogel with antimicrobial effect.[22] Marchesan and co-workers have also synthesized phenylalanine derivative *N*-(4-Nitrobenzoyl)-Phe which self-assembled to form hydrogel showing significant antimicrobial property.[145]

2.3.5.2 Short and ultrashort peptide based hydrogels: Peptide sequences having amino acids chain length less than 20, is termed as short peptides, while sequence having less than 7 are ultrashort peptide.[146] Zhang and co-workers have designed several self-assembling short peptides.[147] Features of these peptides include regularly alternating hydrophilic and hydrophobic amino acids, where positive charges are juxtaposed to negative ones.[148] Due to ionic self-complementarity encouraged by the presence of salts, these peptides self-assemble to form nanofibers that interweave further to form β-sheet hydrogels.[148] Diphenylalanine is frequently incorporated as a backbone to generate short peptide based hydrogelators because it (FF) promotes π-π stacking interactions.[149] The N- terminal capping groups also enhance intramolecular interactions, which then can induce hydrogel formation. The protecting groups

which are generally used as a capping groups such as Fluorenylmethyloxycarbonyl (Fmoc),[150] naphthalene,[151] carbazole,[152] and indole[153] are reported to induce gelation. Naresh kumar and co-workers have designed an anthranilamide capped short peptide hydrogel having antimicrobial property.[154]

2.3.5.3 Stimulus responsive peptide hydrogels: In stimulus responsive hydrogel the polymer networks comprising of stimuli-responsive basic building blocks, for example, photoisomerizable units[155] or redox groups,[156] allow the triggered and reversible transitions between hydrogel and solution phases or hydrogel and solid states.[157] The conjugation of p-boronophenylmethoxycarbonyl (BPmoc) or p-nitrophenylmethoxycarbonyl (NPmoc) to the FF peptide yielded redox-active hydrogels.[158] Incorporation of fumaric amide as a conformational switch has proved to be an effective strategy to construct photo-responsive supramolecular hydrogels with potential applications.[155] pH responsive hydrogels have been designed as drug delivery systems. Zhong and co-workers have synthesized an RGD derived peptide conjugate, which entrap doxorubicin and release it under mild acidic conditions paving ways for the controlled release of drug cargos in a typical tumor microenvironment.[159] Ge and co-workers have designed a paclitaxel loaded peptide hydrogel for the localized delivery of paclitaxel *via* intratumoral injection to enhance the therapeutic efficacy against the tumor.[160] Apart from drug delivery systems, stimulus responsive hydrogels have been explored for tissue engineering,[161] self-healing materials,[162] and sprays.[163]

2.3.5.4 Amyloid based Hydrogels: Amyloid-based hydrogels are water-laden, three-dimensional materials formed by cross-linking of protein fibrils. They hold large amount of water because they have a large number of hydrophilic functional groups present in their polymeric chain.[164] Several proteins and peptides are known to form hydrogels through the cross-linking of amyloid fibrils.[165] Amyloid based hydrogels are useful in the development of materials such as drug delivery systems and tissue engineering.[59]

2.3.5.5 Fmoc Based Hydrogels: Janmey and co-workers reported for the first time the formation of fibrous networks with fluorenylmethoxycarbonyl (Fmoc)-protected amino acids and dipeptides,[166] while Xu and co-workers were the first to report that certain Fmoc-protected amino acids and dipeptides spontaneously formed fibrous scaffolds.[167] Fmoc-modified diphenylalanine (Fmoc-FF) has been widely

studied as the simplest and most effective hydrogelator.[167-168] Recently, Fmoc-FF-based hybrid gels were also used as drug delivery systems.[169] Ikeda and co-workers have synthesized a new Fmoc-dipeptide, comprising α-methyl-L-phenylalanine.[170] Few examples of Fmoc based peptide hydrogels are listed in table 2.1.

Table 2.1. Fmoc based peptide hydrogels

S.No	Sequence	References
1	Fmoc-FF	171
2	Fmoc-F,Fmoc-W, Fmoc-Y	172
3	Fmoc-FRGD-OH, Fmoc-RGDF-OH, Fmoc-FG-OH	150
4	Fmoc-VLK(Boc), Fmoc-K(Boc)LV	173
5	Phosphorylated Fmoc-FFpY	174
6	Fmoc-FFY	175
7	Fmoc-RGDS, Fmoc-RGDS, Fmoc-GRDS and Fmoc-GRDS	176

2.4. Properties of self-assembled Nanostructures

2.4.1 Mechanical Properties: Several previous studies reported the mechanical strength of the FF peptide nanostructure.[177] Atomic force microscopy (AFM) measurements have indicated an average point stiffness of 160 Nm^{-1} and a calculated Young's modulus of about 20 GPa for nanotubular peptide assemblies.[178] Density functional theory (DFT) calculations show that the high mechanical strength of FF nanostructure was the result of an aromatic zipper present in the nanotubes.[179] Gazit and co-workers have designed dipeptide based on β,β-diphenyl-Ala-OH (Dip), Dip-Dip, cyclo-Dip-Dip, and *tert*-butyloxycarbonyl (Boc)-Dip-Dip.[180] The phenyl-enriched structures showed material performance superior to that of FF nanotubes, with improved mechanical rigidity, thermal stability, and piezoelectricity. The mechanical properties of the nanostructure can also be tuned by using two peptides of different stereochemistry. Elevating the level of FF peptide in the peptide mixture, decreases the nanostructure's stiffness.[177]

2.4.2 Electrical Properties: Among the amino acids, some side chains include hydrogen donor and acceptor groups. These side chains are commonly involved in proton transfer and proton coupled electron transfer processes.[181] In the context of protein and peptide-based films, these side chains give rise to long-range proton transport.[182] Nakayama and co-workers have shown conductivity in the designed peptide, GFPRFAGFP, which self-assembled to form fibers.[183] Ashkenasy and co-workers have demonstrated that the aromatic stacking in D,L, α-cyclic peptide self-assembled nanotubes was found to promote long range conductance in peptide self-assembly, and hence could increase the conductivity.[184] However, due to the inherently low dielectric constant, energy translocation through peptide architectures is inefficient, which severely hinders their practical application.[185] Incorporation of water molecules can improve the conductivity of bioinspired supramolecular structures.[182] Another way to improve charge transfer inside peptide assemblies is by the utilization of doping, such as through chemical conjugation or co-assembly with functional moieties.[186] By concerning these points, Gazit and co-workers have designed L,D- amino acid containing Trp dipeptide (Ww), which crystallized into a layered organic-water structure.[187]

2.4.3 Optical Properties: The molecular arrangement during self-assembly determines the optical properties of peptide nanostructures. The elementary building block of FF-nanotubes or Boc-FF-nanospheres was shown to have the optical properties of zero dimensional quantum dots (QD).[188] However, FF was also reported to form 2D quantum-wells during thermal deposition at high temperature.[189] The change in optical property was attributed to the alteration of their nanoscale packing, during vapour deposition process. Besselievre and co-workers have used the lanreotide octapeptide cyclized peptide scaffold to form nanotubes.[190] The high-resolution structure of the nanotube walls, show that the cyclic peptides are stacked in a 2D crystal which resembles quantum well.[191]

Some of the most promising quantum-sized physical effects, found in these nanomaterials, are the electron-optical spectral properties such as light absorption and luminescence.[192] The nanoscale architecture comprising the supramolecular structure revealed pronounced electron-optical effects which are highly specific for different quantum confinement ordering and could be recognized optically for understanding of quantum confined shapes, and dimensions.[19]

2.5 Factors affecting nano-assemblies

Peptide self-assembly occurs due to the association of two or more molecules mediated by physical interactions. In aqueous solution and in equilibrium, a peptide molecule adopts a conformation that minimizes its free energy. The main driving forces in the intramolecular interactions include hydrophobic interactions, hydrogen-bonding (intermolecular and intramolecular), Van der Waals, aromatic, and electrostatic interactions.[193] These non-covalent interactions are relatively insignificant for isolated peptides because they are generally weaker than covalent interactions. pH,[194] electric field,[195,196] magnetic field,[197] and temperature[198] also modulate nano-assemblies.

2.5.1 Aromatic π-π Interactions: Burley and Petsko first reported the aromatic interactions in proteins.[199] They have reported that phenyl ring centroids are separated by a preferential distance, between 4.5-7.0 Å, and dihedral angles of 90° are commonly found to have aromatic π-π interaction.[199]

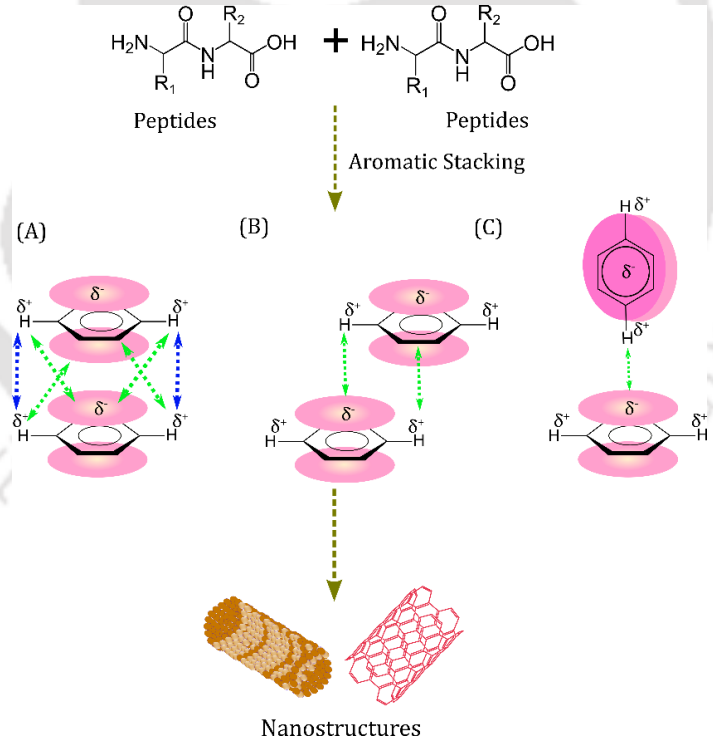

Figure 2.6 Schematic representation of aromatic interactions; (A) sandwich, (B) Parallel displaced, and (C) Edge- to- face stacking leading to the formation of nanostructure. Blue line represents repulsive interactions, and green line represents attractive interactions.

In supramolecular chemistry, aromatic-π interaction is considered as a non-covalent interaction between the organic molecule having aromatic moieties.[200] On the basis of interactions between π electron rich aromatic species, aromatic interactions can be classified as edge-to-face, parallel displaced, and face-to-face stacking[201](Figure 2.6). The small, unsubstituted aromatic compounds prefer edge-to-face geometry, whereas substituted and large multi-ring aromatic compounds prefer parallel displaced geometry.[202] Chakrabarti and co-workers examined the specific interactions and packing preferences of tryptophan (Trp) with other aromatic amino acids. They reported that interaction of Trp with Phe was more favourable in face-to-edge (FtE) geometry as compared to face-to-edge (FtE) geometry.[203] The bulky indole side chain of Trp amino acid is capable of establishing multiple interactions, including π···π, C-H···π, band N-H···π, in which the indole nitrogen can also act as a hydrogen bond donor.[204] Aromatic interactions are also crucial for the stability of the helix bundle proteins. The different nanostructures formed by the π-π interactions are nanotube,[205] nanofibers,[206] nanoflowers,[207] and nanorods.[208]

2.5.2 Hydrogen bonding: Hydrogen bonds are the interactions between hydrogen atoms and the electronegative atoms.[209] The selectivity and high directionality of hydrogen bonds can convert short peptides into diverse one-dimensional, two-dimensional, and three-dimensional nanostructures.[210] Li and co-workers have demonstrated the formation of FF microrods by hydrogen bond based self-assembly.[211] The characterizations of the self-assembled microrods indicated that 1,1,3,3,6,6-Hexafluoro-2-propanol (HFIP) formed stable intermolecular hydrogen bonds with an FF peptide, leading to the solvation of peptide molecules. The intermolecular hydrogen bond strength modulated by elevated temperature and sonication enables structural transitions between nanowires and nanotubes.[212] Hydrogen bonding between peptide backbones is unique and plays a critical role in the one dimensional growth of many peptide aggregates.[213] Lu and co-workers have compared the self-assembly of I_3K and L_3K peptide, and found that replacing isoleucine residues with leucine leads to a morphological change from long nanotubes to spherical aggregates, with the corresponding secondary structure transition from β-sheet to random conformation.[214]

2.5.3 Hydrophobic Interactions: Peptide resemble conventional surfactants in terms of possessing hydrophobic and hydrophilic moieties.[121] Stupp and co-workers have shown that the self-assembly of amphiphilic peptide is prominently governed by the relative strength of hydrogen bonding, compared

with the hydrophobic interactions.[215] The aromatic residue of peptide plays crucial role in determining the interactions between molecules. The organizational mode of the aromatic residues in the hydrophobic interactions is commonly disordered, while in π-π interactions, it is well-ordered.[216]

2.5.4 Electrostatic Interactions: Electrostatic interactions play a significant role in the self-assembly of biomolecules.[217] The strength of an ionic bond is dependent on the solvent (particularly its dielectric constant) and the presence of mobile ions. Ionic bonds are generally stronger and of longer range than hydrogen bonding.[218] Electrostatic bonds based on the Coulombic attractions between opposite charges lead to the formation of ion-pairs. Bernier and co-workers have described the self-assembly of a crown ether functionalized peptide through the mediation of electrostatic interactions.[219] Su and co-workers have fabricated an artificial peptide nanofibers with peptide motif, VIAGASLWWSEKLVIA, further metallized to synthesize nanofiber-based silver nanowires.[220] A novel hybrid nanomaterial was obtained successfully by assembling the prepared silver nanowires on graphene nanosheets. In another study, Liu and co-workers fabricated micelle-induced protein nanowires through an electrostatic interaction when the electronegative cricoid stable protein one (SP1) assembled with positively charged cross-linked micelles.[221]

2.5.5 Van der Waals Interactions: Van der Waals forces, such as the interaction between aliphatic tails in peptide amphiphiles, provide a crucial contribution to various non-covalent interactions and are ubiquitous in assembly systems.[222] There are however only a few examples that employ Van der Waals interaction as a dominant force for the control of a peptide nanostructure.[223,222]

2.5.6 Solvent Effects: Solvent affects the self-assembled nanostructure owing to different polarity, dielectric constant, and hydrogen bonded network. Murphy and co-workers investigated the effect of solvent system on the self-assembly of beta amyloid peptide.[224] In pure dimethylsulfoxide (DMSO), Aβ peptide had no detectable β-sheet content. In 0.1% trifluoroacetate, however content went upto 33% β-sheet, and in 35% acetonitrile/0.1% trifluoroacetate, Aβ peptide had two-third amino acids in β-sheet conformation, equivalent to the fibrillar peptide in physiological buffer. Hamley and co-workers have demonstrated that the short peptide fragments, derived from β-amyloid peptide, AAKLVFF, exhibited distinct structural differences depending on solvent polarity.[225] Zhimin and co-workers examined the

effect of solvent system on the FF peptide to form either nanofibers or nanotubes after heating to 95°C and subsequent cooling in solution, or alternatively, deposition on the surfaces.[226] Interestingly, they have reported that upon cooling from mixed water-methanol systems, nanofibers formation was observed, but they could not observed any structure in when the percentage of methanol exceeds 70%. In these conditions, nanofibers are formed only upon drying on glass surfaces. Authors attributed this behaviour to the ability of methanol to form hydrogen bonds with the diphenylalanine molecules, leading to good solvation of peptide molecules.[226] Roy and co-workers have investigated the solvent effect on the gelation of laminin derived peptide.[227] They have chosen the solvents of different polarity varying from highly polar phosphate buffer saline (pH 6) to 10% DMSO/water (0.1% TFA) and comparatively weak polar 50% ACN/ water (0.1% TFA). The gelation results clearly revealed that aqueous-organic mixtures are more favourable for inducing hierarchical self-assembly in more hydrophobic peptide derivatives by promoting hydrophobic and aromatic interactions between gelator moieties, which otherwise could not have been possible in aqueous solvents due to their poor solubility.[228]

2.6 Applications of de novo designed peptide constructs

Peptide based nanomaterials have been used for a myriad of biological applications, leveraging in large part their property to self-assemble (Figure 2.7).

2.6.1 Tissue Engineering: Bioinspired materials for tissue repair have been amongst the most exhaustively explored fields in biomaterials research.[229] Pedone and co-workers have designed the peptide, QK, mimicking the vascular endothelial growth factor (VGEF).[230] VGEF is the principle regulator of angiogenesis. Hartgerink and co-workers have incorporated the QK peptide to the nanofiber forming peptide sequence, which self-assembled to form hydrogel.[231] The conjugated peptide sequences potentially promoting VEGF receptor activation, dimerization, clustering, and intracellular angiogenic signalling at the site of nano-fibrous hydrogel delivered.[231] Stupp and co-workers have designed a peptide nanoribbons mimicking the activity of fibroblast growth factor-2 (FGF-2),[232] which is a regulating factor in angiogenesis, cell differentiation, and wound healing.[232] Peptide sequences have also been designed as anti-inflammatory motifs,[233] surface adherence molecules,[234] and corneal tissue repair.[235]

2.6.2 Drug Delivery Systems: The clinical efficacy and effect of conventional chemotherapeutics against tumors are compromised by several factors including poor solubility, short half-life *in vivo*, the weak penetration capability, and the low specificity.[236] Ingeniously designed drug delivery systems can improve the bioavailability of drugs or minimize the adverse effects of drugs. Among the different drug delivery systems, peptide based drug delivery systems are important because; (i) the unique biochemical functionality encoded by peptide sequences enables an active targeting,[237] (ii) the structure of peptide assembly can be programmatically modulated by intrinsic and external stimuli to achieve a controllable release of the payload into the target region,[238] (iii) peptides are biocompatible compared to the synthetic organic compounds, and (iv) the reactive terminus and side chains of peptides can be used as a reactive site to conjugate chemotherapeutics.[239]

2.6.3 Antimicrobial Peptide Hydrogel for wound healing: Despite advancements in medical technology, infectious diseases caused by micro-organisms such as bacteria, virus, fungi, remain major threat to public health. Furthermore, over-prescription and misuse of antibiotics also have escalated the drug-resistance. Chronic wound infections and development of antibiotic resistance are affecting people world-wide. Antimicrobial peptides kill bacteria effectively, but their susceptibility to degradation, limit their use for topical application only. In recent years, tremendous research has been conducted to utilize hydrogels either as an antimicrobial agent[240] or as a drug carrier.[241] Chitosan, a natural linear polysaccharide, was investigated to form hydrogels and subsequently as a potential antimicrobial hydrogel. Hsieh and co-workers have reported a chitosan-γ-poly(glutamic acid) polyelectrolyte complex hydrogel possessing antimicrobial property against *Staphylococcus aureus* and *E. coli*.[242] Interestingly, the formed hydrogels also promote the 3T3 fibroblast cell proliferation, and so induced wound healing. In addition to polymer based hydrogels, peptide based antimicrobial hydrogels are also reported recently. Schneider and co-workers have designed a 20-residue β-hairpin peptide hydrogel scaffold for tissue regeneration which also have an inherent antimicrobial property.[20] Diabetic foot ulceration and infections are one of the prominent cause of mortality and morbidity in developing countries. The microbiological profiling of diabetic foot infection shows the presence of pathogens such as *Pseudomonas aeruginosa*, *Staphylococcus aureus*, and *Enterobacter* species.[243]

Table 2.2. Peptide based hydrogels for diabetic foot ulcer

S.No.	Hydrogels	Compositions	Ref
1	Chitosan-peptide-collagen hydrogel	Chitosan-collagen hydrogel with peptide : QHREDGS	244
2	Hydroxyethyl cellulose peptide hydrogel	Peptide : RQPKIWFPNRRKPWKKRPRPDDLEI entrapped in cellulose	245
3	Multidomain peptide hydrogel	Peptide: $K_2(SL)_6K$	246
4	Dispersin B-KSL-W hydrogel	Dispersin B Peptides: KKVVFWVKFK, and KKVVFKVKFK Pluronic F-127	247
5	ODEX/HA-AMP/PRP hydrogel	Oxidized dextran Platelet-rich plasma Peptide: SWLSKTAKKLFKKIPKKIPKKRFPRPRPWPRPNMI-NH2	248
6	Chitosan-peptide hydrogel	Chitosan Peptide: LLGDFFRKSKE-KIGKEFKRIVQRIKDFLRNLVPRTES	249
7	Glucose oxidase loaded antimicrobial peptide hydrogels	Glucose oxide Peptide : IKYLSVN	250

Peptide hydrogels and its composite with chitosan have been investigated as an antimicrobial agent useful in the diabetic foot ulcer (Table 2.2).

2.6.4 Biosensors: Peptides have also been employed as recognition elements in bio-sensing.[251] For instance, peptides with short chains of amino acids generally have better chemical and conformational stability than proteins. Peptide based biosensors have been fabricated for the detection of several analytes, including cells proteins, metal ions, proteases, kinases, bacillus species, nucleic acids and antibodies.[251] Electrochemical biosensors based on screen-printed electrodes and peptides are interesting alternatives for molecular diagnosis.[252] Chai and co-workers have developed an electrochemical peptide cleavage-based biosensor for the detection of prostate specific antigen using silver deposition on electrode.[253] Other

recently explored applications of peptide based molecular constructs are in energy storage devices,[254] bioimaging,[255] antifouling agents,[256] and metal organic framework.[257]

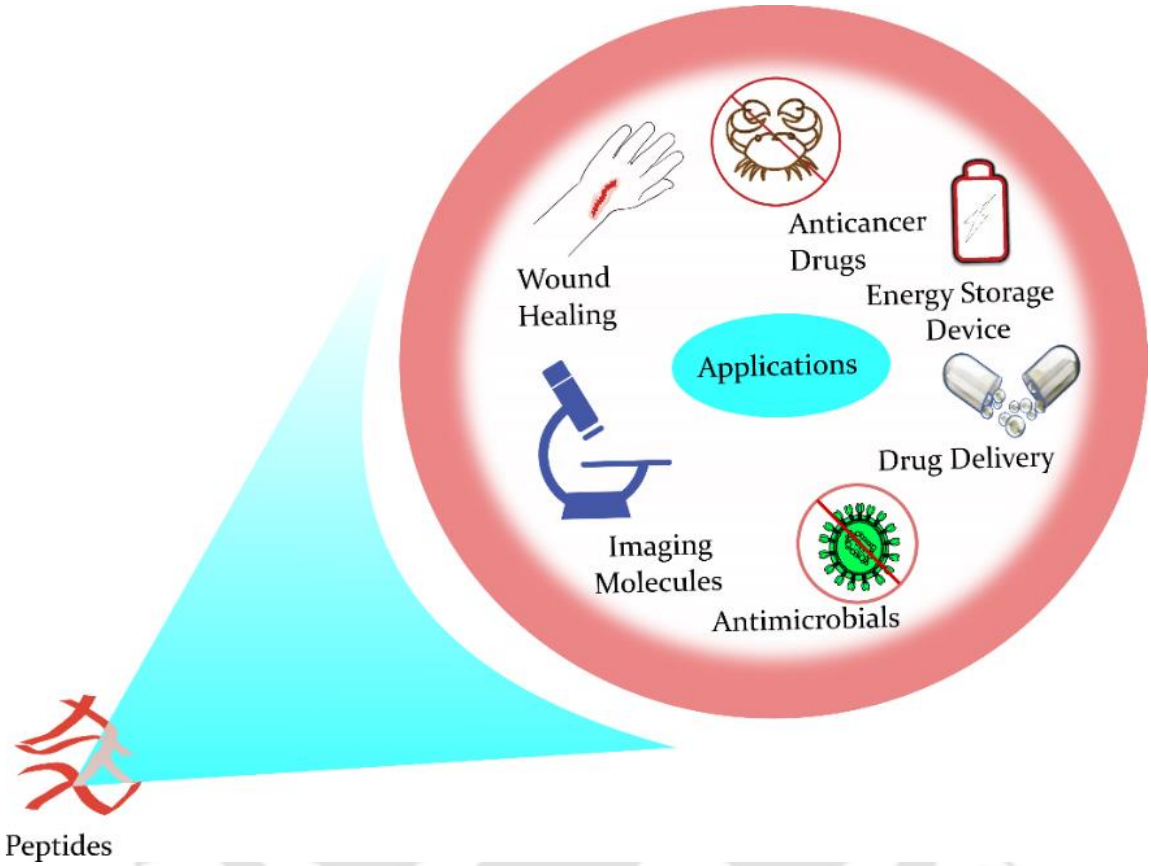

Figure 2.7 Applications of self-assembled nanostructures

2.7 Conclusions and Future Directions

Extensive research has been performed in the field of supramolecular self-assembly of peptides in the last 20 years. The wide range of self-assembled architecture, formed by these molecules have been explored in various fields. Research work has been conducted to address different problems such as, to deliver the small drug molecules to the target areas,[258] to increase the efficiency of anticancer drug, sustained release

of drug molecules, find the replacement of conventional vaccine for reducing side effects, and replacement of hazardous batteries with biodegradable materials etc. Here we have provided an overview of different nanomaterials fabricated by peptide molecules with possible applications. The stimulus responsive materials have opened a different field of research, in the area of drug delivery systems where drugs can be released only by changing the pH of the surroundings. Peptides and small molecule-based nanostructures can be good alternatives as drug delivery systems as they possess certain characteristics such as good biocompatibility, ease of synthesis, and functionalization. The efforts to replace the conventional vaccines with peptide based vaccines offer several advantages such as less toxicity, easy to synthesis protocol, and stability. Although several methods have been applied to control the formation of self-assembled structures, total control of the designed peptide conformation and assembled supramolecular structure, still remains elusive.

3

Research Design and Objectives

3.1 Research Design

The design and development of bioinspired molecules for different application fronts is the primary goal of this thesis. It is mainly focused on the de novo design of peptide based molecular systems and their chemical modifications for targeted applications. The peptides are designed to have enhanced aromatic π-π interactions leading to self-assembly forming functional nanostructures. The objectives of this thesis may be broadly summarised as follows:

3.2 Objectives

The central objective of this thesis is the design of aromatic extended molecular networks directed by aromatic π-π interactions forming supramolecular assemblies at nano-scale. Based on this central objective, four application fronts have been formulated.

1. De novo designed artificial blue fluorescent protein

The specific objective of this study is to design a naturally folded fluorescent mini protein that can potentially be modified as an artificial biosensor. The work involves the following steps:

- **i.** Design of a mini protein fold using automated protein design methods.
- **ii.** Identification of fluorophore implantation site in the hydrophobic core of the protein.
- **iii.** Incorporation of β-(1-azulenyl)-L-alanine which has a fluorescence emission in the visible region of the electromagnetic spectrum, in the core region of protein.
- **iv.** Redesign protein core, and verify the stability of the newly designed molecules by molecular dynamic simulations.
- **v.** Synthesis and characterization of the designed artificial functional protein.

2. Quantum confinement of peptide nano-assemblies

- **i.** Design of syndiotactic phenylalanine hexamer peptide
- **ii.** To study the quantum confinement effects of the designed peptide

3. Ultrashort peptide hydrogel with antimicrobial property for topical applications

i. Synthesis of Fmoc mediated ultra-short peptide hydrogels
ii. Study the rheology of synthesized ultra-short peptide hydrogel
iii. Validation of antimicrobial property of peptide hydrogel, specifically aimed to use for wound healing.

4. Heavy metal removal and reduction by metal-organic systems and biodegradable adsorbents

i. Generation of trityl based organic nano assemblies
ii. Synthesis and characterization of metal organic systems
iii. To explore the possibility of using such aromatic molecular systems as heavy metal sorbents for water remediation
iv. To explore the possibility of human hair, as a cost effective adsorbent, for removal and reduction of chromium

3.3 Experimental approach and broad outcome

In the subsequent chapters, we will discuss the design of a minimalistic blue fluorescent mini-protein. The designed mini protein has an unnatural amino acid, β-(1-azulenyl)-L-alanine, impregnated in the hydrophobic core. Further, we have studied the quantum confinement of a phenylalanine based peptide nanoassembly. Diphenylalaline has been reported to form quantum dots in methanol with an average diameter of 2.1 nm.[19] We have taken the complexity to the next level and designed a syndiotactic phenylalanine peptide hexamer, FfFfFf-OH, adopting gramicidin A like helical structures. The designed peptide also self-assembled in methanol to form an organogel.

To further explore the possibilities of peptide based molecular constructs, we have designed an ultrashort peptide molecule, N- terminus modified with a fluorenylmethoxycarbonyl (Fmoc) group. Such N-terminal modifications help in enhanced aromatic stacking, subsequently resulting in the self-assembly of molecules, forming a hydrogel. A series of biophysical experiments were performed to characterize the peptide self-assembly. We have also addressed the question of their stability in biological fluids. A successful hydrogel is characterised by its high storage or holding capacity. Rheological studies have been

performed to establish the visco-elastic property of the synthesized hydrogel. The self-healing property of hydrogels opens up the possibility of using the designed hydrogel to be used in wound dressing and tissue regenerative biomaterials.

Ramakrishnan and co-workers have reported the single crystal organic Nanoflower, 1,2-bis(tritylthio)ethane, obtained during the deportation of histidine containing peptide.[259] The molecule responsible for the crystal formation was reported to be a trityl compound, which is generally used as a side-chain protecting group of amino acids. In our work, we have explored the possibility of 1, 2-bis(tritylthio)ethane crystal, used as a heavy metal adsorbent. We have also explored the heavy metal removing ability of a keratin polymer, human hair, which is generally a biological waste. Human hair was processed by different methods such as pulverization and inceneration, and metal adsorbent capacity was established by employing a series of adsorption experiments.

4

De novo Designed Artificial Blue Fluorescent Protein

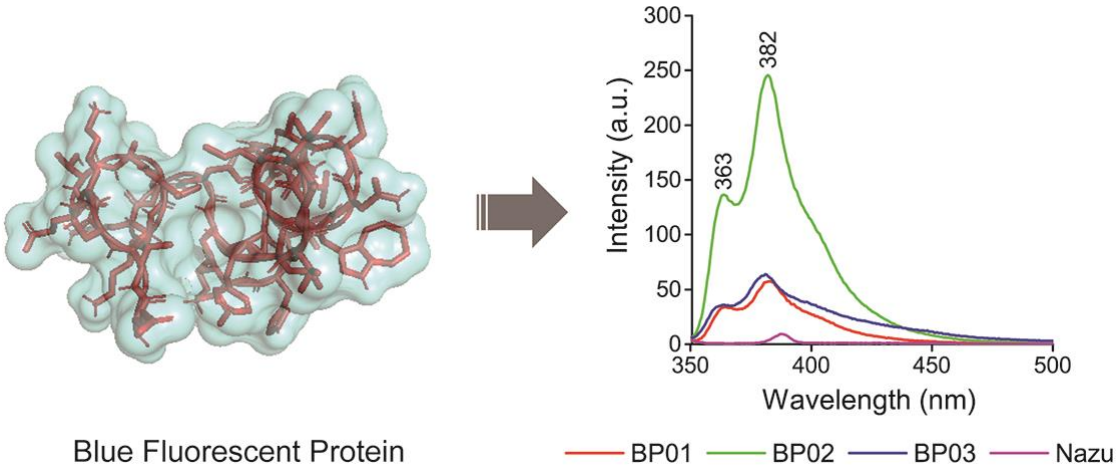

Diversification of chain stereochemistry offers tremendous increase in protein design space. We have designed a minimal fluorescent protein, carrying β-(1-azulenyl)-L-alanine in the hydrophobic core of a heterotactic protein scaffold, employing automated design tools such as AR-SAMD and IDeAS. The *de novo* designed heterochiral protein can be selectively excited at 342 nm, quite distant from the intrinsic fluorophore, and emits in the blue region. The structure and stability of the designed proteins were evaluated by established spectroscopic and calorimetric methods.

4.1 Introduction

Protein molecules found in nature are polymers of amino acids with definite handedness or chirality, with their spatial orientation being preferentially left handed or L-chiral.[260,261] Of late, this disproportionate or rather complete excess of L- amino acids is argued to be preordained and eventually turned out to be one of the most powerful arguments of creationists who believe that species on earth are not formed by evolution but by 'intelligent design'.[262]

Tacticity is a relative term in stereochemistry, which deals with the arrangement of adjacent chiral centers within a given polymeric molecule. Based on the spatial arrangement, a polymer can be isotactic, syndiotactic or heterotactic in nature. An isotactic polypeptide sequence is characterized by amino acids having L- or D- stereochemistry, whereas, a syndiotactic sequence is having a stereo-regular arrangement with alternate L- and D- amino acids (or vice versa) in succession, and a hetero-tactic polymer is a random distribution of L- and D- amino acids in a sequence.[263,264] If we can hypothetically add one more variable as 'stereochemistry of amino acids' in the backbone, by adding D- amino acids at 'n' sequence positions, number of stereo-isomeric diversity increases exponentially from 1^n to 2^n, but the entire protein universe is made of just only one of them, which means (2^n-1) is yet to be explored.[261] The origin of this apparent stereo-chemical filtration in protein biogenesis remains unclear; however, its consequence on peptide assemblies can be investigated and explored for the future design of bioinspired materials.[265] Our primary interest is to use the backbone stereochemistry as an additional variable; exploring novel architectures in the 2^n-1 design space available for novel peptide based molecular constructs.

In one of the pioneering studies, P.J. Flory observed that isotactic polypeptides are far more "stiff" than could be explained on the grounds of his statistical coil model with effects of atomic excluded volumes included.[266] The stiffness is measured in terms of characteristic ratio, which is unusually high in poly L-chiral peptides with a limiting value of 9.0.[267] But when the random polypeptide is modified from poly L (isotactic) to alternating L, D (syndiotactic), the characteristic ratio deflates from 9.0 to 0.9, which is a value lower than the theoretical minimum for the unperturbed random coil. The drastic drop in stiffness without making any difference in its residue level inter-amide electrostatics remained a 'puzzle' to him.[268]

In an apparent attempt to study this phenomenon, we simulated equilibrium ensembles of octa-alanine peptides in poly L and alternating L, D chiral stereo-chemical sequence in the water at different temperatures. We observed that the short and long-range electrostatic interactions are found to be in the opposite directions in the folded state and in harmony in the unfolded state.[28] The ying-yang of these two opposing interactions enables a third variable like amino acid side-chain sequence or solvent dielectric to be detrimental in selecting the conformational fold. It may be this effect that makes an isotactic polypeptide like protein, so powerfully responsive to stimulus, and eventually manifest themselves as a sensor transducer apparatus in living systems.[269] In this work, we introduce the next level of complexity in 'polypeptide stereochemistry', by adopting a heterotactic (random L and D) backbone, and examine the scope of this prototype, for the design of future biomaterials.

The *de novo* design of proteins and the determination of minimum requirements for the formation of protein-like structures are currently the subjects of active research.[270,271] Significant advances have been established toward the design of stable, well-folded proteins with novel sequences.[272,273] The design of the stable protein-like structure with a smaller number of residues requires both an exquisite optimization of hydrophobic packing and a strategy to decrease the backbone configurational entropy of the unfolded state.[274] The discovery of a small and fast folding protein, a 20 residue Trp-cage (NLYIQWLKDGGPSSGRPPPS), by Anderson and co-workers, folds in 4 μs to the native state, contributed much to the understanding of protein structure and folding mechanisms.[274,275]

The NMR structure reported by Neidigh et al. [274] reveals a compact hydrophobic core where three proline residues (Pro-12, Pro-18, Pro-19) and a glycine (Gly-11) pack against the aromatic side chains of Tyr-3 and Trp-6. The central buried Trp-6 residue is surrounded by residues Tyr-3, Leu-7, Pro-12, Pro-18 and Pro-19 (Figure 4.1). The secondary structure elements include an α-helix extending from residues 2 through 8, followed by a 3_{10}-helix (residues 11-14), and a polyproline II helix at the C-terminus. Owing to its small size and fast folding rate, Trp-cage has been an extremely popular model for computational studies of protein folding dynamics.[276]

The aromatic amino acids responsible for fluorescence, are relatively rare in proteins.[277] Tryptophan's (Trp) significant red shift, while compared to all other amino acids, high sensitivity to the local

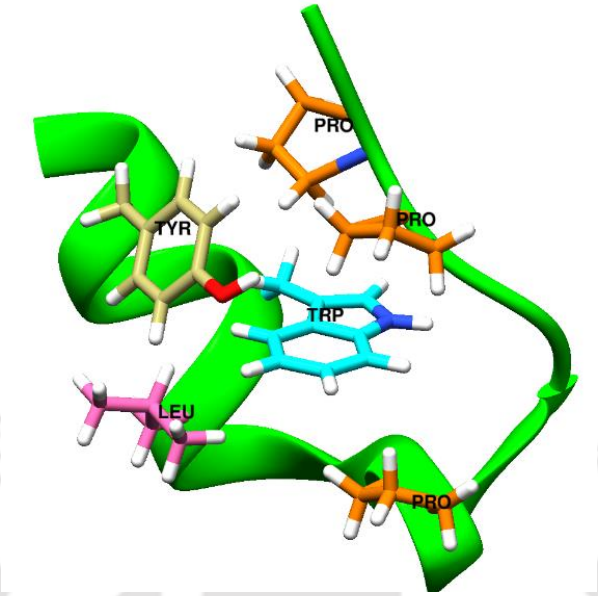

Figure 4.1. Structure of Trp-cage. Trp-6 is surrounded by residues Tyr-3, Leu-7, Pro-12, Pro-18 and Pro-19.

environment and low abundance in proteins are particularly well suited for the study like protein structure, function, and dynamics.[278] However, Trp needs to be excited by UV light with wavelengths less than 300 nm, which interferes with other chromophores often present in a biological sample.[279]

One approach to address this problem is to use the unnatural analog of Trp which can be excited above ~300 nm, where Trp absorption is negligible. A pseudoisosteric analog of Trp, β-(1-Azulenyl)-L-Alanine (AzAla) which is an azulene moiety,[280] fulfils the above criteria. This can be excited at 342 nm, independently of Trp, and the emission is in the visible region.

The limitations of such methods are low protein yields, unpredictability of efficiencies and complicated working protocols.[281] Peptides have been in use as reliable scaffolds for novel biomaterials.[282,283] Many sensitive fluorophores can respond rapidly to environmental changes by way of a change in their spectral characteristics. We report design, synthesis, and characterization of a hetero-chiral artificial protein of just 30 amino acids long, which was further examined to explore the possibility of converting it to a fully

functional molecule. An unnatural amino acid AzAla is incorporated in a heterotactic protein scaffold which has a clear distinction in spectral characteristics compared to the native tryptophan signal.

4.2 Experimental Procedures

4.2.1 Protein Design: The design and sequence optimization of the de novo protein was performed employing the protocol described elsewhere.[284,269,285] First the amino acids were folded in space by using Automated Repetitive Simulated Annealing by Molecular Dynamics (AR-SAMD) protocol. In brief, energy minimized polypeptides were submitted to AR-SAMD cycles with customized GROMOS-96 parameter. A fairly large family of structures was generated sequentially, simulating a long high-temperature MD trajectory and performing simulated annealing periodically. The starting structure was first energy minimized followed by Molecular Dynamics simulation with parameter set customized for randomization of either stereochemical structure or conformation of a polypeptide, using GROMOS-96 force field. The final conformer resulting from each Simulated Annealing Molecular Dynamics (SAMD) cycle was stored for later processing. The possibility of redesigning stable folds to a possible functional protein molecule was further evaluated by an automated sequence design tool, IDeAS. The input files for IDeAS was cartesian coordinates of the most stable fold specifically in PDB format. The coordinates over L-side-chain rotamers were applied inversion-symmetry transform, generating the database of D enantiomers.

4.2.2 Materials: All chemicals and solvents used for experiments are of analytical reagent grade. Amino acids, solvents, Trifluoroacetic acid, Thioanisole, and 1,2-ethanedithiol were purchased from Sigma-Aldrich. Diethyl ether, m-cresol, were purchased from Merck. AzAla was purchased from Iris Biotech GMBH, Germany. Ultrapure water used throughout the experiments.

4.2.3 Peptide synthesis and Characterization: Peptides were synthesized manually by SPPS (solid phase peptide synthesis) method using Fmoc chemistry. Peptides were cleaved from the resin using a cleavage cocktail comprising trifluoroacetic acid, ethanedithiol, thioanisole, and m-cresol (20:1:2:2). Purification was done by Shimadzu Prominence Modular HPLC instrument with a reversed-phase C18

column using a linear gradient of water and acetonitrile (10–100%) containing 0.1% TFA. Peptides were further characterized by verifying mass using a Bruker, Autoflex Speed MALDI TOF/TOF spectrometer.

4.2.4 UV-Vis Absorption Spectroscopy: Cary 60 UV-Vis spectrophotometer (Agilent Technologies) was used to record UV-Vis absorption of synthesized peptides. Absorption spectra were scanned from 200 to 700 nm and the data was recorded at medium mode using a quartz cuvette of 10 mm path length.

4.2.5 Fluorescence Spectroscopy: The fluorescence of the synthesized protein samples was measured using Horiba Florimax-4 spectroflorimeter at room temperature in a quartz cuvette at 10 mm path length. Equimolar concentration (10 μM) was prepared by using Molar absorption coefficient of tryptophan 5690 $M^{-1}cm^{-1}$, tyrosine 1490 $M^{-1}cm^{-1}$, and AzAla 4212 $M^{-1}cm^{-1}$.

4.2.6 Circular Dichroism Spectroscopy (CD): CD spectra were recorded in a Jasco 700 CD spectropolarimeter (Jasco Labor- und Datentechnik GmbH, Groß-Umstadt, Germany). Scans were recorded at 25°C between 190 and 260 nm as an average of five scans and smoothed using the Savitzky-Golay algorithm to obtain the final data. Spectra were collected at 1.0 nm intervals, bandwidth of 1 nm, in a buffer containing 10 mM phosphate buffer. Spectra of all peptides were measured at concentrations of 100 μM and recorded in a 1 mm quartz cuvette. CD spectra were presented as a plot of mean residue ellipticities.

4.2.7 Fourier Transform Infrared Spectroscopy: Peptide samples were cast on potassium bromide pellets and FT-IR spectra were recorded on a Micro FTIR-200 (Jasco Co., Japan) equipped with an MCT detector at 4 cm^{-1} resolutions between 4000 cm^{-1} to 400 cm^{-1}. The 16 scan data were collected, and processed using spectral manager software (Jasco Co., Tokyo, Japan).

4.2.8 Differential Scanning Calorimetry (DSC): DSC scans were carried out using Netzsch (Model: STA449F3A00 DSC/TGA) instrument. Peptides were dissolved in deionized water with a concentration 1mg/mL. The same solution but without the protein was used in the reference cell. Both the sample and reference were scanned from room temperature to 200°C at a scan rate of 1 K/min.

4.3 Results and Discussion

A series of four new 'mini-proteins' have been synthesized by solid phase peptide synthesis (Table 4.1) and characterized by HPLC (Figure 4.2) and MALDI-TOF (Figure 4.3). Structure and stability was examined by calorimetric methods to evaluate its characteristics to be qualified as a self-folding fluorescent mini protein. To facilitate the visible range fluorescence of the protein, we designed and synthesized three sequences, incorporating an unnatural fluorophore that has an emission wavelength in the visible region of the EM spectrum. Trp-cage and AzAla substituted variant of Trp-cage is used as a control for objective analysis. The designs are implemented in three steps.

Table 4.1. Details of the designed proteins

S.No.	Protein Code	Amino acid Sequence	Observed molecular mass (Da)	Expected molecular mass (Da)
1	VG01	ELsKETaLKKsFkFlVlIiLWnNtvDaIhI	3489	3484.1
2	BP01	ELsKETaLKKsFkFlVlIiZWnNtvDaIhI	3574	3568.2
3	BP02	ELsKETaLKKsFkFlVlIiLZnNtvDaIhI	3498.2	3495.2
4	Trp-cage	NLYIQWLKDGGPSSGRPPPS	2169.3	2168.4
5	BP03	NLYIQZLKDGGPSSGRPPPS	2179.5	2179.4

(Amino acids in large fonts are L- amino acids, and small fonts are D- amino acids. Z indicates AzAla)

First, the amino acids were folded, by an already established Simulated Annealing Molecular Dynamics procedure (AR-SAMD).[284,269] At high temperature, polypeptide chain can switch from L to D (or otherwise), and this is achieved by modifying the force function governing the improper dihedral angle in GROMOS force field. As the folds evolve in the prescribed design space, they were assessed and scored on the basis of their potential utility to be sequence engineered as functional foldamers, involving an automated inverse design scheme. The collection of 30-mer polyleucine folds generated as a result of AR-SAMD were subjected to Molecular Dynamics Simulation at 298 K in water. By doing so, we intend to

evaluate the possibility of generating metastable folds that can further be sequence designed as 'artificial proteins'.

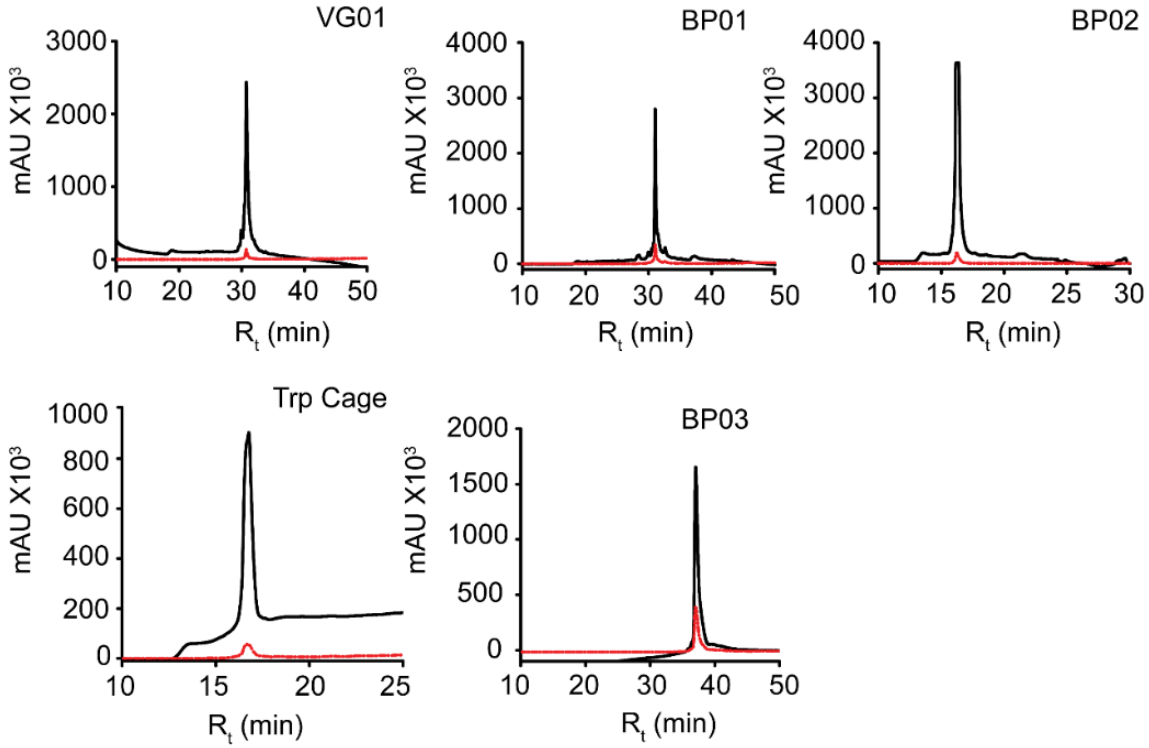

Figure 4.2 HPLC Chromatogram of synthesized peptides. Chromatogram was recorded at 342 nm (for BP01, BP02, and BP03), 280 nm (for Trp-cage and VG01), and 210 nm (for VG01, Trp-cage, BP01, BP02, and BP03).

This is achieved by performing sequence design of a few selected folds using an automated sequence design tool, IDeAS (Figure 4.4). Details of the computational procedure employed for the generation of an optimal sequence solution have been described elsewhere.[284,285] In the third step, we selectively mutate one or two core residues with a blue fluorescent unnatural amino acid. To facilitate the visible range emission, we designed four artificial fluorescent proteins, incorporating AzAla (denoted as Z). Structures of the designed peptides were evaluated for structural stability with a 20 ns Molecular Dynamics (MD) simulation under NVT conditions at 300K. The structures were first energy minimized in vacuum and later in water with the steepest descent algorithm. The structures were stable under the tested conditions

with stable root mean square deviation (RMSD) and radius of gyration distributions throughout the simulation (Figure 4.5).

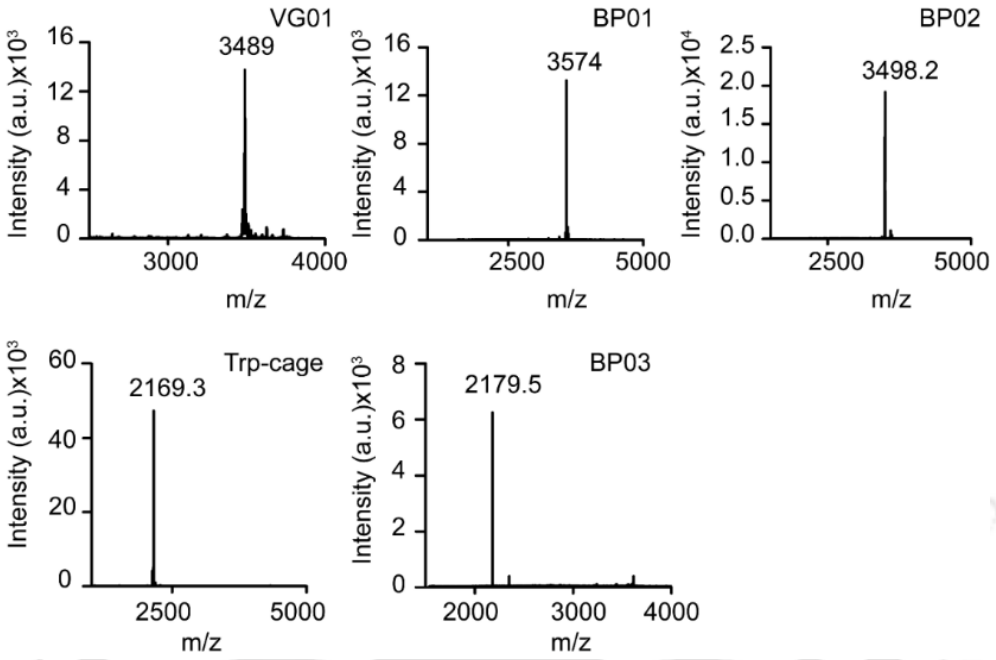

Figure 4.3 MALDI-TOF spectra of synthesized peptides. The observed molecular mass was found equivalent to the expected molecular mass.

The solvent exposure of fluorophore has been verified using Spectrofluorimeter. The earlier established de novo designed mini protein Trp-cage and its W6Z mutant was chosen as the control. The first sequence (VG01) was a *de novo* designed heterochiral fold evolved as a result of systematic stereochemical and sequence selection routines.

BP01 and BP02 are L20Z and W21Z mutants of VG01. BP03 is W to Z mutant of our control protein, Trp-cage. The dihedral angle distribution of all amino acids in the designed sequences, and C-alpha traces of foldamer BP02 are shown in Figure 4.6. The predicted secondary structure of the designed proteins was mainly extended-β and disordered structure which was confirmed by CD spectral analysis (Figure 4.6 D). UV-Vis absorption spectra were recorded to confirm the presence of AzAla in the designed proteins, showed the absorption peak of the proteins BP01, BP02, and BP03 at 280 and 342 nm while VG01 and Trp-cage at 280 nm (Figure 4.7). N-acetyl-L-tryptophanamide (NATA), a Trp analogue, has been used as

a reference for Trp containing proteins. At 280 nm excitation wavelength, the emission of NATA was at 356 nm which shows solvent exposed condition of Trp residue (Figure 4.8).[286]

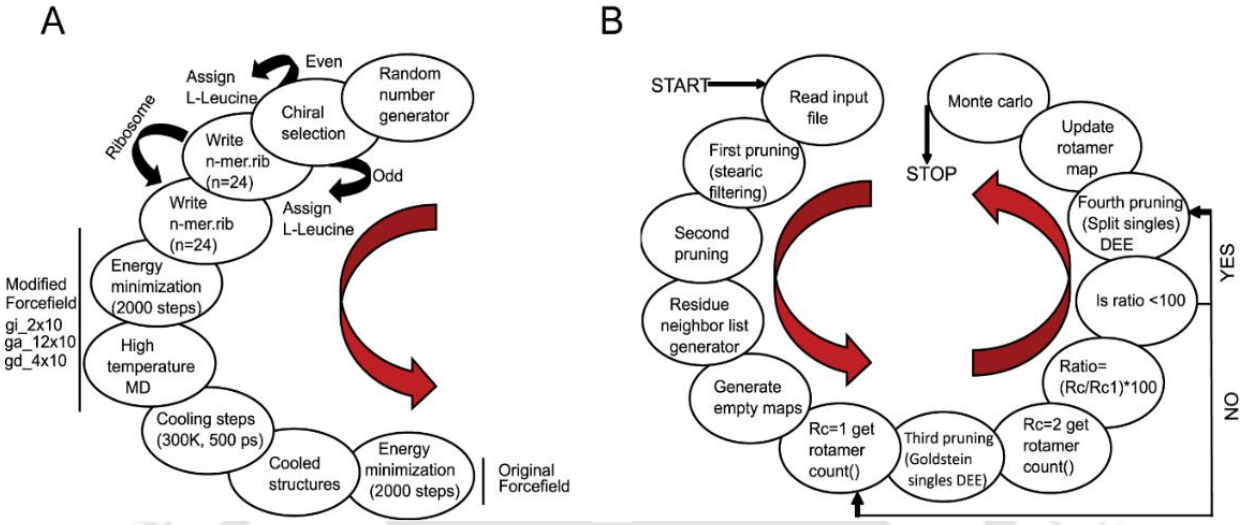

Figure 4.4. Schematic representation of: (A) Generation of folds by Automated Repetitive Simulated Annealing (AR-SAMD); and (B) Flowchart illustrating the sequence optimization steps involved in IDeAS program suite.

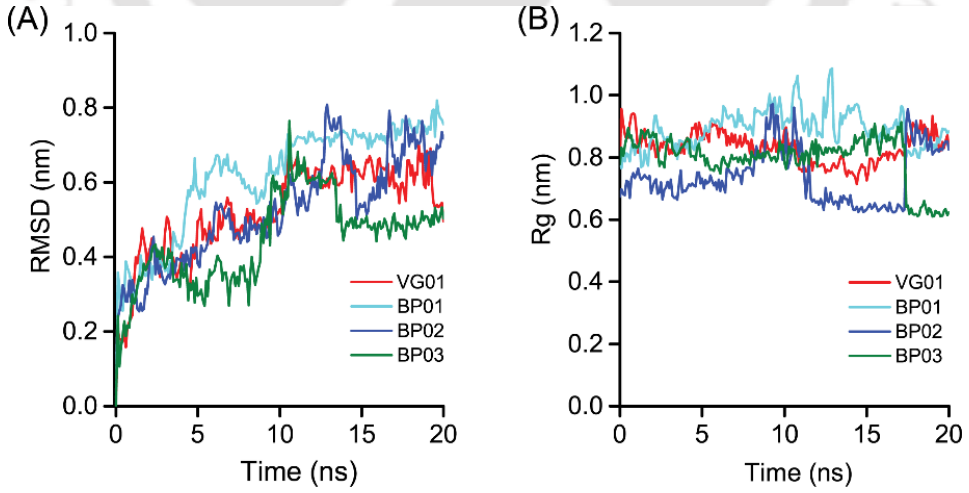

Figure 4.5. Root mean square deviation (RMSD) and Radius of gyration (R_g) of designed peptide sequences.

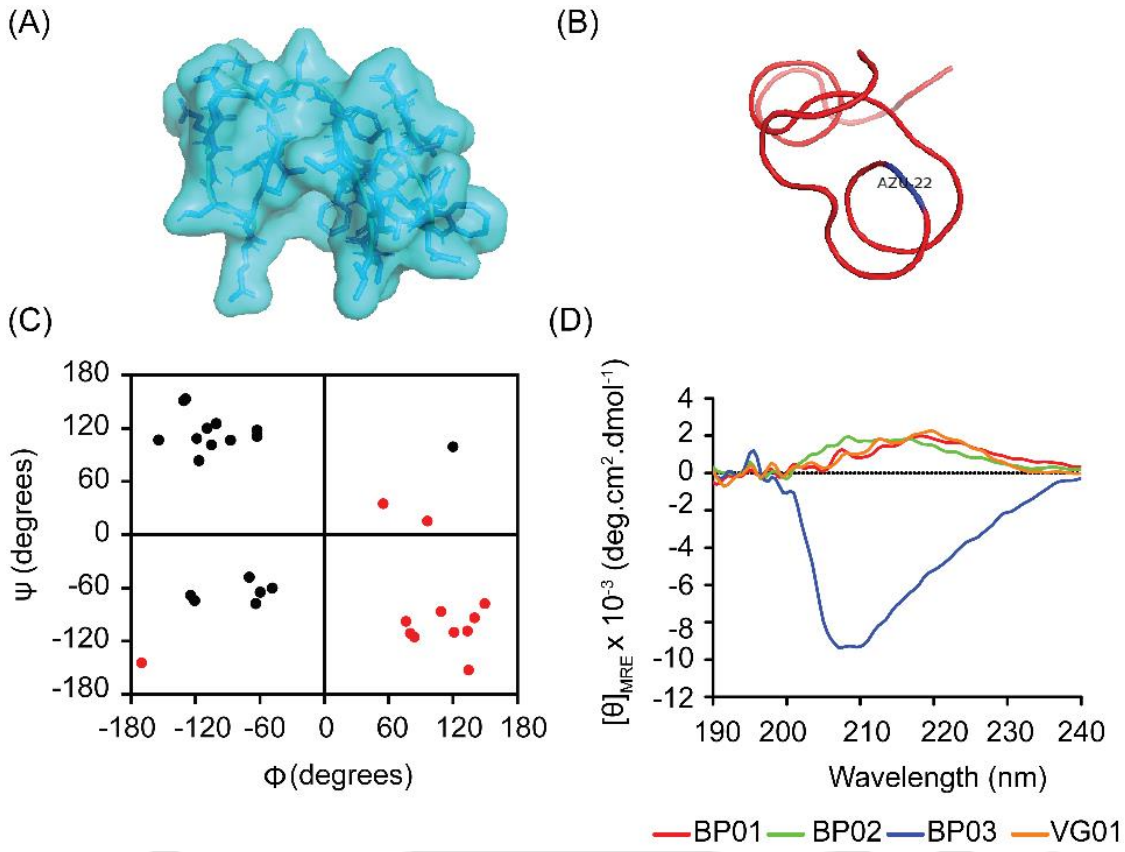

Figure 4.6. Representation of (A) Surface model, (B) C-alpha traces, and (C) Dihedral angles of protein foldamer BP02 where D- amino acids are shown in red circles and L- amino acids are shown in black circles. The representation in all four quadrants of Ramachandran map confirm the heterochiral nature of the designed protein. (D) CD spectra of the designed proteins indicating the disordered conformation of the designed proteins

The Trp side chain in NATA is more exposed to solvent compared to other synthesized proteins, Trp-cage and VG01. The relative low Trp fluorescence intensity indicates the inability of VG01 mini protein sequence to sustain a stable hydrophobic core under ambient conditions. AzAla containing peptides show emission at 363 and 382 nm, which is the characteristic emission wavelength of AzAla. At the excitation wavelength of 342 nm, only protein BP01, BP02, and BP03 show emission at 364 nm and 382 nm. Emission spectra of protein BP01, BP02, and BP03, were compared with that of N-acetyl azulenylalanine (Nazu). Nazu has the AzAla fluorophore almost fully exposed to solvent. This will confirm the formation of a well-

defined hydrophobic core, which is an important criterion for a stable functional foldamer. At the excitation of 342 nm, fluorescence intensity estimate of BP02 is significantly high, compared to Nazu. This observation indicates the burial of AzAla in the containing proteins is expected to have a much more prominent fluorescent peak compared to Nazu.

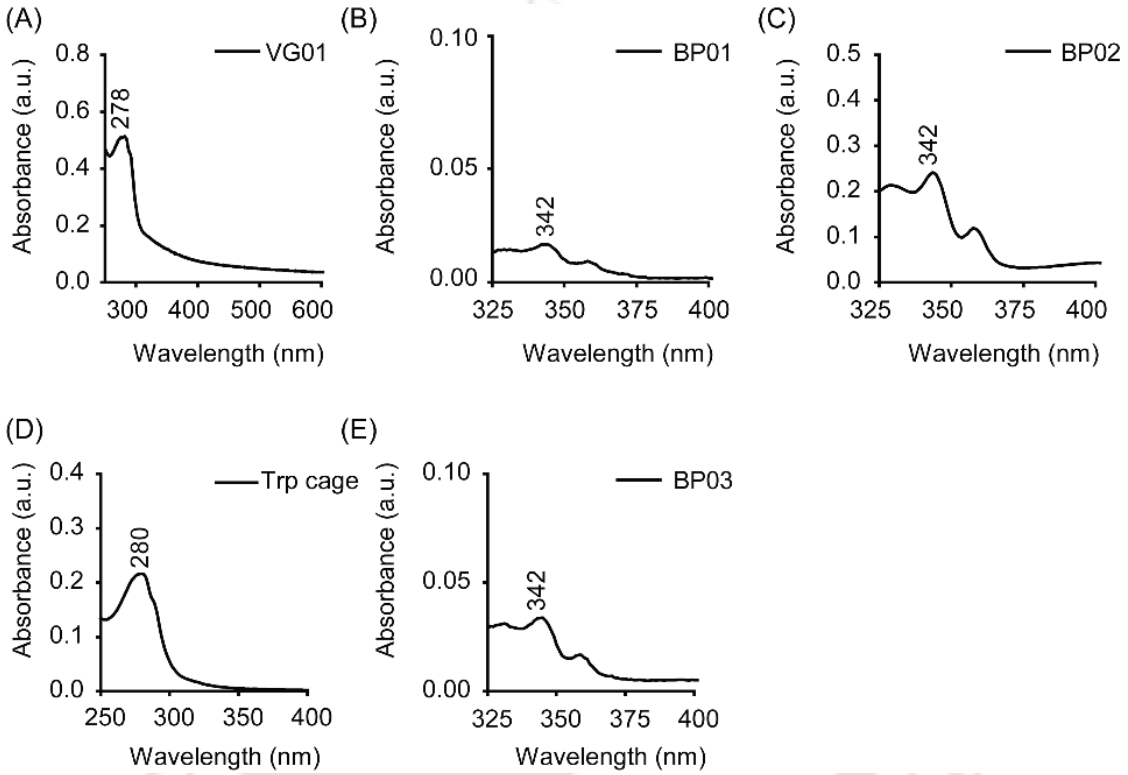

Figure 4.7. UV-vis absorption spectra of the synthesized peptides. The absorption peaks (A) VG01, and (D) Trp-cage showed absorption peak at 280 nm while of (B) BP01, (C) BP02, and (E) BP03 were observed at 342 nm.

However, BP01 and BP03 are not showing significant difference in fluorescence intensity compared to Nazu. The low intensity of proteins BP01 and BP03 suggests quenching of AzAla, due to the solvent. The excitation spectrum of AzAla containing peptides show two major absorption maxima at 280 and 342 nm, respectively, which can be used for excitation of the non-alternating aromatic ring system to yield emission at 382 nm.[280] AzAla, an unnatural amino acid containing azulene in its side-chain, shows a quite strong ^1L_a

absorption band centered at 320–380 nm (ε ~4200 cm^{-1} M^{-1})[287] and a weak ^1L_b absorbance at 600 nm (ε ~ 400 cm^{-1} M^{-1}). Excitation at this wavelength does not result in measurable fluorescence signal while excitation in the ^1L_a band yields an emission band at ~380 nm with a quantum yield comparable to Trp.[279] AzAla can be excited selectively at 342 nm to get the emission at 382 nm. Although the relative fluorescence intensity of AzAla when excited at 342 nm, is lower than that of tryptophan, this amino acid could represent an interesting fluorescence probe in peptides and proteins, as a potential blue-coloured tryptophan analog.[280]

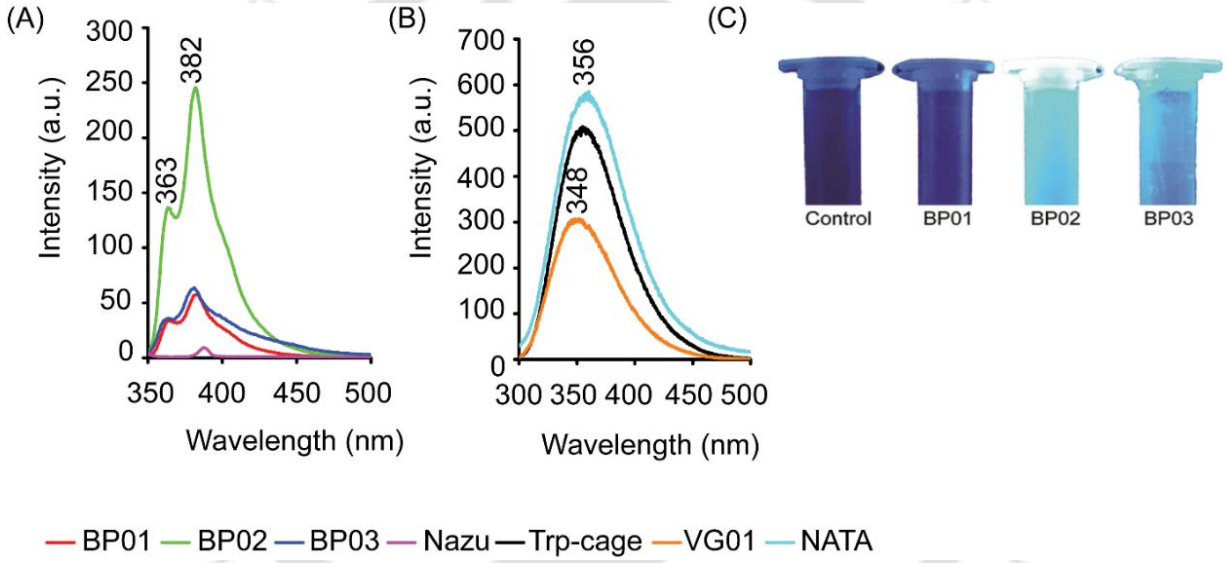

Figure 4.8. Fluorescence emission spectra of synthesized protein foldamers: (A) at an excitation wavelength of 342 nm, BP01 (red), BP02 (green), and BP03 (blue) showed emission at 363 and 382 nm; (B) at an excitation wavelength of 280 nm, NATA (cyan), Trp-cage (black), and VG01 (orange) showed emission at 356, 355, and 348 nm, respectively. (C) UV illumination of synthesized proteins. BP02 shows a more visible bright blue color compared to BP03.

The UV illumination of BP02, is showing visible bright blue colour (Figure 4.8C), compared to BP03, while the intensity of BP01 was significantly less. Empty microcentrifuge tube was taken as a control. BP02, thus qualifies to be a *de novo* designed hetero-chiral protein foldamer, pregnant with a fluorophore in a

well-defined hydrophobic core. The formation of a well-defined hydrophobic core facilitating spontaneous folding to the designed conformation may be indirectly reflected in the thermal stability of the designed proteins. This was characterized by Differential Scanning Calorimetry (DSC). The heat capacity curves obtained from DSC measurements show (Figure 4.9) several characteristic features. Starting from room temperature, the apparent protein heat capacity gradually increases until the onset of thermal unfolding, accompanied by a sharp peak in C_p corresponding to an endothermic unfolding transition. The peak at the transition gives the midpoint temperature (T_m), where the folded and the unfolded forms of the protein are at equilibrium (i.e., $\Delta G = 0$),[288] and the area under the transition gives the enthalpy of unfolding (ΔH_{unf}) at that temperature.[289] The Higher T_m value of proteins indicates higher thermal stability.[290] Under the experimental conditions, the thermally induced transition of proteins BP02 and BP03 occur at 66°C and 42°C, respectively. DSC thermogram of protein BP02 shows more thermal stability compared to BP03.

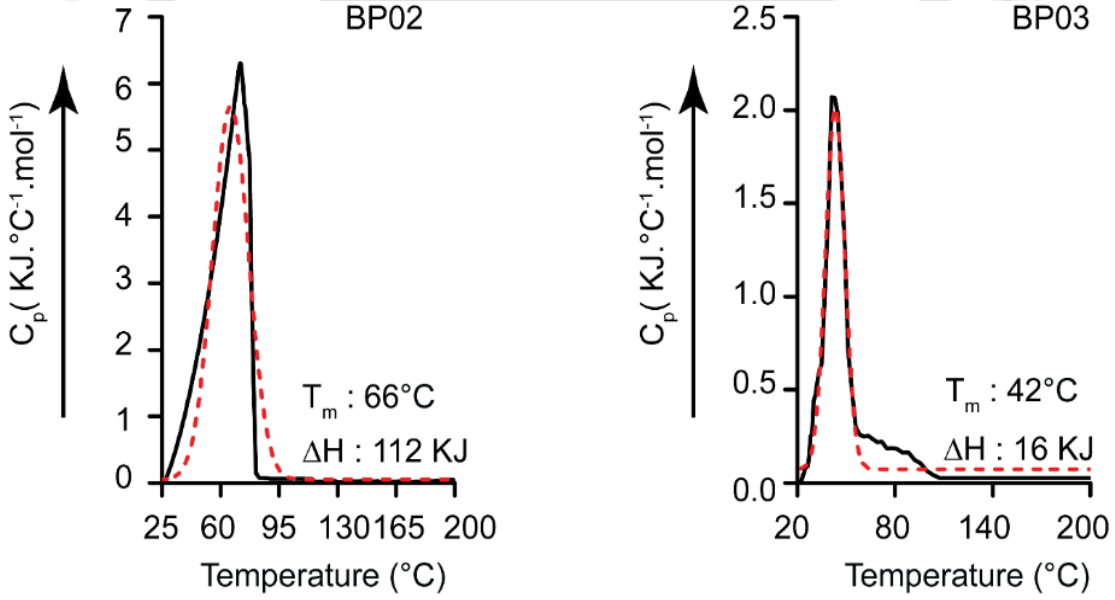

Figure 4.9. DSC thermogram of proteins (A) BP02, and (B) BP03. Tm value of protein BP02 (66°C) is greater than BP03 (42°C). Solid Black line represents experimental data while dashed red line represents curve fit (non-linear curve fit).

BP01 being completely non-fluorescent, was omitted from thermodynamic stability measurements. Secondary structures of the designed protein were analyzed by circular dichroism (CD) and FT-IR spectroscopy. The spectra of synthesized proteins in deionized water was further investigated using CD spectroscopy (Figure 4.6 D). CD spectra of Trp-cage show negative peaks at 208 nm and 223 nm, with a positive peak at 195 nm (spectrum not shown) majorly forms an α-helix as previously reported.[274,291] Similarly, BP03 (a mutant of Trp-cage) shows a negative peak at 208 nm and a positive peak at 195 nm, which constitutes majorly an α-helix. VG01 shows a positive peak at ~219 nm which might be due to the contribution of Trp to the far-UV CD spectra. Previous work by Chakrabartty *et al.* showed that it arises, when the aromatic group is fixed in a particular structure.[292] This spectral feature also has been observed in folded peptides containing well-ordered Trp side chain.[293]

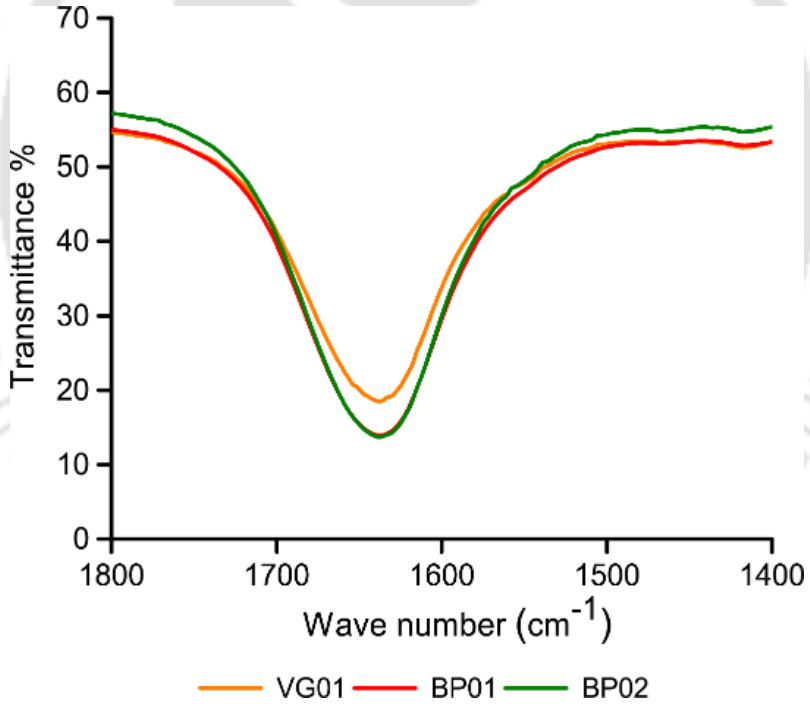

Figure 4.10. FT IR spectra of the synthesized proteins VG01 (orange), BP01 (red) and BP02 (green). Spectra show fingerprint region at 1638 cm^{-1} which confirms β sheet content of the proteins.

The far-UV CD spectrum of VG01, BP01, and BP02 is not suggestive of any specific conformation, because analysis of the CD spectra of heterochiral proteins cannot be compared using the observations usually deduced from Poly L- homochiral proteins, and therefore interpreted with caution.

The secondary structure of proteins was also verified by FT-IR (Figure 4.10). Information on the secondary structure of proteins can be derived from the analysis of a strong amide-I band. Amide-I band arises predominantly from C=O stretching vibrations of the amide group,[294] shows absorption in the region 1600-1700 cm.$^{-1}$Amide I bands in the spectral range 1620 cm^{-1} and 1640 cm^{-1} is attributed to the β-sheet structure.[295] The C=O stretching frequencies of proteins VG01, BP01 and BP02 is similar to β structures although it cannot be confirmed by standard comparisons, because of the heterochiral stereochemical sequence of the polypeptide foldamer.[296]

4.4 Conclusions and Future Possibilities

In this study, we have shown the possibility of the designed heterotactic protein sequence, with an unnatural amino acid, AzAla, as a minimal fluorescent protein. Using UV-Vis and fluorescence spectroscopy, we have shown that the designed protein has blue fluorescence. On comparing fluorescence intensity of Nazu with other proteins, at the excitation wavelength of 342 nm, we found that the protein BP02 has maximum intensity, indicating that AzAla is buried inside a stable core, excluding solvent. The secondary structure reveals the presence of extended-β and disordered structures. The DSC complement well with fluorescence experiments, indicating higher thermal stability of protein BP02. Our observations complement the primary objectives of our work in designing a hetero-chiral mini-protein. The design and experimental protocols employed in BP02 prototype construct may be helpful in the generation of future peptide based biomaterials beyond the limits of natural alphabets.

5

Quantum confinement in a Peptide Nanoassemblies

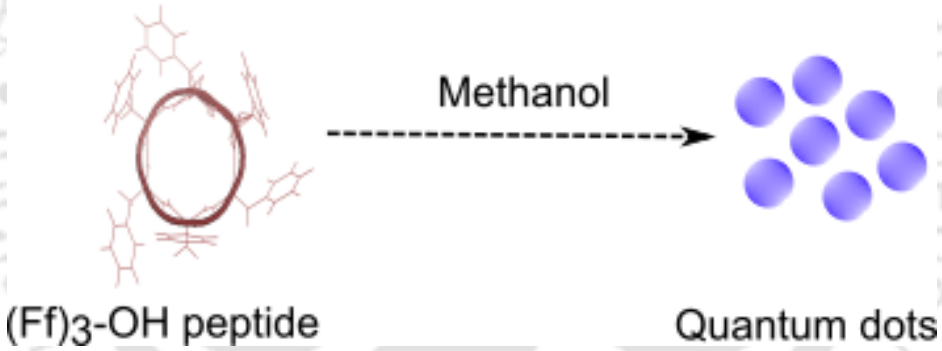

Spatial confinement of excitons in the nano-crystalline region of semiconducting nanostructures differ significantly from the optoelectronic properties exhibited by the bulk material. We report spike-like absorption observed in the UV spectrum of a phenylalanine hexamer peptide ($(Ff)_3$-OH) nano-assembly, which may be attributed to the spatial confinement of electrons to the dimension of quantum dots (QDs). Interdependency of the UV and PLE spectrum of the peptide confirms the existence of quantum confinement in $(Ff)_3$-OH nano-assemblies.

5.1. Introduction

QDs are semiconductor nanocrystals exhibiting three-dimensional quantum confinement that lead to unique quantum sized effects in their electronic and optical properties.[297] QDs have electronic properties intermediate between discrete molecules and bulk materials.[298] QD demonstrates exceptional physical properties induced by electron-hole space confinement.[188] The phenomenon that constrains excitons in QDs is known as quantum confinement (QC). A key feature of QC is that, it occurs when a particle's diameter is too small and comparable to the wavelength of the electron.[299] Their electronic and optical properties deviate substantially from bulk materials.[300]

The QD research so far has mainly been conducted with inorganic materials.[301] Several studies have focused on the complex systems, comprising conventional inorganic QD, conjugated with organic molecules with several applications.[302] Organic polymers, being mechanically robust, lighter than inorganic materials and tunable in solution, offer ample opportunities to develop new electronic devices.[303] Peptides have been emerged as an ideal molecule for organic electronics due to their intrinsic ability to form a spectrum of ordered self-assembled supramolecular nanostructures.[304] In recent years, peptide conjugated QDs are studied for cellular imaging,[305] enhancement of cellular uptake,[306] and drug delivery.[307] Peptides engineered with different amino acids have served as ligands for producing water-soluble QDs.[308] Incorporating cell-penetrating peptides on QD surfaces has allowed the translocation of functionalized QDs into cells for intracellular imaging applications.[309]

The QC effect in peptide nanostructures leading to better optoelectronic and charge transport behaviour is well-demonstrated by Gazit and co-workers in self-assembling peptide semiconductors based on diphenylalanine nanotubes.[310] The size of peptide QDs is usually governed by the specific amino acids. Therefore, a large number of naturally occurring and unnatural amino acids could be used in different combinations. It offers the possibility to tweak the size and properties of peptide QDs. Amdursky et al. have shown that peptides of phenylalanine and tryptophan form QDs with different optical and electronic properties from the diphenylalanine analogues.[19]

The elementary building blocks in peptide QDs are entirely different in comparison to inorganic systems.[16,19] Studies demonstrate that aromatic peptide molecules such as diphenylalanine (FF) with the same building block, can self-assemble into nanostructures with distinguished optical,[123] electrical,[311] and ferroelectric properties.[17] Gazit and co-workers have observed that FF peptide in methanol, self-assemble into nano-crystalline structures having optical properties similar to QDs. They observed a very narrow photo-excitation peak in nano-crystalline assemblies. But at low-concentration, only a broad excitation peak was obtained suggesting that individual dipeptide molecules are not QDs.[19] Gazit and Rosenman's groups have also reported QC in peptide nanostructures,[312] and demonstrated that FF dipeptides can assemble to form quantum wells. The formed quantum wells structure exhibited strong blue luminescence.[123] Rosenman and co-workers have reported QDs, formed by the self-assembly of tertbutoxycarbonyl-Phe-Phe-OH (Boc-FF), an organic molecule.[188] Tao et al. have demonstrated the modulation of tryptophan based aromatic cyclo-dipeptides, self-assembling to form quantum confined structures with photoluminescent properties.[39]

Peptide QDs represent one of the simplest forms of the quantum dot, but they also offer distinct advantages over other types. They are made of natural amino acids, synthesized by plants and animals and can preclude adverse effects of nanomaterials on organisms and ecosystems. This is a distinct advantage compared to inorganic QDs, especially those made of heavy metals.[297] Due to the availability of a wide range of amino acids that have diverse properties, peptide QDs may have properties not yet observed in inorganic materials.

The success of diphenylalanine QDs prompted us to explore the possibility of extending the aromatic π-π interaction mediated diphenylalanine systems from a dimer to a hexamer. This extension is possible only by adopting an alternating L, D (LDLDLD stereochemistry) for the phenylalanine hexamer peptide (figure 1). Ghadiri and co-workers have already demonstrated that cyclic peptides based on alternating D- and L- amino acid residues assemble to form hollow nanotubes forming peptide-based supramolecular tubular structures.[121,313] Self-assembly of these nanotubes is a result of the stacking of cyclic peptide rings through backbone hydrogen bonding.[28] In this work, we have examined the absorption and photoluminescence of a hexamer peptide having alternate L- and D- phenylalanine (FfFfFf-OH, denoted as $(Ff)_3$-OH), self-assembled to form an organogel. From the optical properties, we were able to

characterize the formation of a quantum-confinement in nano-assembled organogels of $(Ff)_3$-OH molecules.

5.2 Experimental Procedure

5.2.1 Molecular Dynamics Simulations: Molecular Dynamics (MD) simulations were performed using GROMACS 5.0.4 package with a GROMOS96 force field (54a7 parameter set). Each peptide was placed in a dodecahedron box with a spacing of 1.0 Å from the edge of the box. A flexible SPC/E water model was used. The solvated system was neutralized to zero. Energy minimization was carried out using the steepest descent until a tolerance of 1000 KJ mol^{-1} nm^{-1} was reached. Periodic boundary conditions were deployed in all the systems. The energy minimized system was then equilibrated, followed by the production run for 50 ns at 300 K, with periodic boundary, at an integration time step of 2 fs. The entire system comprising of the peptide and the solvent were maintained at a constant temperature of 300 K using the modified Berendsen thermostat with a time constant of 0.1 ps. Pressure of 1 bar was maintained using isotropic pressure coupling with the Parrinello-Rahman barostat at a time constant of 2 ps. Electrostatics (Particle-mesh Ewald) and van der Waal cut-off were fixed at 1.2 nm. Bond lengths were constrained using LINCS algorithm. The MD trajectories for the 50 ns production run were analyzed using the GROMACS analysis toolkit. The analysis was carried out to determine the dihedral angles of the peptide backbone over the simulation time, using standard tools in GROMACS package.

5.2.2 Materials and Methods: Amino acids, solvents, trifluoroacetic acid, thioanisole, and 1,2-ethanedithiol were purchased from Sigma-Aldrich. Diethyl ether, methanol, m-cresol were purchased from Merck. Hexafluoroisopropanol (HFIP) was purchased from TCI chemicals. Ultrapure water was used, from a Millipore Milli-Q water purification system, with an electric resistance 18.2 MΩ.

5.2.3 Peptide synthesis and Characterization: Peptide was synthesized manually by solid-phase peptide synthesis method using Fmoc chemistry. HMPA resin was used for the synthesis. Peptide was cleaved using a cleavage cocktail comprising of trifluoroacetic acid, ethane dithiol, thioanisole and m-cresol in the ratio 20:1:2:2, and further precipitated in ice-cold diethyl ether. Purification was performed by Shimadzu Prominence Modular HPLC instrument with a reversed-phase C-18 column using water

and acetonitrile gradient (10–100%) containing 0.1% TFA. Synthesized peptides were further characterized by verifying mass using a Bruker, Autoflex Speed MALDI TOF/TOF spectrometer.

5.2.4 Organogel formation: Peptide stock solution was prepared in HFIP. For gelation, peptide was subsequently diluted in methanol to 8mg/mL concentration and kept undisturbed at room temperature. Self-supporting organogel was formed after 12 h.

5.2.5 Field Emission Scanning Electron Microscopy: The structural characterization of the organogel formed by $(Ff)_3$-OH peptide were performed using JSM-7610F Field-Emission Scanning Electron Microscope. Organogel was diluted 50 times with methanol before analysis and allowed to air-dry at room temperature.

5.2.6 Atomic Force Microscopy: For AFM analysis, peptide was diluted 50 times with methanol, drop-casted on glass slides and allowed to air-dry. AFM images were acquired in non-contact mode using silicon probe on an Asylum MFP-3D Origin atomic force microscope (Oxford Instruments).

5.2.7 Dynamic Light Scattering (DLS): The DLS was recorded on a Malvern Zetasizer Nano-ZS instrument for the $(Ff)_3$-OH peptide solution in methanol. Twenty measurements were recorded at 25°C in the 173° backscatter configuration. The size and the polydispersity index were determined using the inbuilt software.

5.2.8 Circular Dichroism Spectroscopy (CD): CD spectra were recorded on a Jasco 700 CD spectropolarimeter (Jasco Labor-und Datentechnik GmbH, Groß-Umstadt, Germany). Peptide was first dissolved in HFIP and further diluted to 100 μM concentration in water. Scans were recorded at 25°C from 190 to 240 nm, and a bandwidth of 1.0 nm (average of eight scans).

5.2.9 Fourier Transform Infrared Spectroscopy (FT-IR): Peptide sample was casted on potassium bromide pellets. FT-IR spectra were recorded on a micro FTIR-200 (Jasco Co., Japan) at 4 cm^{-1} resolution between 4000 and 400 cm^{-1}. The scanned data were processed using Spectra Manager software (Jasco Co., Tokyo, Japan).

5.2.10 Rheology: The rheological property of the organogel was analyzed by using Physica MCR-301 (Anton Paar, Austria) rheometer. The storage modulus (G') and loss modulus (G") of the organogel were characterized. The rheological experiment was conducted at a temperature of 37°C in cone-plate geometry, with a cone angle of 1°.

5.2.11 Optical Absorption: Synthesized peptide $(Ff)_3$-OH was dissolved in HFIP to prepare the stock solution. Subsequently methanol was added to obtain the desired concentrations (0.05, 0.5, 1, 2, 4 mg/mL). All five concentrations were analyzed for optical absorption. Experiments were carried out in Agilent Carry 60 UV-Vis spectroscopy.

5.2.12 Photoluminescence Emission (PL) and Photoluminescence Excitation (PLE): The PL and PLE spectra of the different concentrations of the peptide were carried out in Jasco Spectroflourometer. The PL was recorded at excitation wavelengths of 252, 258 nm and PLE was recorded at emission wavelengths of 282, and 290 nm.

5.3 Results and Discussion

5.3.1 Modeling and simulation of $(Ff)_3$-OH peptide: The conformational possibilities of the phenylalanine residue (F) in a diphenylalanine (FF) peptide can be understood from Figure 5.1. A typical amino acid can broadly adopt any three φ, ψ basins in a Ramachandran diagram (Figure 5.1(B)); a β basin extending up to the polyproline II helix region (basin 1), a right-handed α-helical basin (basin 2) and a left-handed (LH) α-helical basin (basin 3). Two diphenylalanine (FF) monomeric units can in principle have nine geometric combinations, with each phenylalanine residue adopts any one of the three conformational basins (Figure 5.1(C)). For favorable quadrupole interactions, the distance between two benzene rings should be in the range 4.0 to 6.0 Å, with an equilibrium distance of 4.96 Å, where it has a maximum energetic advantage of 3–4 kcal/mol. This distance can be achieved only by a (13) combination of Ramachandran geometric basins for first and second phenylalanine residue, and interestingly this basin combination is observed in the crystal structure of FF nanotubes solved by Görbitz (CCDC 16340).[205] A detailed explanation of these geometrical calculations can be found in an earlier published work.[136]

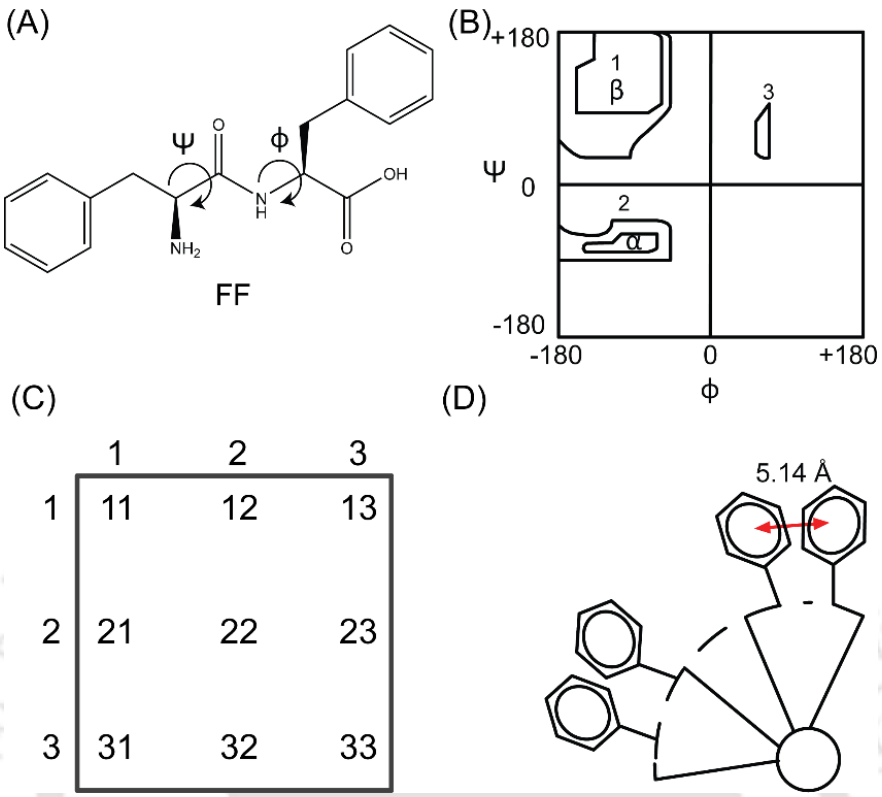

Figure. 5.1 (A) Chemical structure of FF Peptide. (B) Ramachandran map depicting allowed basins 1–3, and (C) their respective combinations for FF peptide. (D) Representative image of the distance between geometric centers of two benzene rings in FF peptide.

The QDs behaviour of FF molecule is primarily facilitated by this geometric combination. In an extended phenylalanine system, this distance can be achieved by alternating the phenylalanine residues in the two β basins corresponding to L and D chiral amino acids (Figure 5.1(C)). A typical (ϕ, ψ) combination of (-120, 120) for L-Phe and (120, -120) for D-Phe will have an average of 5.28 Å between the two CB atoms of consecutive phenylalanine residues. This combination is stabilized by favorable short range and long range electrostatic interactions of a typical polypeptide chain.[28] To verify the stability of alternating beta basin combinations of a typical extended phenylalanine system, we performed molecular dynamics simulations of $(Ff)_3$-OH peptide for 50 ns. The average FF backbone geometrical combination of the largest cluster, suggests (ϕ, ψ) backbone dihedral angles alternating between the β basins of L and D chiral amino acids, suggesting the stability of the designed structure with phenylalanine side-chains positioned

at geometrical distances within the limits of favorable quadrupole interactions, thus forming an extended π-π interaction network (Figure 5.2, 5.3 and 5.4, Table 5.1).

Molecular Dynamics simulations were repeated in methanol, to objectively compare the results. The RMSD and Rg of structures sampled (Figure 5.3) during the course of MD, is qualitatively similar to the results in water. Average structure of the largest cluster of both $(FF)_3$ (Poly L) and $(Ff)_3$ suggests high degree of structural similarity. This confirms the observations of our earlier investigations on the interplay of short range and long range electrostatic interactions in modulating peptide conformations (Table 5.1).[28] It confirms how, peptides with favourable long and short range interactions (as in the case of $(Ff)_3$) becomes insensitive to the stimulus (solvent in this case), while poly-L $(FF)_3$ peptide having countervailing short and long range interactions becomes sensitive to the stimulus. The significant decrease in the number of clusters sampled by $(Ff)_3$ during the simulation of both hexamer peptides further confirms this theory. The Gibbs free energy landscape of both simulations presents a distinct Global Minimal Energy Conformation (GMEC) for $(Ff)_3$, while energy landscape of $(FF)_3$ peptide is not showing any clear conformational directive (Appendix 1).

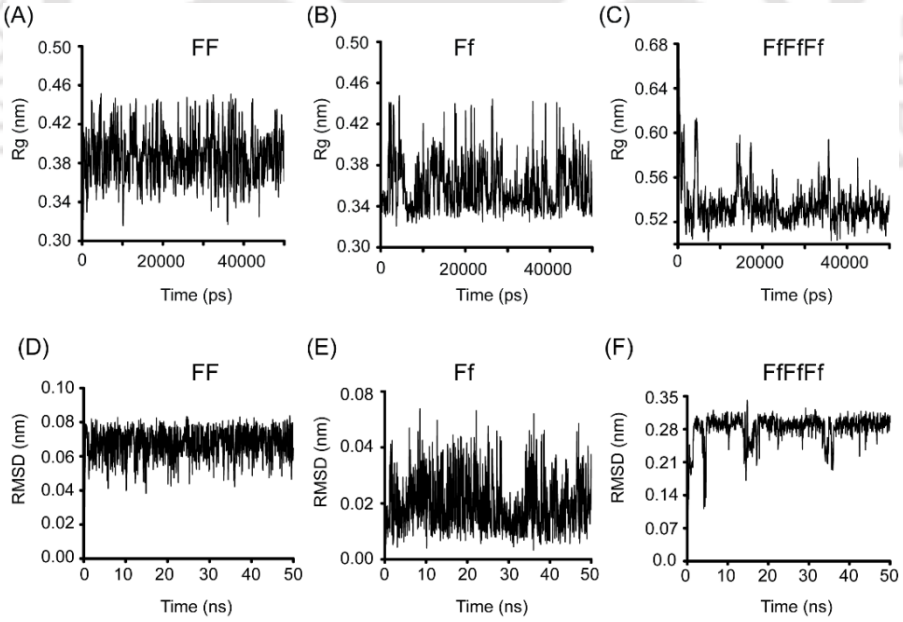

Figure 5.2. Radius of gyration suggesting the folded conformation of $(Ff)_3$-OH peptide. Root mean square deviation (RMSD) as a function of time is shown. Cluster analysis based on RMSD with respect to the starting structure, suggesting 85.8% of structures are populating the largest structure.

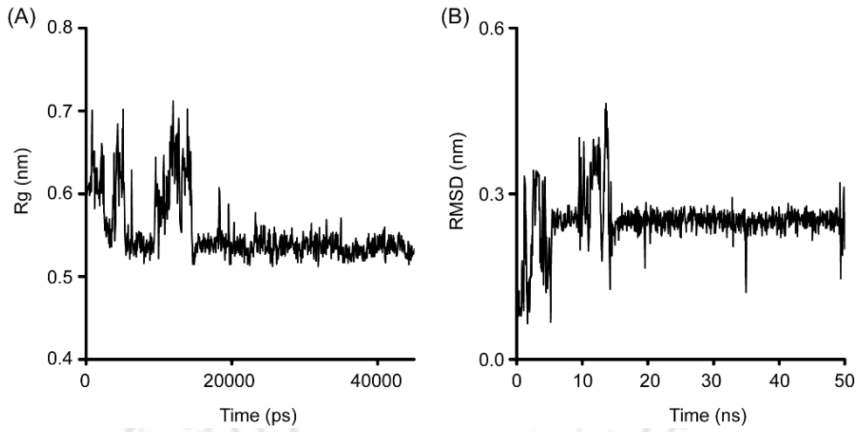

Figure 5.3. Radius of gyration (Rg) and RMSD of $(Ff)_3$-OH in methanol.

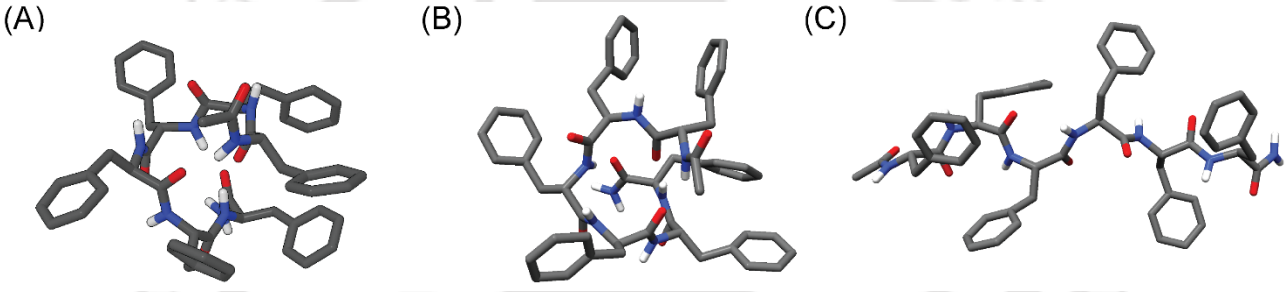

Figure 5.4 Average structure of the largest cluster in an RMSD based cluster analysis. (A) $(Ff)_3$-OH in water, (B) $(Ff)_3$-OH in methanol, and (C) $(FF)_3$-OH in methanol

Table 5.1. ϕ,ψ dihedral angle combinations of the largest cluster

	Water		Methanol	
Residue	**Φ**	**Ψ**	**Φ**	**Ψ**
Phe -1	-118.193	101.98	-144.936	125.8458
(D) Phe -2	87.36	-117.04	67.30651	-109.814
Phe -3	-114.339	84.69	-119.77	82.20351
(D) Phe -4	85.06	-99.69	81.62392	-97.2331
Phe -5	-121.07	74.13	-136.15	81.19471
(D) Phe -6	116.04	-132.154	110.0318	-112.387

5.3.2 Characterization of synthesized $(Ff)_3$-OH peptide organogel: HPLC and MALDI-TOF spectra of the synthesized peptide is shown in Figure 5.5. Secondary structure was analyzed by CD and FT-IR spectroscopy (Figure 5.6). CD spectra shows a positive peak at 195 nm, and negative peaks near 212 and 226 nm. It suggests that $(Ff)_3$-OH peptide majorly constitute the gramicidin β helical conformation. CD spectra of Gramicidin A was recorded for comparison which shows a positive peak at 195 nm, and two negative peaks at 210 and 230 nm. Gramicidin A is a syndiotactic peptide having typical $\Pi_{(L,D)}$ or gramicidin β helical conformation.

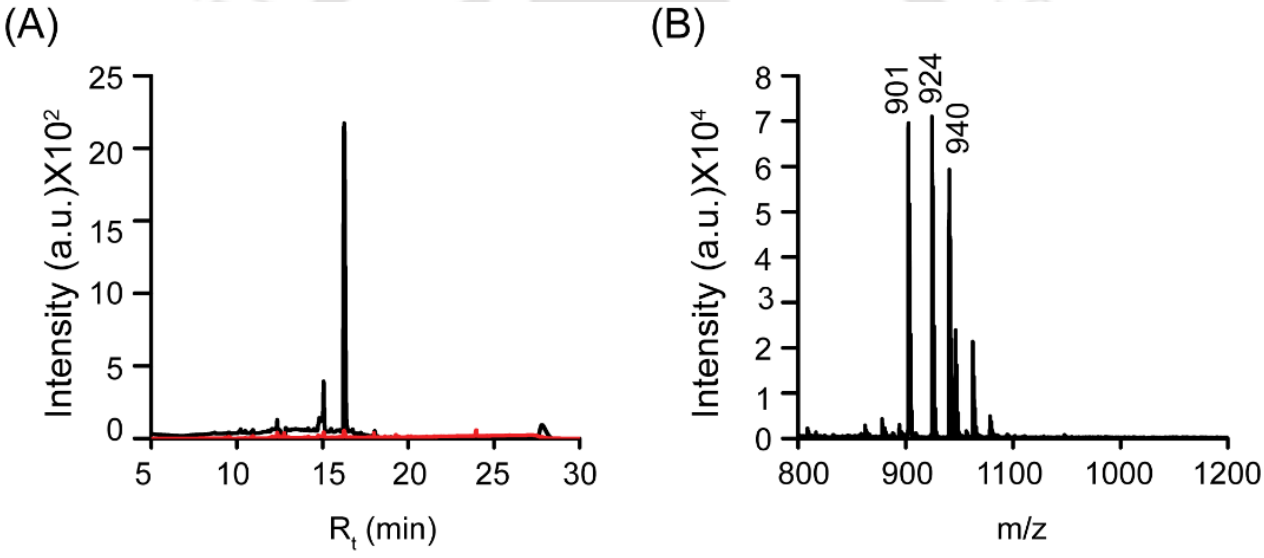

Figure 5.5 (A) HPLC chromatogram of the synthesized peptide. Chromatogram was recorded at 210 nm (black solid line) and 254 nm (red line). (B) MALDI-TOF spectra of synthesized peptide. Observed molecular mass (901 Da) was found equivalent to the expected molecular mass (901.05 Da). Na^+ (924 Da) and K^+ adducts (940 Da) were also observed.

Secondary structure of $(Ff)_3$-OH peptide was also verified by FT-IR spectroscopy. Information about the secondary structure of the peptide is derived from the analysis of strong amide-I band. The amide-I band

arises predominantly from the C=O stretching vibrations of the amide group and shows absorption in the region 1600-1700 cm^{-1}.

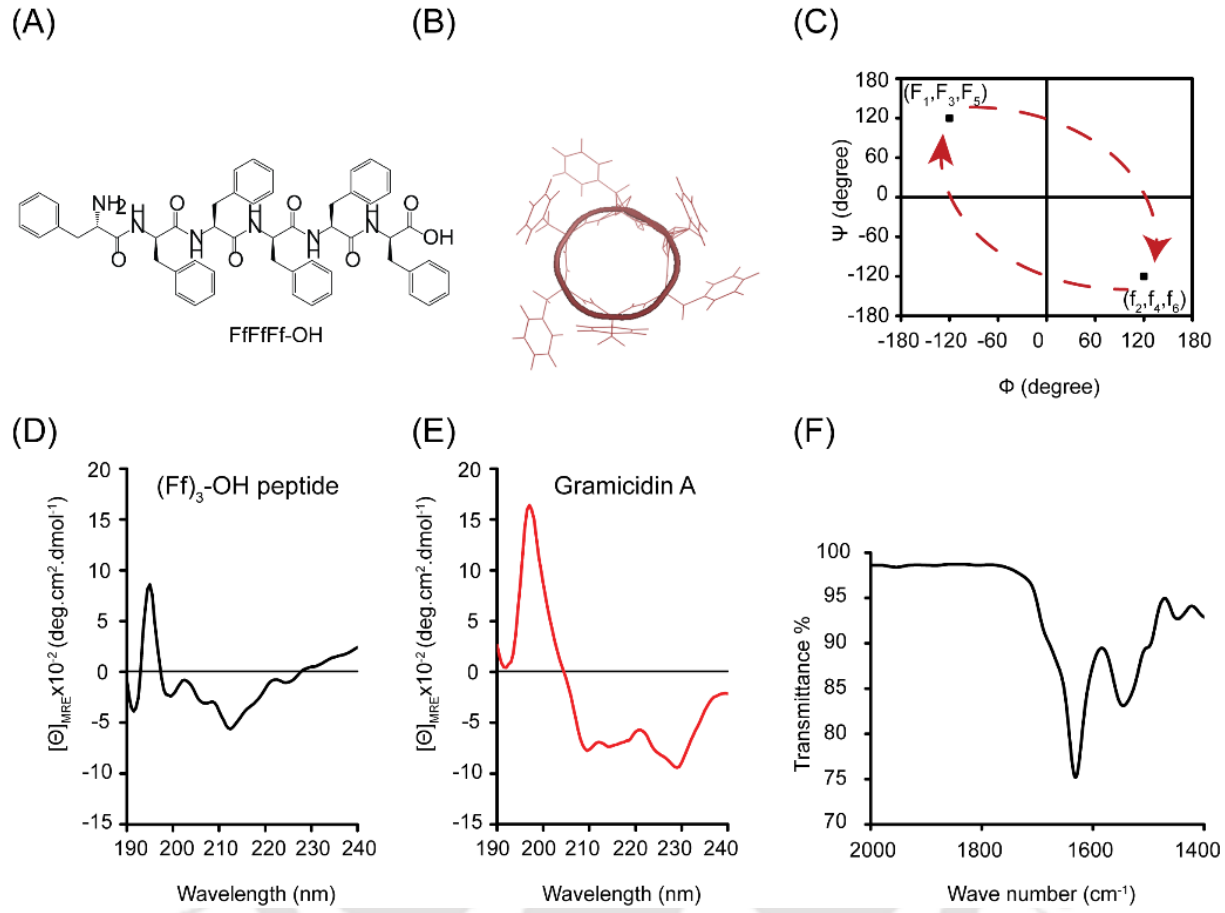

Figure 5.6. (A) Chemical structure of $(Ff)_3$-OH peptide. Capital letter denotes L- amino acid, and small letter denotes D-amino acid. (B) Designed structure of $(Ff)_3$-OH peptide. (C) Ramachandran plot of designed peptide, with geometrical basins alternating between L and D chiral regions, (D) CD spectra of $(Ff)_3$-OH peptide showing a positive peak at 195 nm, and negative peaks at 212 and 226 nm. (E) CD spectra of Gramicidin A showing a positive peak at 195 nm, and two negative peaks at 210 and 230 nm. CD results suggest that overall conformation of the $(Ff)_3$-OH peptide may be similar to that of Gramicidin A. (E) FT-IR spectrum of synthesized peptide confirming β structure

FT-IR spectra of $(Ff)_3$-OH peptide shows dominant peak position at 1632 cm^{-1} which is in the signature region of β structures.[314] Peak at 1548 cm^{-1} attributes to amide-II absorption band.[315] Spectroscopic

analysis indicates odd and even numbered phenylalanine residues alternating conformational basins of β structures of L and D chiral amino acids resulting in a tube like architecture similar to that of a Gramicidin helix, already reported by Ghadiri and co-workers. FESEM analysis of $(Ff)_3$-OH peptide showed formation of nanostructures that self-assemble to form nanofibers as reported earlier (figure 5.8).[136] AFM analysis showed nanospheres formation which self-assembled to form fibers (Figure 5.7 A). Further Self-assembly of nanospheres to form nanofibers is elaborated by FESEM analysis and shown in Figure 5.8. At higher concentration (8mg/mL), peptide self-assembled to form organogel (FESEM analysis, Figure 5.7 (C)), which was subsequently verified by rheology experiments (Figure 5.7 (E)).

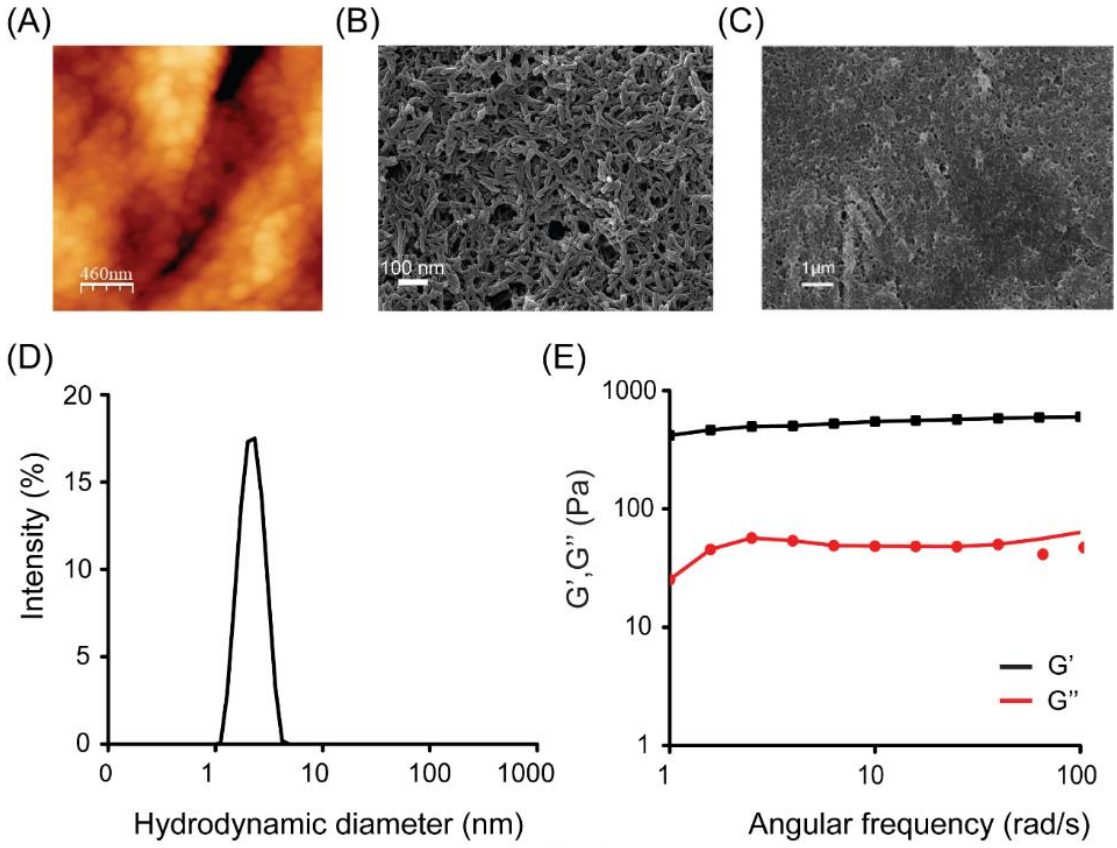

Figure 5.7. FESEM images of (A) $(Ff)_3$-OH peptide, (B) $(Ff)_3$-OH organogel. (C) DLS analysis, and (D) Rheology of $(Ff)_3$-OH organogel. Solid black line represents storage modulus, and red line represents loss modulus

The visco-elastic property of organogel was characterized by frequency sweep analysis. The storage modulus (G') and loss modulus (G") were measured with a fixed strain constant, at 1%. As shown in figure 5.7 (E), the storage modulus (G') and loss modulus (G") were observed in the range between 0.1 to 100 rad/s. Storage modulus of the synthesized peptide was found to be in the order of 10^2, which is similar to the previously reported peptide hydrogel.[316] The synthesized organogel exhibited higher G' (solid-state property), compared to G" (fluid-state (sol) (Figure 5.7 (E)), validating a semisolid-like physical state. DLS was performed to determine the particle size. The size distribution of the peptide is shown in Figure 5.7 (D), and single peak corresponding to the hydrodynamic diameters 2.16 nm was observed.

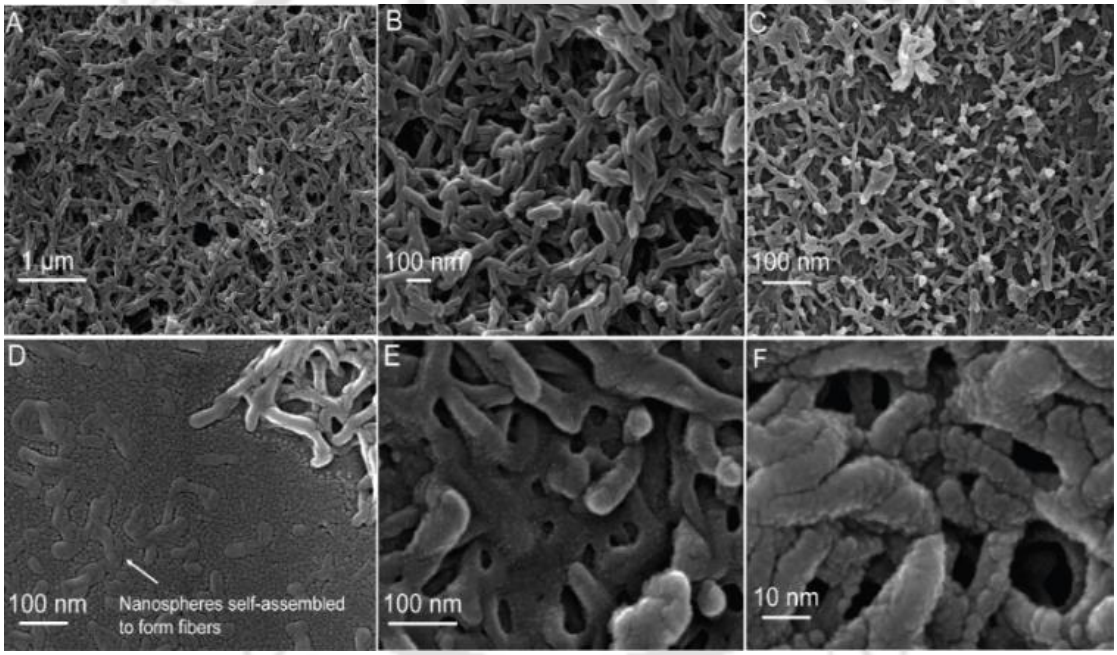

Figure 5.8. FESEM images of $(Ff)_3$-OH peptide at different magnification confirming nanofibers formation by self-assembly of nanospheres; (A) 15K (B) 30K (C) 35K (D) 75K (E) 200K (F) 300K

5.3.3 Validation of Quantum dots: The optical absorption (OA) spectra of the peptide, recorded for different $(Ff)_3$-OH concentrations (Figure 5.9 (E)), has multiple peaks in 240–300 nm range. The position of the individual peak and the spectral structure of the optical absorption curves do not change,

but the intensity of the peaks increases with increase in peptide concentration. In a semi-conductor, electron hole pairs can be created by irradiating the sample with electromagnetic radiations having photon energy larger than the energy gap of the semiconductor.[317] The number of electron hole pairs generated will be dependent on the number of absorbed photons, decided by the number of available states, given by the density of states function.[318] The quantum efficiency of this process will more close to unity, if the energy of light is more than the band gap energy. The recorded optical absorption spectra (Figure 5.9 (E)) have identical spike-like spectral signatures, supporting QD formation. The Photoluminescence emission (PL) and Photoluminescence excitation (PLE) spectra of the peptide at different concentrations are shown in Figure 5.9. At low concentrations, when no nanostructure is formed, the PLE spectrum is wide with multiple peaks. As the concentration increases, more basic building blocks self-assemble triggering epitaxial growth forming nanospheres (which self-assembled to form nanofibers), which results in sharp PL and PLE peaks. We observed that both OA and PLE spectra are identical and their peaks are located at 263 nm (4.71 eV), 258 nm (4.80 eV), 252 nm (4.91 eV), and 248 nm (4.99 eV). The experimental data shows that the peak at 263 nm has the highest intensity (Figure 5.9 (A), (B)). Intensity of other PLE peaks declines gradually. As explained, the intensity of the absorption peaks decreases with increase in band gap energy. Such absorption and PLE behavior is observed when the excited electron interacts with lattice vibrations.[188] The energy interval between the resulting maxima is equal to the phonon energy $\hbar\omega_{ph}$ = 0.08 – 0.11 eV, which actively interacts with the excitons.[188] By following the PLE spectrum, we can clearly observe the high intensity exciton peak at 263 nm, followed by distinct nanostructure formation. The formation of the narrow peak is a direct evidence to the crystallinity in the nanostructures.[319] The optical properties of QDs critically depend on their size. From the OA and PLE spectra, we can calculate the dimensions by using theoretical model of organic QD.[19, 188] The electronic structure of the exciton is

defined by

$$R = \pi r_B^0 \sqrt{\frac{\frac{m_0}{M}}{\frac{\mu}{m_0 \varepsilon_\infty^2} - \frac{E_{ex}^{QD}}{R_y}}} \qquad (1)$$

Where, R is the QD radius, and $r_B^0 = \frac{\hbar^2}{m_0 e^2}$ = 0.53 Å is the Bohr radius of hydrogen atom , and m_0 is the free electron mass, $R_y = \frac{m_0 e^4}{2\hbar^2}$ = 13.56 eV is the Rydberg constant, $\mu = \frac{m_e m_h}{(m_e + m_h)}$ is the reduced exciton

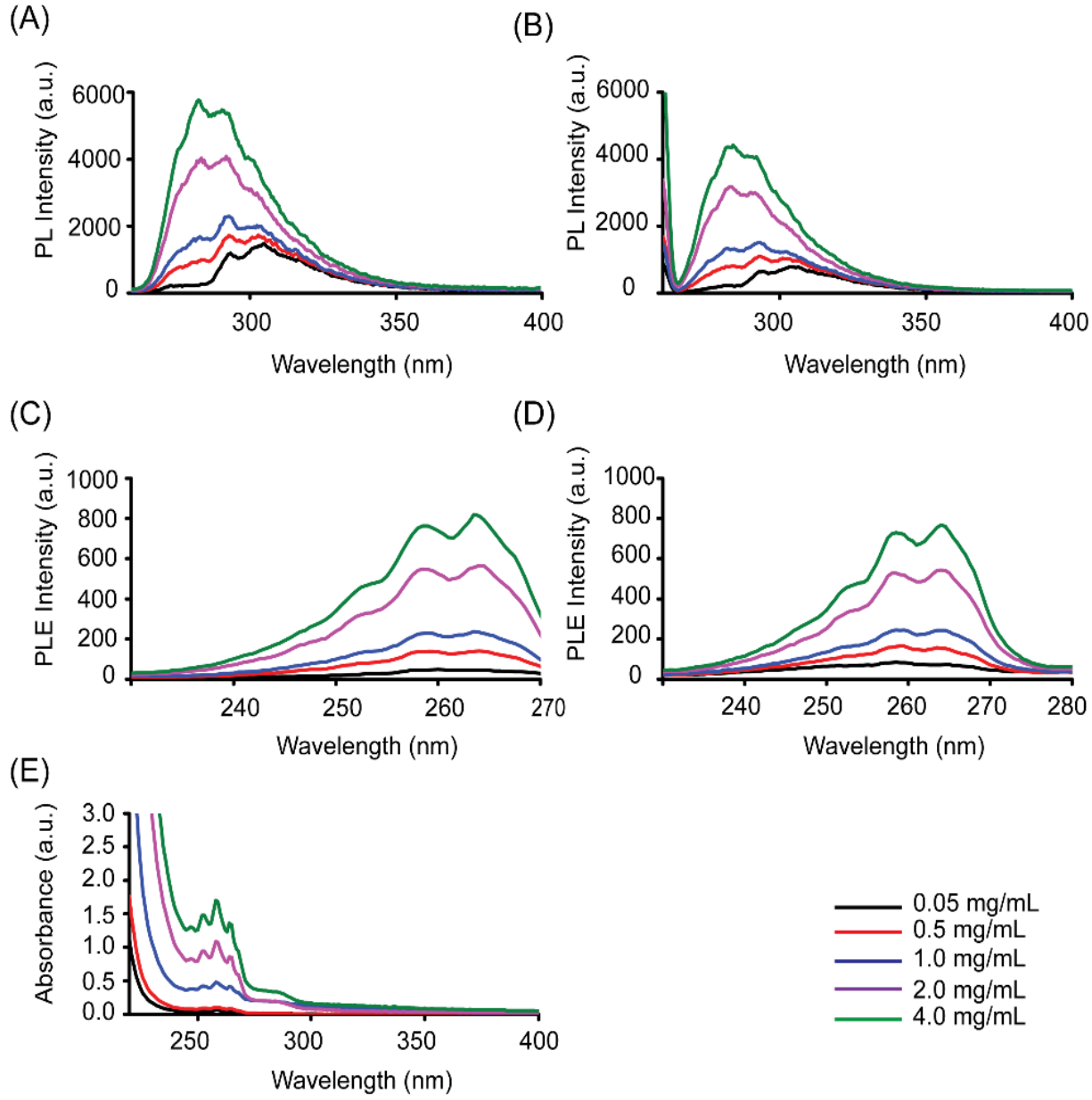

Figure 5.9. PL spectra of $(Ff)_3$-OH peptide at the excitation wavelengths (a) 252 nm and (b) 258 nm. PLE spectra of the peptide at emission wavelengths (c) 282 nm and (d) 290 nm. (e) Optical absorption spectra at different concentrations.

mass, m_e and m_h are the effective mass of electron and hole, $M = (m_e + m_h)$ is the translational mass of exciton, ε_∞ is the high frequency dielectric constant of the QD, and E_{ex}^{QD} is the exciton binding energy.

Due to the lack of known electronic parameters of the $(Ff)_3$-OH building blocks, we have used the refractive index of the similar benzene crystal, with n = 1.5,[320] for calculating ε_∞. This defines $\varepsilon_\infty = n^2 = 2.253$.

In the case of QD, the main peak or high-intensity peak in PLE represents a phononless excitation of the electron in excitons. The other less intensity peaks, is reported as the interaction of the excited electron with the lattice vibrations (or phonons).[321] Thus, other peaks are a result of phonon replicas. Larger the energy interval, less will be the intensity of the peaks and the energy gap gives the phonon energy $\hbar\omega_{ph}$. The peak position where the continuous absorption starts (rises) gives the energy for breaking of binding exciton state, $\hbar\omega_{ion}$. The energy difference between $\hbar\omega_{ion}$ and the phononless band $\hbar\omega_g^0$ gives the exciton binding energy E_{ex}^{QD}:

$$\hbar\omega_{ion} = 5.060\ eV\ (245\ nm)$$

$$\hbar\omega_g^0 = 4.714\ eV\ (263\ nm)$$

$$E_{ex}^{QD} = 5.060 - 4.714 = 0.346\ eV$$

The effective masses of electrons and holes are almost equal and close to $0.5m_0$ [322]. Consequently, $\mu = 1/2m_e = 0.25m_0$, and $M = m_0$. The radius of QD can be estimated by using equation (1) and estimated as R = 1.07 nm. This value seems reasonable and consistent with QD sizes found by other methods in different materials.[323]

5.4. Calculation of Quantum dot radius: The energy difference between $\hbar\omega_{ion}$ and the phononless band $\hbar_g^0$ gives the excitation binding energy E_{ex}^{QD}.

$$h\omega_g^0 = 4.714\ \text{eV}\ (263\ \text{nm}) \qquad (2)$$

$$E_{ex}^{QD} = \hbar\omega_{ion} - \hbar\omega_g^0$$

$$E_{ex}^{QD} = 5.060 - 4.714 = 0.346\ eV$$

$$\hbar\omega_{ion} = 5.060\ \text{eV}\ (245\ nm)$$

Then radius of the QD can be calculated by using formula

$$R = \pi r_B^0 \sqrt{\frac{\frac{m_0}{M}}{\frac{\mu}{m_0\varepsilon_\infty^2} - \frac{E_{ex}^{QD}}{R_y}}}$$

Where, $r_B^0 = \frac{\hbar^2}{m_0 e^2}$ = 0.53 Å is the Bohr radius of hydrogen atom, and m_0 is the free electron mass

$R_y = \frac{m_0 e^4}{2\hbar^2}$ = 13.56 eV is the Rydberg constant,

$\mu = \frac{m_e m_h}{(m_e + m_h)}$ is the reduced exciton mass, m_e and m_h are the effective mass of electron and hole,

$M = (m_e + m_h)$ is the translational mass of exciton,

ε_∞ is the high frequency dielectric constant of the QD

We have used the refractive index of the similar benzene crystal, with n = 1.5,[320] for calculating ε_∞. This defines $\varepsilon_\infty = n^2 = 2.253$

$$m_e = \frac{m_0}{2}\ and\ \mu = \frac{m_e}{2}$$

So,

$$\mu = \frac{0.5\ m_0}{2} = 0.25 m_0$$

Replacing these values in the equation (1),

$$R = \pi(0.53)\sqrt{\frac{1}{\frac{0.25m_0}{m_0(2.253)^2} - \frac{0.346}{13.56}}}$$

R = 10.7 Å or 1.07 nm

5.5 Conclusions

A molecular self-assembly is an emerging tool in the synthesis of functional nanoscale structures. Among different self-assembling molecules, peptides are interesting building blocks for the construction of supramolecular assemblies. Amino acids, the basic building block of peptides, provide great diversity depending on their side-chain properties. The supramolecular assembly is governed by noncovalent interactions such as hydrophobic interactions, π- π stacking and van der Waals interactions. Naturally occurring peptides and proteins are generally made of amino acids of poly L chirality. In such polypeptides, conformational stability is not very significant. Therefore, proteins and polypeptides hops from one conformation to another, with small variations in temperature, pH or any such external stimulus. Unlike in poly L chiral isotactic polypeptide sequence, alternating L,D syndiotactic peptides have their short range and long range electrostatic interactions complementing each other, contributing to their overall stability.[28] This offers the much needed stability in retaining the designed backbone conformation, which facilitates the optimum geometric positioning of phenylalanine side-chains. $(Ff)_3$-OH is a classic example of syndiotactic polypeptide, folding to a helical architecture (gramicidin helix), facilitating an extended phenylalanine network forming quantum confinement. This further validates our earlier efforts in tuning the basic building block geometry, for the development of new nano-assembled materials.[136]

6

Ultrashort Antimicrobial Peptide Hydrogels

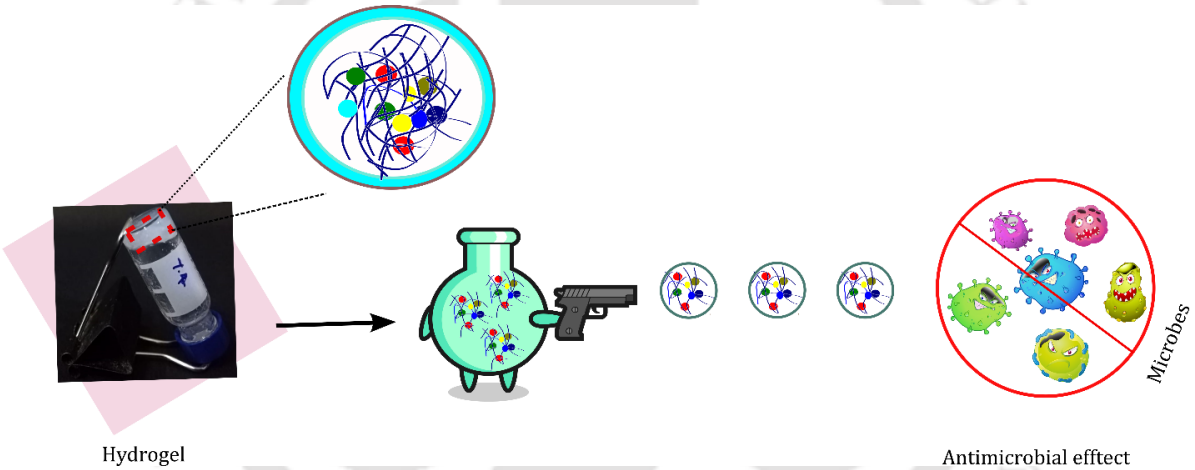

Molecular self-assembly of simple building blocks may lead to the fabrication of complex and ordered structures at nano-scale, thus, offering new functional supramolecular systems in biology and material science. We report three tripeptide hydrogels formed by the aromatic interactions between Fmoc and phenylalanine amino acid side chain. Hydrogelation properties were verified by rheology experiments. The hydrogels formed were further evaluated for their antimicrobial properties, with a long term goal of using them for the treatment of diabetic ulcers.

6.1 Introduction

Among different self-assembling molecules, peptides are an exciting option for the construction of supramolecular assemblies because amino acids, that constitute peptide molecules, provide great diversity depending on their side-chain properties.[324] These bioinspired nanostructures are attractive due to their biocompatibility, ability for molecular recognition, and ease of chemical modification. The supramolecular organization of peptide assemblies is modulated in molecular designs by exploiting the hydrogen-bonding properties of amino acid residues, their hydrophobicity,[325] and amino acid chirality.[326] Short peptides have some unique advantages such as good biocompatibility and low immunogenicity, while we consider them for designing functional biomaterials.[327] Recent seminal works suggests that short peptides bearing aromatic group at their N-termini have great propensity to self-assemble, forming stable hydrogels.[328] N-terminal modifications with Fluorenylmethyloxycarbonyl (Fmoc) group-containing amino acids, have also been investigated for their ability to form hydrogelators. These hydrogels have physical and mechanical properties, comparable to those formed from longer peptides and covalently cross-linked polymers.[329] Janmey and co-workers reported the formation of hydrogels from Fmoc-protected dipeptide, Fmoc-Leu-Asp,[166] and this study caught the attention of researchers in designing short peptides, that can potentially form stable hydrogels.

The use of hydrogels has gathered significant interest in developing drug delivery vectors for anti-infective applications. Hydrogels have been established as frequent biomaterials for the infection treatment and wound dressing.[330] Hydrogels are highly desirable for such applications because of their similarities to the host's extracellular matrix, providing improved biocompatibility, high water content, and fibrous architecture to support cell attachment and growth.[331] Antimicrobial peptides have been studied extensively as a new class of drugs. The self-assembling peptide hydrogels with inherent antimicrobial ability have recently come to the fore. Charge density of self-assembled peptides at the bacterial membrane surface and charge-to-surface area ratio are the important factors deciding optimal membrane interactions, enabling detergent-like effect, forming membranous pores in the bacteria leading to bacterial death.[332,333]

Single Fmoc-protected amino acids, Fmoc-F [22] and Fmoc-L,[334] have shown selective antibacterial activity against Gram-positive bacteria when mixed to form hydrogel co-assemblies. However, no activity was reported against Gram-negative bacteria *P. aeruginosa* and *E. coli.* Cell wall and membrane disruption were thought to be the primary mode of action for these peptides. However, Thakur and co-workers have reported the efficacy for Fmoc-F hydrogels against *S. aureus,* including methicillin-resistant strains.[22] They postulated that the antibacterial activity of Fmoc-F is due to the release of solubilized Fmoc-F fragments from the hydrogel. At higher micelle forming concentrations, Fmoc-F was shown to trigger osmotic and oxidative stress in Gram-positive bacteria to alter its membrane integrity**.**

Although limited, these studies have prompted us to work towards the synthesis of new Fmoc- based antimicrobial peptides. In this study we have synthesized three ultrashort peptides Fmoc-FFH, Fmoc-FHF, and Fmoc-HFF. We designed histidine (His) containing short peptides or amphiphilic histidine derivatives as basic building block. His shows cation-pi interactions and π-π interactions with aromatic amino acids such as phenylalanine. His containing peptides can be functionalized with aromatic moieties including 9-fluorenylmethyloxycarbonyl (Fmoc) group as N-terminal capping group,[326] or aromatic amino acids to promote self-assembly by exploiting the directional nature of π-π interactions along with hydrogen bonding and hydrophobicity. Furthermore, His containing peptide amphiphilic building blocks have been developed to acquire pH-sensitivity in the self-assembly of aromatic imidazole side chains.[335]

6.2 Experimental Procedures

6.2.1 Materials: All peptides were synthesized manually by Solid Phase Peptide synthesis (Fmoc chemistry). Fmoc protected amino acids were used for peptide synthesis. Nova PEG Rink amide Resin was purchased from Nova Biochem. Amino acids, piperidine, 2-(1*H*-benzotriazol-1-yl)-1,1,3,3-tetramethyluronium hexafluorophosphate (HBTU), Hydroxybenztriazole (HOBT), N, N-Diisopropylethylamine (DIPEA), trifluoro acetic acid and phenol were purchased from Sigma Aldrich. Triisopropyl silane (TIPS), and HFIP were purchased from TCI chemicals. Human serum was purchased from Sigma Aldrich.

6.2.2 Peptide synthesis and characterization: Peptides were synthesized by SPPS at the micromolar (μM) scale. The resin was soaked overnight before Fmoc removal using 20% piperidine. After

adjusting the pH to 7, the resin was incubated for 1h with activated amino acids along with DIPEA. N_2 gas was purged for 3-5 minutes, for complete mixing and removal of moisture content. For each amino acid attachment, coupling was repeated twice. The whole process was repeated until all the amino acids in the designed sequence were attached to the resin. Cleavage of the peptide from the resin was carried out using a de-protection reagent cocktail with, TFA, phenol, water, and TIPS in the ratio 88:5:5:2, and kept for 4 hours. After 4 hours, the deprotection mixture was allowed to precipitate in ice-cold diethyl ether by passing through glass wool. The peptides obtained after filtration was washed with diethyl ether. In each step, peptide was collected in ice-cold diethyl ether and incubated for 30 minutes followed by centrifugation at 3000 rpm for 5 minutes. The centrifuged peptide was washed with ether after vortexing, and incubated for 20 min at room temperature.

6.2.3 Purification and Characterization of peptides: The purity of peptide was checked by HPLC (Shimadzu, LC 20AD) and Mass Spectrometry (MALDI-TOF and ESI-MS). HPLC was performed by running a gradient of 10 % Acetonitrile in MQ water to 100 % Acetonitrile at a flow rate of 0.5 mL/min, using a C-18 reverse phase column. ESI (Electrospray ionization) mass spectrometer was used to characterize the mass of the synthesized peptide.

6.2.4 Preparation of peptide hydrogel: Peptide was completely dissolved in a minimum volume of HFIP, and then phosphate buffer (pH 7.4) was added to get 2% gel.

6.2.5 Morphological characterization of hydrogels: FESEM analysis was performed using a Zeiss Sigma-300 FE-SEM instrument. Hydrogel samples were loaded on a glass slide and air-dried. AFM analysis was performed in Asylum MFP-3D AFM instrument.

6.2.6 Fourier Transform Infrared Spectroscopy (FT-IR): FT-IR spectra were recorded in a Shimadzu IR Affinity-1S Fourier transform infrared spectrophotometer in the attenuated total reflection (ATR) mode. Peptide hydrogels were deposited (10 µl) on the crystal and allowed to air-dry. ATR-FTIR spectra were recorded at a resolution of 4 cm^{-1}, and an average of 20 scans were recorded for final spectra.

6.2.7 Thioflavin T fluorescence assay: ThT binding assay was performed by mixing 7.5 µL, 1 mM peptide to a solution of 10 µM ThT in 25 mM sodium phosphate buffer at pH 7.4. ThT fluorescence was

recorded at 482 nm (emission slit width = 5 nm) for 60 s at regular time intervals on a spectrofluorometer (Jasco FP 8500) at 25 °C, using a 1 cm path length quartz cuvette (Helma, Sigma-Aldrich). The excitation wavelength was set at 450 nm (slit width at 2.5 nm).

6.2.8 Characterization of hydrogels: Peptides were dissolved in a minimum volume of HFIP (20 mg in 20μL of HFIP) and phosphate buffer (25mM) was added to obtain different concentrations. Hydrogel formation was checked by tube inversion test. To optimize the pH for hydrogel formation, peptides were dissolved with different phosphate buffer pH ranging from 5.8 to 10. Hydrogel formation was validated by tube inversion test.

6.2.09 Rheological study of hydrogels: Rheological analysis of hydrogels was carried out using a rotational rheometer, Physica MCR301 (Anton Paar, Austria). All experiments were performed through a cone-plate geometry, 50 mm diameter cone (1^{o} angle) and parallel plate while the gap between cone and plate during experiments was kept at 0.1 mm. The temperature was maintained at 25^{o}C by a heating and cooling system, and a Peltier system. The amplitude sweep tests were carried out at constant frequency (1Hz) to determine the linear viscoelastic region (LVE) where gel-sol transition occurs and storage modulus crossover the loss modulus. The frequency sweep test was carried out in the range of angular frequency from 0.1 to 100 rad/s at constant strain corresponding to under LVE region. The self-healing property of peptide-based hydrogels was examined by a step-strain dependent rheological experiment. The strain was varied from low shear strain 0.1% to deforming strain 300%, followed by recovering at low shear strain. In each step, the strain was employed for 200s and step-strain cycle was repeated three times.

6.2.10 Serum stability Test: The serum stability assay of the designed peptides was performed using HPLC.[336] For this, 100 μl of peptides (1 mM concentration) were mixed with 100 μl of 100% human serum (sterile; Sigma) and incubated for 2 h at 37 °C at 150 rpm. After 2h, 100 μl of 0.6% trichloroacetic acid was added to precipitate serum proteins. The samples were kept at 4°C for 15 min, and then centrifuged at 13,000 rpm for 5 min. The supernatant was collected, and 20 μl was injected to the HPLC column (Shimadzu, LC 20 AD). Procedure was repeated for control experiments.

6.2.11 Antimicrobial Assay: Antimicrobial assay was performed with Gram-positive (*Staphylococcus aureus,* strain MTCC 96*)* and Gram-negative (*Pseudomonas aeruginosa,* strain PA01) bacteria.

Hydrogels for antibacterial assays were prepared in separate wells of 96-well tissue culture treated polystyrene plates. Hydrogels were allowed to incubate at 37°C for 2 hours. Following incubation, hydrogels were equilibrated with 200 µL Nutrient Broth media (N.B. media) overnight at 37°C. Before the assay, N.B. media was removed from the top of the hydrogels and replaced by 100 µL of fresh Nutrient broth. Bacterial stock solutions were quadrant streaked on a nutrient agar plate, followed by incubation at 37°C overnight. After sufficient colony growth, a single colony was transferred to a fresh broth and incubated overnight at 37°C. 10 µL of this culture was used to inoculate the working solution of cells to be used at their log phase. The optical density of this suspension was adjusted to O.D. = 0.1 a.u., resulting in 10^8 colony forming units (CFU/mL) bacterial stock solution. 100 µL of this culture was introduced to the surface of the hydrogels and serial dilutions (1:10) were performed across the plate and incubated for 24 hrs at 37°C. Readings were recorded at 600 nm, and each experiment was performed in triplicate with control.

6.2.12 Membrane disruption analysis by FESEM: Mid-log phase cells (10^8) were treated with peptide hydrogels and incubated at 37 °C. Incubated cells were centrifuged at 5000 x g for 5 minutes. Obtained pellets were treated with 2.5% glutaraldehyde and incubated at 4 °C for 3 hours. Subsequently, cells were centrifuged again at 5000 x g for 5 minutes. Bacterial cells were washed twice with phosphate buffer (pH 7.4), and loaded on a glass coverslip. The loaded samples were washed with deionized water and ethanol gradient ranging from 30–100%. Samples were air-dried, sputter-coated with platinum, and analysed using FESEM.

6.2.13 Determination of intracellular Reactive Oxygen Species (ROS) generation: The intracellular ROS generation was measured using 2,7-dichlorodihydrofluorescein diacetate (DCFH-2-DA) as described earlier.[22] Bacterial cells were grown to mid-log phase and 200 µL of bacterial cells (10^6 CFU/mL) were incubated with peptide hydrogels. Each samples were incubated with 5µL of DCFH-2-DA at 37°C for 3 h. After 3 h, fluorescence emission (λ_{em}) was recorded at 523 nm by exciting the samples at 503 nm (λ_{ex}). The increase in the fluorescence intensity was calculated by using the formula

$$\text{Fold increase} = \frac{(F - F_0)}{F_0}$$

Where F is the final fluorescence intensity, and F_0 is the initial fluorescence intensity.

6.2.14 Outer membrane permeabilization Assay: Outer membrane permeabilization assay was performed on Gram-negative bacteria *Pseudomonas aeruginosa,* by monitoring 1-N-phenylnaphthylamine (NPN) uptake. NPN is a non-polar probe that exhibits enhanced fluorescence in a hydrophobic environment.[337] Mid-log phase *Pseudomonas aeruginosa* cells were grown and washed twice with phosphate buffer (pH 7.4). Washed cells were diluted with phosphate buffer to a concentration of 10^8 CFU/mL, and incubated with peptide hydrogels. After 2 h of incubation, cells were transferred to cuvette and 8μL of NPN (final concentration 10 μM) was added. Fluorescence emission (λ_{em}) was recorded at 425 nm by exciting the samples at 356 nm (λ_{ex}) using spectrofluorometer (Jasco FP 8500). Polymyxin B (10 μg/mL), a known outer-membrane permeabilizing agent, was used as a positive control.[338]

6.3 Results and Discussion

6.3.1 Design, Synthesis and Characterization of peptides: In the designed sequences, the phenylalanine moiety is important for gelation because it facilitates the π stacking through the phenylalanine side-chain. Tripeptides Fmoc-FFH, Fmoc-FHF, and Fmoc-HFF were synthesized by solid phase peptide synthesis, purified by reverse phase HPLC and verified by mass spectrometry (MALDI-TOF) (Figure 6.1). The hierarchal self-assembly of the synthesized peptides was controlled by the hydrophobic sidechains, peptide backbones with different hydrogen-bonding abilities, and the hydrophilic imidazole sidechain of Histidine.

6.3.2 Secondary structure determination and ThT fluorescence assay: The secondary structure of the peptide was analyzed using FT-IR spectroscopy (Figure 6.2). The analysis of peptide IR spectra is based on correlations of characteristic amide I (amide C=O stretch, 1600-1700 cm^{-1}) band frequencies with structure. The FT-IR spectra of the synthesized peptide hydrogels show dominant peak position in 1632-1635 cm^{-1} range which is the signature region for β structures. The peak at 1548 cm^{-1} attributes to amide-II absorption band. The values found for the amide I band for these hydrogels are in the range of 1636–1641 cm^{-1} and for amide II, the values are in the range of 1539–1566 cm^{-1}. These frequency values

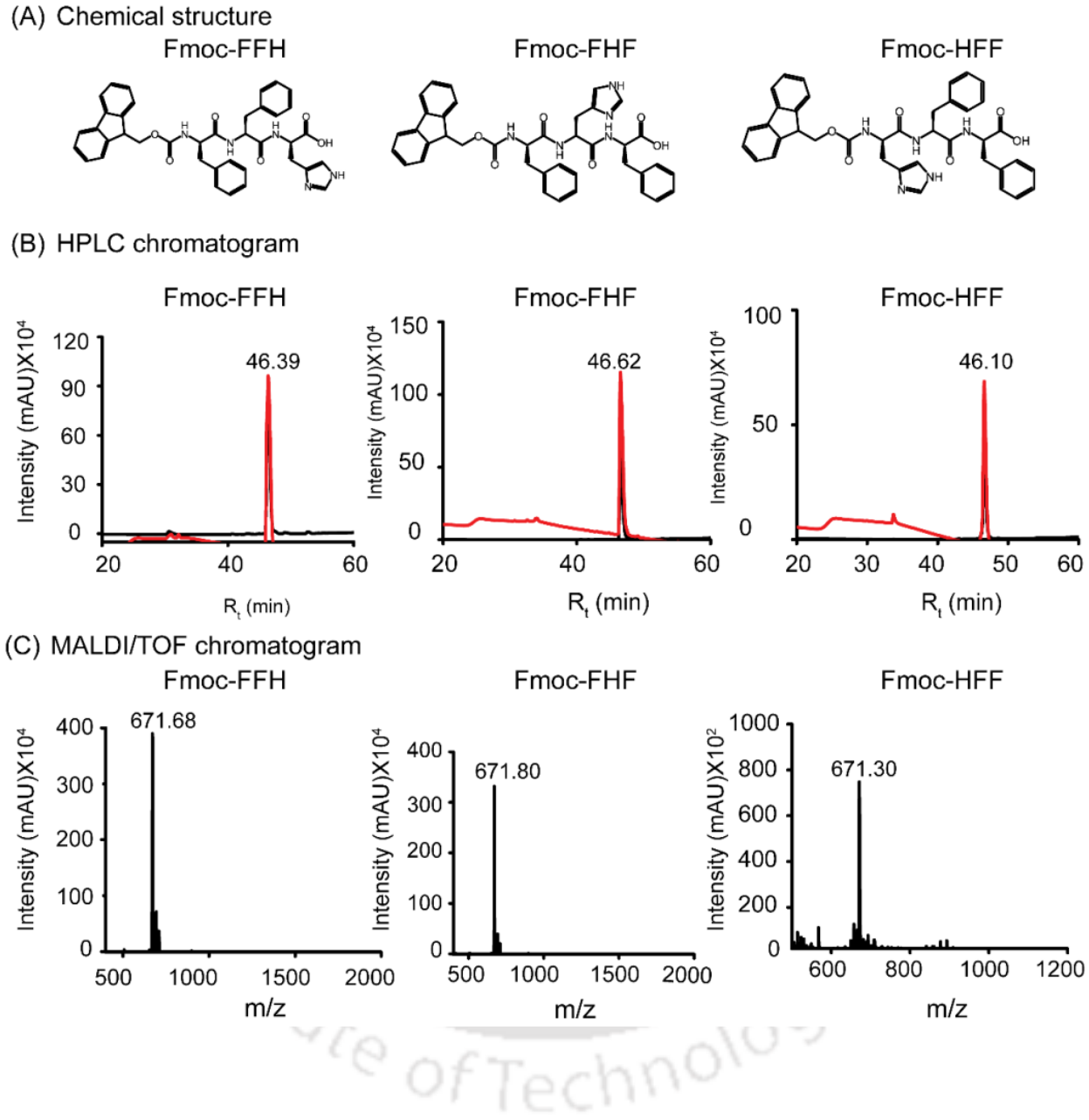

Figure 6.1. Characterization of synthesized peptides; (A) chemical structure of the designed sequences, (B) HPLC chromatogram of the synthesized peptide, and (C) Mass spectrum for primary characterization by verifying the mass of the synthesized peptide.

suggest an aggregation model similar to the β-sheet arrangement found in peptides.[339] Thioflavin T (ThT) assay was performed to determine the presence of β structures that can potentially form amyloid like fibers. Thioflavin T, a benzothiazole dye, binds to the hydrophobic grooves of the fibril's surface

composed of β-sheet. The free ThT molecules show weak fluorescence in aqueous solution. In the presence of fibrils, it intercalate between the grooves present on the solvent exposed side chains of the fibrils.[340] The mechanism of fluorescence enhancement after binding to fibrils is attributed to the immobilization of C-C bond connecting the benzothiazole and aniline ring after binding to the fibrils, resulting in enhanced fluorescence intensity.[341]

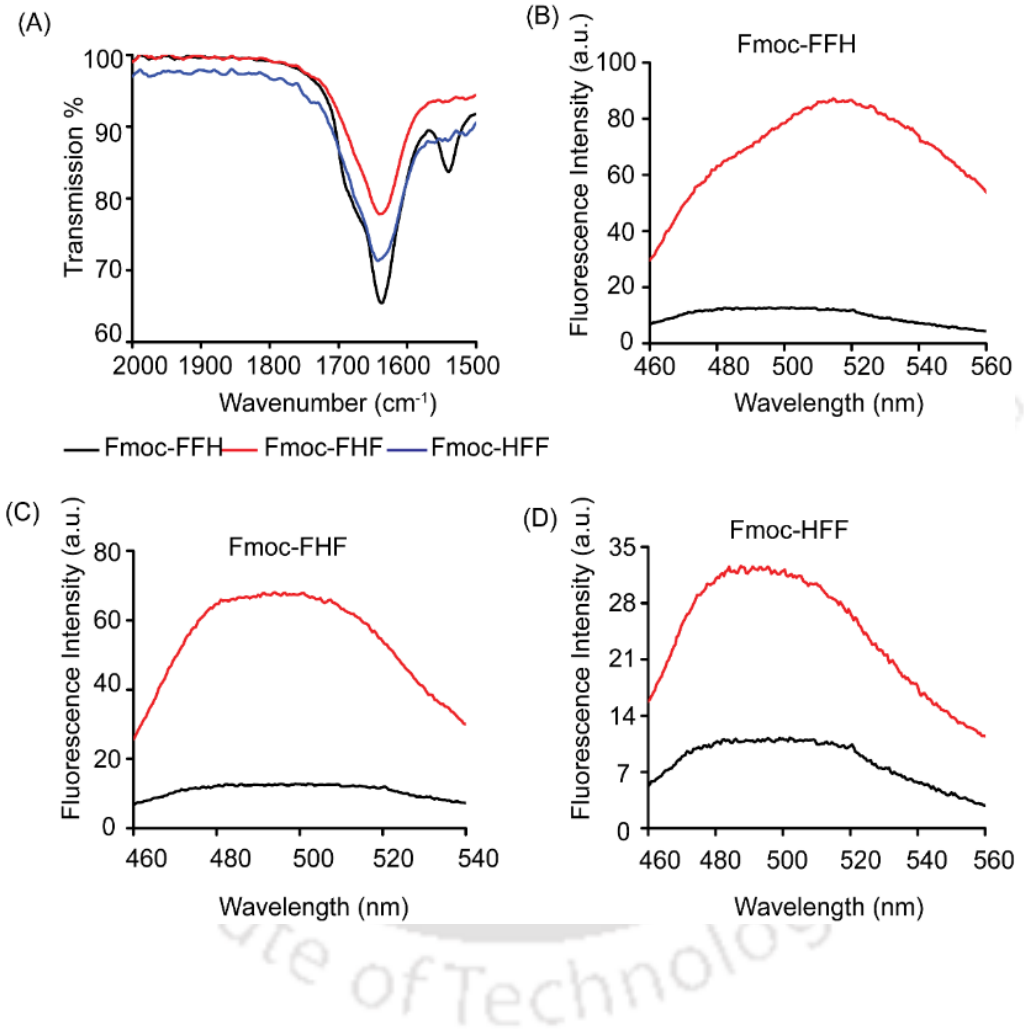

Figure 6.2 (A) FTIR analysis of peptide hydrogels suggesting β structure. B, C, and D showing ThT fluorescence spectra of the three peptides, Fmoc-FFH, Fmoc-FHF, and Fmoc-HFF respectively

The intensity of fluorescence is directly proportional to the extent of fibrillogenesis. All the designed peptides displayed marked enhancement in fluorescence after binding to the ThT dye, confirming the presence of beta fibrils. (Figure 6.2 B,C, and D).[342]

6.3.3 Characterization of hydrogel formation: Peptides were dissolved in phosphate buffer (pH 7.4) at different concentrations, and gelation was observed by tube inversion test (Figure 6.3A). The results are summarized in table 6.1, which shows that the gelation starts at 1% concentration (w/v), and immediate hydrogel formation was observed at 2% concentration for all the peptides.

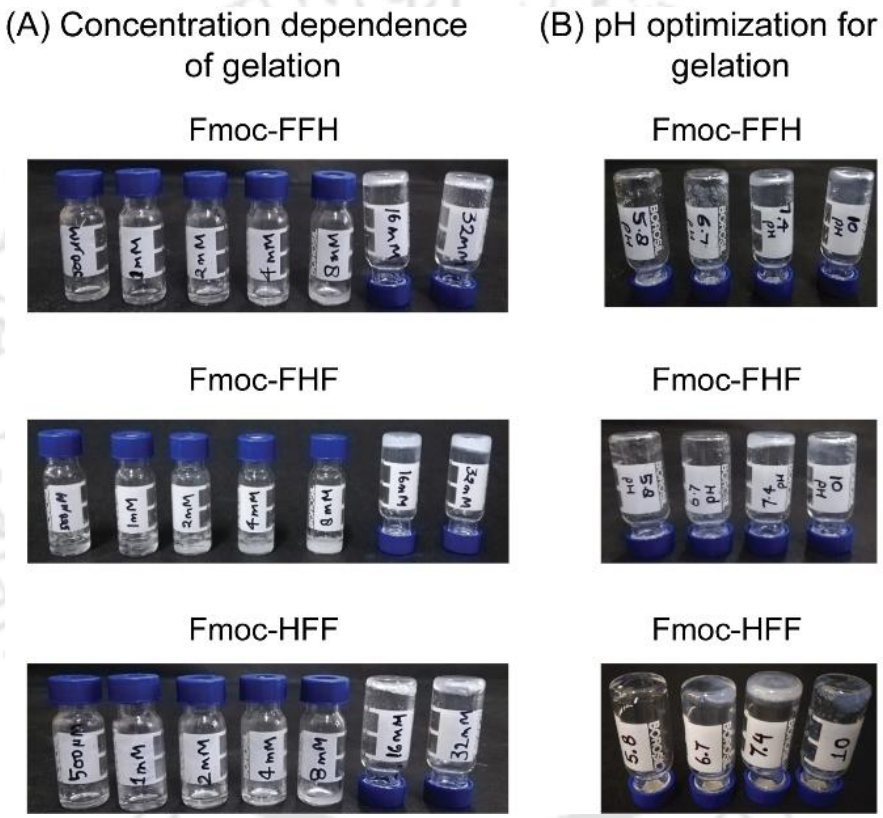

Figure 6.3. (A) Concentration dependence of Hydrogelation (concentration of peptides: from left to right; 500μM, 1mM, 2mM, 4mM, 8mM, 16mM, 32mM). (B) Optimization of pH for hydrogel formation (pH of peptides: from left to right; 5.8, 6.7, 7.4, 10).

Temperature, solvent system, and pH of the solvent will also affect hydrogelation. We tested the effect of pH on hydrogel formation within the buffering range of phosphate buffer (pH 5.8 to 8.0). No hydrogel was formed at pH 5.8, and 6.7 whereas, gelation is observed at pH 7.4 (Figure 6.3 B, Table 6.2.). The pKa

of Fmoc-F is approximately 3.5.[343] Therefore, the peptide is negatively charged at the gel forming pH of 7.4. It may be postulated that the negative charge may cause an electrostatic repulsion and inhibit self-assembly. However, as reported in the case of Fmoc-F, there is an apparent increase in pKa of this molecule due to its more hydrophobic nature, which puts the charged carboxylate group in a hydrophobic environment.[344] Similarly, it might result in more neutral species of Fmoc-F at pH 7 than the anionic ones. Moreover, assembly formation at pH 7 hints towards the possibility of major contribution from hydrophobic interactions, superseding the electrostatic repulsive forces that impede gel formation. The gel forming ability changes with pH, and this was confirmed by treating hydrogels with 1N HCl and 1N NaOH (Figure 6.4).

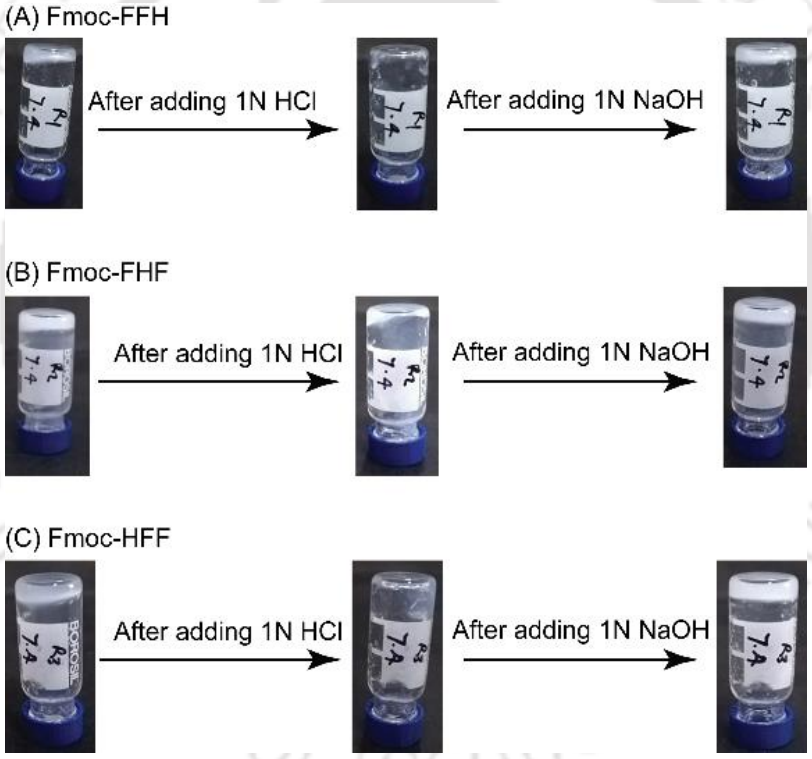

Figure 6.4 Dependence of hydrogelation property with pH switch. Hydrogels lose their gelation property in acidic pH but regained again when switched to basic conditions.

Table 6.1. Determination of gelation concentration for peptide hydrogels

Concentration	Concentration % (w/v)	Gelation Property
500 μM	0.03125%	No gel formation
1 mM	0.0625%	No gel formation
2 mM	0.125%	No gel formation
4 mM	0.25%	No gel formation
8 mM	0.5%	No gel formation
16 mM	1%	Gel formation
32 mM	2%	Immediate Gel formation

Table 6.2. Effect of pH on gelation

pH	Gelation Property	Gelation time
5.8	No gel formation	-
6.7	No gel Formation	-
7.4	Gel formation	Immediate
10	Viscous solutions	-

6.3.4 Morphology of peptide hydrogels: FESEM and AFM images of nanostructures formed by peptides are shown in Figure 6.5. FESEM analysis showed that hydrogels are in fibrous form, which was further validated by AFM.

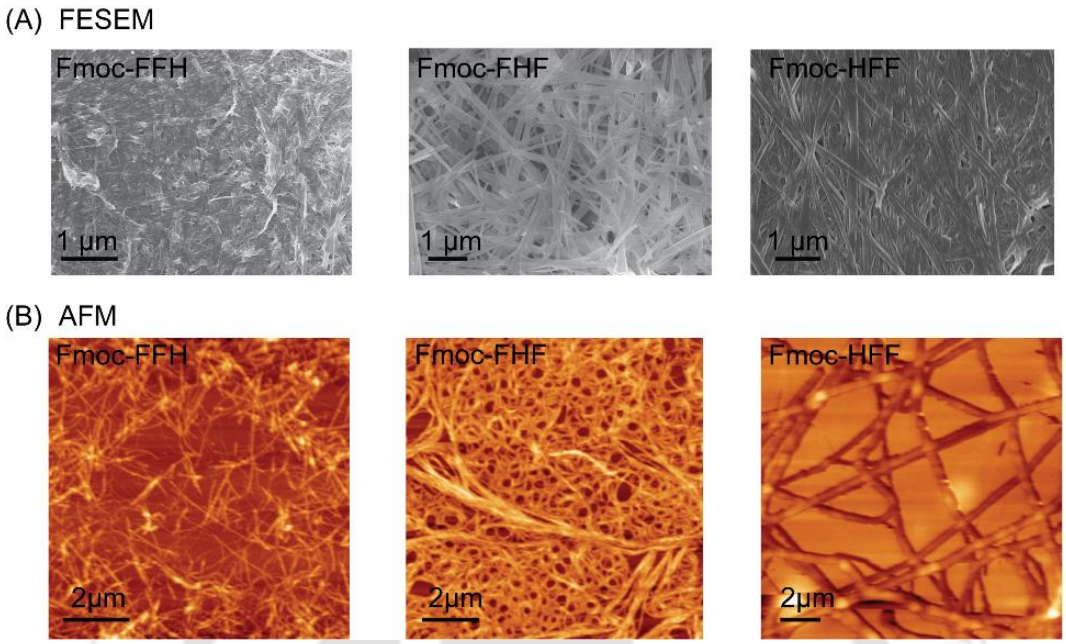

Figure 6.5. Morphology of hydrogels confirmng fibrous structures by (A) FESEM and (B) AFM

6.3.5 Rheology of peptide hydrogels: The rheological analysis of the synthesized peptide hydrogels under different parameters are presented in this section. The self-healing property of hydrogel plays a pivotal role in tissue engineering and drug delivery applications. During high strain, the self-healing hydrogel changes into a low-viscous liquid and regains its original structure after removal of high strain. It also exhibits an appropriate mechanical property to endure the biomechanical loading and allow temporary support for cells attachment. The amplitude sweep tests were conducted to examine the physical strength of the prepared hydrogels. The amplitude sweep results provide the storage modulus (G′) and loss modulus (G″) with deforming strain (%).The Linear visco-elastic region (LVE) of hydrogels was determined by varying the strain from 0.01% to 1000%, wherein the hydrogels can maintain their physical integrity and return to their original structure once the strain is removed. The gel to sol transition appears when storage modulus (G′) crossover the loss modulus (G″). The shear-thinning property of the hydrogels was found to be different as the crossover point of peptide Fmoc-FFH occurred at 15.92%, while for Fmoc-FHF and Fmoc-HFF, it was found to be 4.05 %, and 3.87 % respectively; beyond this

strain the network is broken. All remaining rheological analysis were conducted within the LVE region. The storage modulus represents the solid-state behavior, whereas the loss modulus indicates the liquid-state behavior of a hydrogel. Intuitively, when the solid-state component is higher than the liquid-state component (G' > G''), it represents gel-like behavior. The amplitude sweep results are shown in Figure 6.6. All hydrogels show higher storage modulus compared to the loss modulus, thus validating its gel-like property. Frequency sweep analysis was performed within the LVE region.

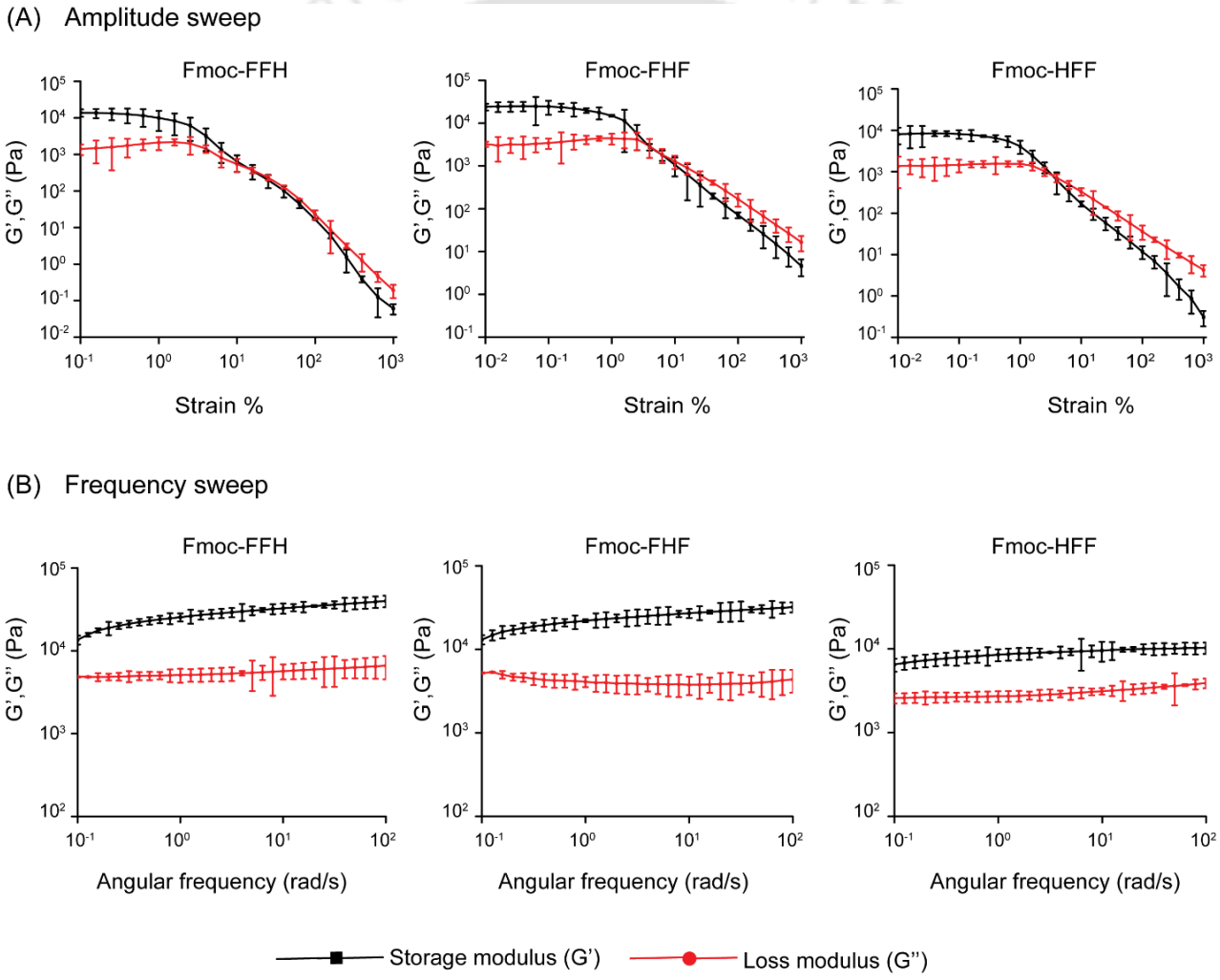

Figure 6.6 Rheology of peptide hydrogels; (A) amplitude sweep and (B) frequency sweep of the synthesized hydrogels. The error bars represent the standard errors of three independent observations.

As shown in Figure 6.6 B, non-significant change in storage modulus and loss modulus for Fmoc-FHF and Fmoc-HFF hydrogel was observed in the complete angular frequency range, confirming the strong mechanical property of hydrogels. In contrast, Fmoc-FFH hydrogel exhibited a significant change in storage modulus as it increased, with an increase in angular frequency. Overall, storage modulus values obtained with different peptide-based hydrogels were in the following order: Fmoc-FFH > Fmoc-FHF > Fmoc-HFF. The storage modulus of the peptide hydrogels was found to be in the range between 32.38 kPa and 9.30 kPa (average value of Fmoc-FHF and Fmoc-HFF). This trend is attributed to increased π-π interactions in peptides which enhances the mechanical property. The aromatic interaction between Fmoc and Phenylalanine moieties is mainly responsible for improving the storage modulus, and it increases with an increase in Phenylalanine content in the peptides.

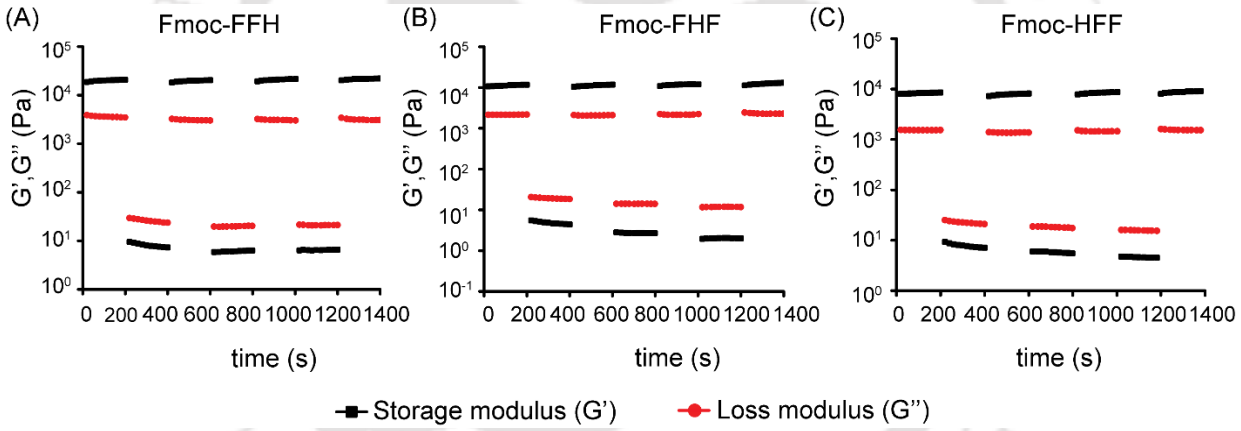

Figure 6.7 Continuous step strain measurements at alternate 0.1% and 300% strains over time, for peptide hydrogels showing self-healing behavior.

The observed increase in storage modulus with increasing aromatic interactions may also be attributed to additional entanglement of the peptide chains, resulting in the increase of cross-linking, thereby enabling the formation of the fiber network. Although the visco-elastic property of the peptide-based hydrogel plays a crucial role in conserving the structural and physical integrity, it is also crucial in regulating the viability, morphology, and differentiation of cells. Depending on the mechanical properties of tissues, the

elastic modulus of mammalian tissue ranges between 0.1 kPa to 10 kPa.[345,346] It has been reported that the epithelial cells and neurons were proliferated on soft structures, possessing a storage modulus of 0.1 kPa.[347,348] Hydrogel stiffness has been shown to affect stem cell growth. Considering such property, endothelial cells were proliferated onto the soft matrix in the presence of conditioned media and formed capillary-like structures, suggesting the importance of the substrate's mechanical properties for cell proliferation and triggering its biochemical response.[349] The mechanical properties observed in our peptide-based hydrogels show the necessity of such an investigation.

In regenerating tissues, cells continuously interact with the extracellular environment and remodel their extracellular matrix to carry out various proliferation, differentiation, and migration activities. During incubation of cells within the hydrogel, the cross-linking of the substrate degrade irreversibly, resulting in a reduction in mechanical strength and poor attachment of cells to the substrate. A new class of hydrogels was required to address this issue, with optimum cells attachment and proliferation using self-healing property. Such adaptable hydrogels possess polymer networks with reversible linkage that can be broken and repaired reversibly without the use of external stimuli. To ensure that peptide-based hydrogels are adaptive, we conducted rheological recovery tests, which involved subjecting the hydrogel to high deforming shear and then allowing it to recover at low shear (Figure 6.7). The gel-sol transition of Fmoc-FFH, Fmoc-FHF, and Fmoc-HFF was evaluated by applying a high strain (strain = 300%, frequency = 1Hz) deforming shear. Variation in the step-strain dependent modulus was analysed between the three samples. Variation in the sol–gel transition of the hydrogels was attained by applying low strain (strain = 0.1%, frequency = 1Hz). During gel-sol transition, the storage modulus value of Fmoc-FFH reduced from 20.03 kPa to 8.19 Pa, while in sol-gel transition it recovered to 19.61 kPa. For Fmoc-FHF hydrogel, the storage modulus decreased from 11.27 kPa to 4.85 Pa at high strain and recovered to 11.23 kPa at low strain. A similar self-healing process was observed for Fmoc-HFF hydrogel, as high strain storage modulus decreased from 8.31 kPa to 7.91 Pa, and at low strain storage modulus value regained to 8.3 kPa. The rapid recovery to original micro-network confirmed the self-healing capability of hydrogels without the need for a healing agent or external stimulus.

6.3.6 Serum stability of the designed peptide: We have performed the serum stability assay of the designed peptides using HPLC. The results indicate that none of the peptides were degraded after serum treatment (Figure 6.8).

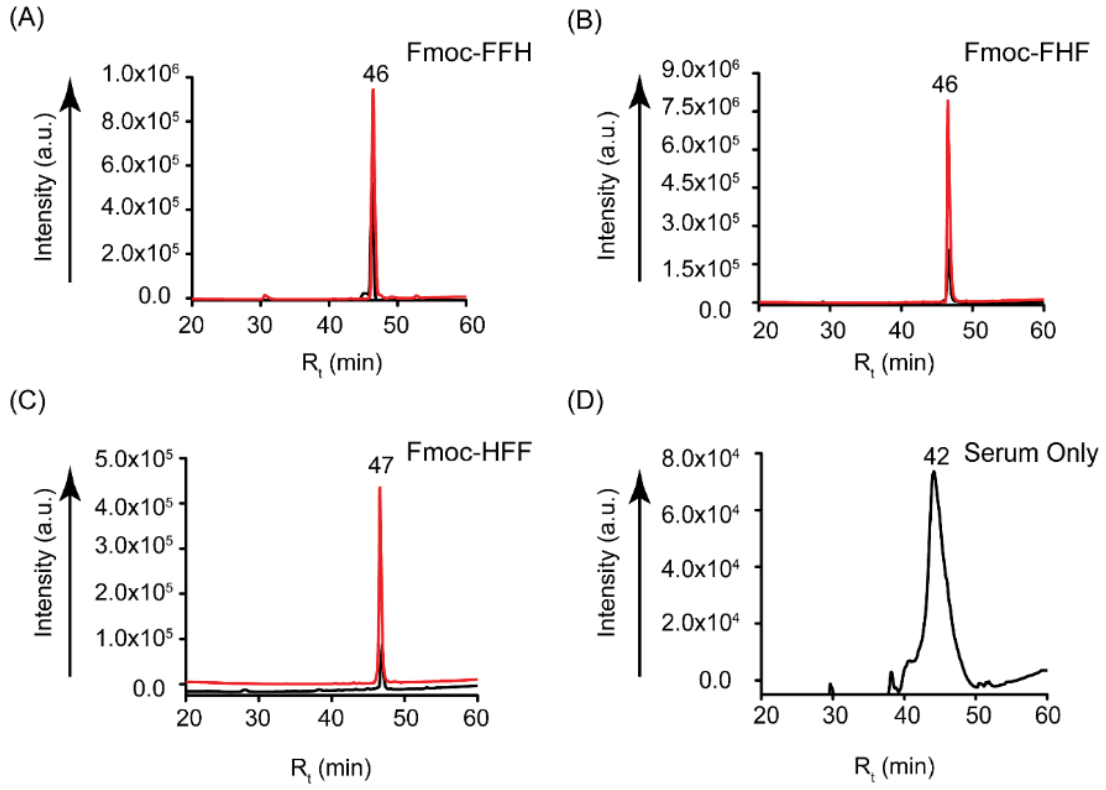

Figure 6.8 Serum stability test of peptides showing stability in the presence of human serum

6.3.7 Antimicrobial potency of designed peptide hydrogels: We have investigated the antimicrobial potency of the synthesized hydrogels (2%) against Gram-positive (Staphylococcus aureus) and Gram-negative (*Pseudomonas aeruginosa*) bacteria. Previous reports of Fmoc based diphenylalanine hydrogels have shown the antimicrobial effect against Gram-positive bacteria (*Staphylococcus aureus*) only.[22] Our synthesized peptides have shown significant antibacterial activity against both Gram-positive (*Staphylococcus aureus*) and Gram-negative (*Pseudomonas aeruginosa*) bacteria, though hydrogels are more effective against Gram-positive bacteria (Figure 6.9). Antibacterial effects of hydrogels were also

validated by FESEM analysis (Figure 6.10). As shown in Figure 6.10, membrane disruption occurred in the presence of hydrogels, while no membrane disruption was observed in the control sample. The mechanism of action of peptide hydrogels could be attributed to a combination of two factors: the fibrillary β-sheet structure, and the peptide hydrophobicity. Self-assembled FF peptides can bind to the surface of the bacterial membrane, aggregate, and orient themselves to optimize hydrophilic-hydrophobic interactions, thus inducing a surface tension leading to membrane depolarization, pore formation and release of cellular content.[350] Antibacterial activity of self-assembled Fmoc-F was attributed to the peptide release from the hydrogel inducing oxidative and osmotic stress as well as altering bacterial membrane

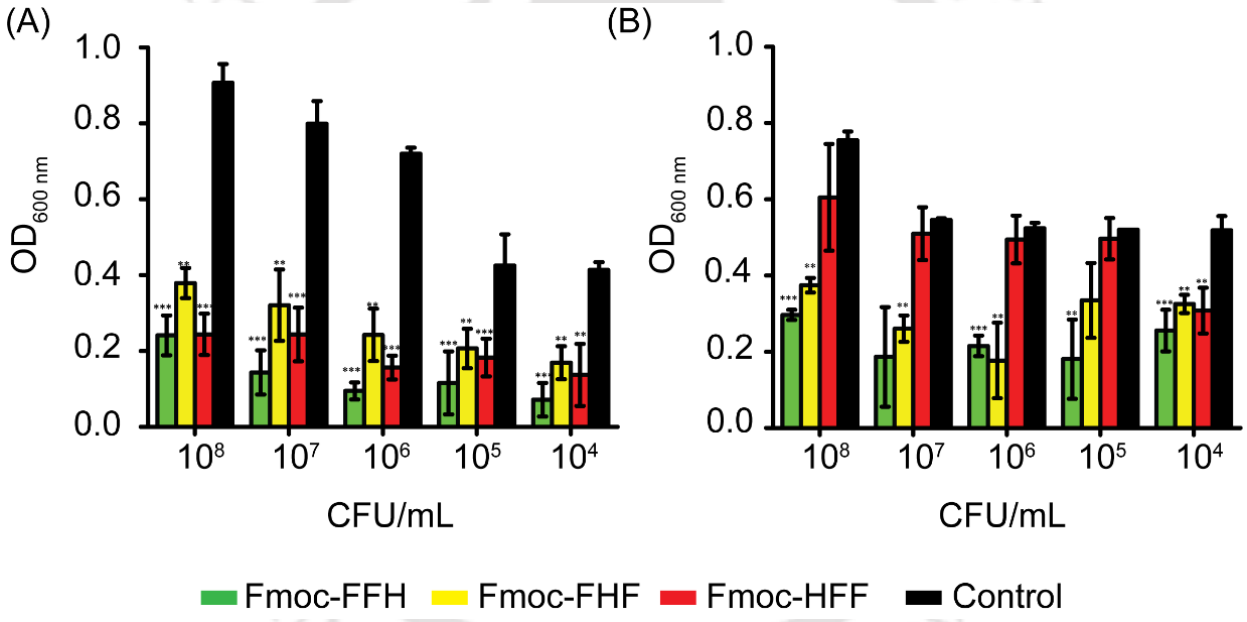

Figure 6.9 Antimicrobial potency of peptide hydrogels on (A) Staphylococcus aureus, and (B) Pseudomonas aeruginosa. For each treatment group, the control and hydrogel treated bacterial cells were compared by Two-tailed Student's t-test. (*p<0.05, n=3)

integrity.[22] We haveinvestigated the level of ROS generation in bacterial cells after hydrogel treatment. Fluorophore 2,7-dichlorodihydrofluorescein diacetate (DCFH-2-DA) was used to measure the ROS generation. DCFH-2-DA is a cell permeable molecule which diffuses into cells and is de-acetylated by the

esterases, forming 2,7 dichlorodihydrofluorescein. In the presence of ROS, 2,7-dichlorodihydrofluorescein oxidizes to dichlorofluorescein (DCF) which is highly fluorescent. Fluorescence intensity of DCF is used to measure the ROS generation in bacterial cells. We observed increased ROS generation in peptide hydrogel treated Staphylococcus aureus cells, but we could not get any significant increase of ROS levels in Pseudomonas aeruginosa (Figure 6.11 A). The increased ROS level disrupts cellular processes which lead to osmotic and oxidative cellular stress, resulting in bacterial death.[351] Therefore, to investigate the mechanism of antibacterial activity in Pseudomonas aeruginosa, we performed the outer membrane permeabilization assay. Alternation in the outer membrane permeabilization was investigated using NPN fluorophore (Figure 6.11 B). NPN weakly fluoresces in aqueous medium, but exhibits enhanced fluorescence in a hydrophobic environment.

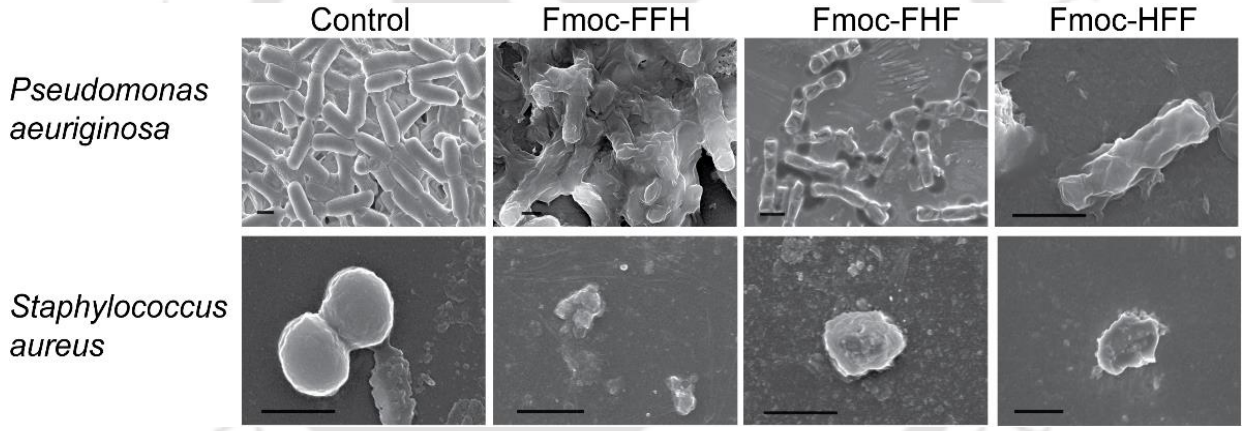

Figure 6.10 FESEM analysis describing bacterial membrane disruption after hydrogel treatment. Scale bar represents 1µm scale.

Perturbation of lipid bilayer provides NPN to get into the hydrophobic environment, causing enhancement in the fluorescence intensity. Significant increase in NPN fluorescence was observed in Fmoc-FFH and Fmoc-FHF treated samples, confirming bacterial membrane disruption by peptide hydrogels. A recent study also reported that the antibacterial effect of diphenylalanine is due to the membrane permeability, and osmotic stress which finally lead to bacterial cell death.[352]

In summary, the antibacterial property of the peptide hydrogels may be attributed to their ability to form β-sheet self-assembled nanofibers, which aggregates and bind onto the surface of the bacterial membrane, creating an oxidative and osmotic stress, leading to the death of the bacteria. In contrast to Gram-positive bacteria, Gram-negative ones have an additional outer bilayer membrane, formed by lipopolysaccharides and phospholipids, that makes the diffusion of molecules difficult across the membrane and renders them more resistant to break.[353] This may be the reason of lesser activity of peptide hydrogels against Gram-negative bacteria.

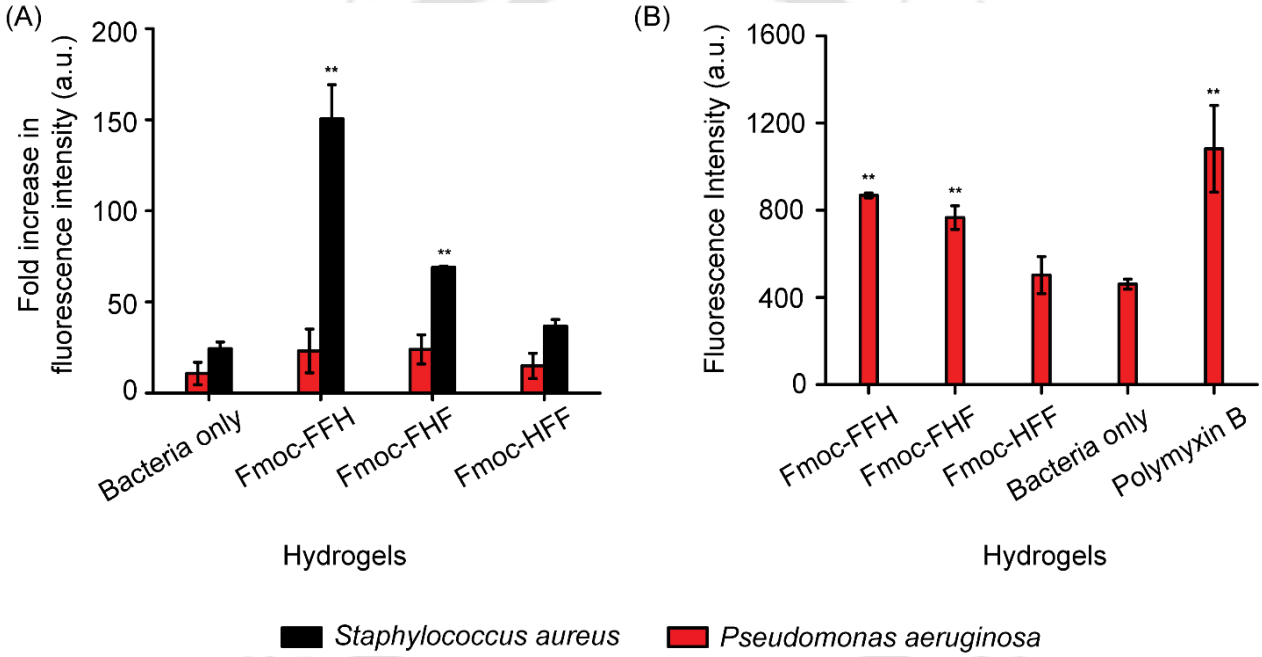

Figure 6.11 (A) ROS generation in *Staphylococcus aureus*, and *Pseudomonas aeruginosa*. (B) Outer membrane permeabilization assay for *Pseudomonas aeruginosa*. For each experiment, the control and hydrogel treated bacterial cells were compared by Two-tailed Student's t-test. (*p<0.05)

6.4 Conclusions

We have synthesized the tripeptide hydrogels by altering position of His amino acids to change the distance between Phenylalanine and Fmoc moieties. We have evaluated the mechanical properties of

hydrogels and reported that the storage modulus of hydrogels depends on the aromatic stacking. We have observed G' value in the order of Fmoc-FFH>Fmoc-FHF>Fmoc-HFF which may be due to enhanced aromatic π-π interaction between Fmoc and phenylalanine (F) moieties in Fmoc-FFH. Peptide hydrogels have shown pH dependent switching and self-healing properties, which may be further explored for targeted drug delivery and tissue engineering. We have shown antibacterial effects of tripeptide hydrogels on Gram-negative bacteria and to a much greater extent Gram-positive bacteria for potential use against diabetic foot ulcers and wound healing. The mechanism of action of peptide hydrogels may be attributed to the osmotic stress developed by Fmoc-F group that alters bacterial membrane permeabilization, eventually leading to the bacterial death. Bacterial membrane morphology by FESEM also supports this hypothesis. The peptide hydrogel Fmoc-FFH have shown inherent antimicrobial properties, and may not require any antimicrobial drugs as active pharmaceutical ingredient. Therefore, the broad spectrum antibacterial effects of our hydrogels may be explored as topical agents in wound healing, burning area and diabetic foot ulcers, where it may work in two complementary ways; moistening the affected area and bactericidal effects.

7

Heavy Metal Removal by Metal-Organic Systems and Biodegradable Adsorbents

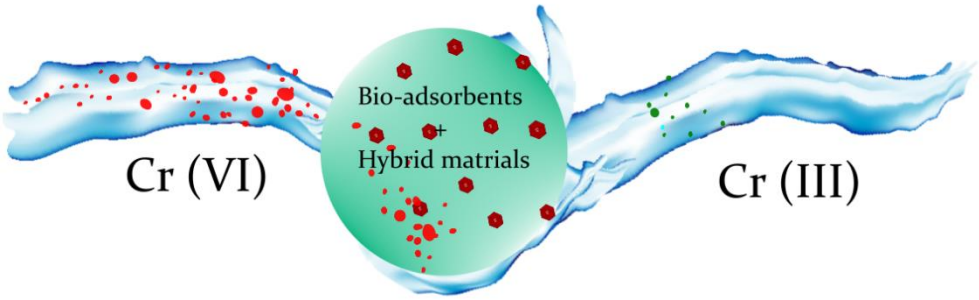

Hexavalent chromium ion (Cr (VI)) is one of the most toxic contaminant released in the water bodies by anthropogenic activities. Despite extensive studies on adsorbents for chromium removal, an effective optimized solution is still in demand and therefore, new cost-effective adsorbents derived from natural sources are still an active research area. In this study, we have investigated the application of 1,2-bis(tritylthio)ethane crystals as an adsorbent for Cr removal. During this investigation using different hybrid systems, we have serendipitously discovered the utility of human hair as a cost effective natural bio-adsorbent.

***Note**: This work was not a part of the designed research project, leading to PhD thesis. We started this investigation after obtaining 1, 2-bis(tritylthio)ethane crystals while performing solid phase peptide synthesis. We then followed and systematically investigated the utility of trityl based hybrid systems and human hair to address the long standing health hazards, resulting from the heavy metal contamination in drinking water in eastern states of India, Bangladesh and western regions of China. The significance of the results prompted us to include it in this thesis.*

7.1 Introduction

Over the last few decades, waste water containing significant amount of hexavalent chromium (Cr (VI)) was expelled as industrial effluent, that causes severe threat to the environment because of their mutagenic and carcinogenic side effects.[354] In aquatic systems, Cr (VI) present in solution as $HCrO_4$, CrO_4^{2}, and $Cr_2O_7^{2-}$, are toxic to the environment.[355] In contrast, Cr (III) present in the solution as Cr^{3+}, $Cr(OH)^{2+}$, $Cr(OH)_3$ and $Cr(OH)_4^{-}$, are less toxic and immobile.[356] Persistent exposure of Cr (VI) may even cause certain types of cancer in digestive tract, and lungs.[357] Therefore, removal of Cr (VI) from the contaminated water is an important problem that has to be addresses affectively.

Several methods such as chemical precipitation,[358] coagulation, flocculation,[359] and adsorption[360] are in practice for heavy metal removal. Among them, adsorption is the most frequently used treatment technique.[361] Various low-cost adsorbents derived from agricultural wastes,[362] natural materials,[363] and modified biopolymers[364] have been tested to remove heavy metals. However, none of them were very effective towards Cr removal. Therefore, a cheap, effective and easily available adsorbent is essential for Cr removal.

Our lab has earlier reported a new organic compound, 1,2-bis(tritylthio)ethane which forms a rare organic nano-flower.[259] We have successfully attempted to verify the possibility of converting this nano-assembly to a functional hybrid material by coating it with magnetite. The resulting magnetite hybrid material was examined for their potential utility as nano-adsorbent for heavy metal removal. Most of the magnetite-based nanomaterials used in the adsorption were surface functionalized or modified,[365] which in turn, is a complicated and intensive process. In this study, we have evaluated the capacity of a hybrid nanomaterial (magnetite coated 1, 2-bis(tritylthio)ethane crystal) for Cr removal. As an extension of this investigation, we have evaluated the possibility of using different forms of human hair as Cr removal bio-adsorbent. Earlier published reports have explored human hair as an adsorbent of oil from wastewater.[366] Basu and co-workers have investigated the utility of human hair as a Cr removal adsorbent by batch experiments.[367] We have extended the study by using different physical form of human hairs and compared their Cr removal efficiency.

7.2 Experimental Procedures

7.2.1 Materials: All the chemicals and solvents used were of analytical reagent grade. 1, 2-ethanedithiol was purchased from Sigma-Aldrich. Ferrous sulfate heptahydrate, ferric nitrate, and diethyl ether were purchased from Merck. Trityl chloride was purchased from Sisco Research Laboratories Pvt. Ltd. Sodium dichromate dihydrate was purchased from Fisher Scientific. Regents for the pre-treatment of human hairs (chloroform, diethyl ether, acetone, and methanol) were purchased from Merck. Hair samples were collected from the local market.

7.2.2 Synthesis and characterization of 1, 2-bis(tritylthio)ethane crystals and magnetite nanoparticles: The compound 1, 2-bis(tritylthio)ethane crystal was synthesized by incubating trityl chloride salts with 1,2-ethane dithiol, in the presence of trifluoroacetic acid for 24 h. After 24 h crystallization and purification were performed using diethyl ether. Magnetite nanoparticles were synthesized by co-precipitation method, by mixing aqueous solutions of ferrous sulfate heptahydrate and ferric nitrate. An anionic surfactant was added for stabilization, and the final mixture was heated at 75°C. Magnetite obtained was washed with distilled water and dried at 60 °C.

7.2.3 Synthesis and characterization of hybrid materials: Synthesis and characterization of hybrid materials were performed by adapting an already published protocol.[259] In brief, synthesized magnetite was dispersed at 0.2% concentration of diethyl ether. 1,2-bis(tritylthio)ethane was then added at a concentration of 0.5 mg/ml. The hybrid materials formed was characterized by Field Emission Scanning Electron Microscopy (FESEM) using Jeol FESEM (Model: JSM-7610F).

7.2.4 pH stability of 1,2-bis(tritylthio)ethane crystals: To study the stability of 1, 2-bis(tritylthio)ethane crystals at different pH, crystals were incubated at different pH ranges, from 2 to 10, for 24 h. After 24 h, stability was checked by studying the changes in morphology by using Jeol FESEM (Model: JSM-7610F).

7.2.5 Pre-treatment of human hair: Human hair samples were washed prior to the experiment as described elsewhere.[368] Human hairs were cut into small pieces and washed thoroughly with distilled

water 4-5 times. Washed samples were treated with an equal ratio of chloroform, methanol, acetone, and diethyl ether to remove extraneous substances. Treated samples were centrifuged at 10,000 rpm for 30 min, followed by supernatant removal and washing with distilled water. The washing process was repeated at least three times for complete removal of dirt and other extraneous materials and dried at room temperature.

7.2.6 Modification of human hair: Washed and dried human hairs were pulverized by employing an earlier reported the protocol.[369] Washed and dried hairs were cut into small pieces (6-7mm). Pulverization was performed in a Ball mill apparatus (Fritsch Pulverisette 6). Size of the human hairs were reduced to 3-4 mm after pulverization. Hair powder was obtained by pyrolysis method which was performed in a muffle furnace at 200°C. Three forms; pulverized hair (PH), hair powder (HP), and raw hair (RH) were evaluated for their ability to adsorb Cr.

7.2.7 Characterization of human hair: Morphology of the adsorbents was characterized by FESEM (Jeol, JSM-7610F) before and after the adsorption experiments. The presence of Cr on the surface of the hair was also analyzed by Energy Dispersive X-Ray Spectroscopy (EDX). Fourier transform infrared (FT-IR) spectra of the adsorbent were recorded on an FT-IR spectrophotometer in 4000-400 cm^{-1} range.

7.2.8 Adsorption study: To estimate the Cr (VI) adsorption, different parameters, such as the effect of different adsorbent dose, pH, initial Cr concentration, and contact time were studied. To investigate the effect of different adsorbent dose, 50 mg/L Cr (VI) solution was added in different conical flasks containing different doses of human hair (0.5, 1, 2, 3, 4, 6, 8, 10 g/L). Flasks were incubated at 25°C for 10 h at 150 rpm. To analyze the effect of pH, 50 mg/L Cr (VI) solution at different pH conditions (from 2 to 10) was prepared and incubated at 25°C for 10 h. To investigate the effect of different initial Cr concentration and time, different flasks containing 100 mg of PH, HP, and RH with Cr concentration (10, 20, 30, 40, 50 mg/L) were incubated at 25°C, and rotated at 150 rpm for 10 h. Cr solutions were collected at regular time intervals. Cr concentration was estimated using Atomic Emission Spectrometer (MP AES 4210). The extent of adsorption and adsorption capacity were calculated by using equations 1 and 2, respectively.

$$\% \text{ Adsorption } = (C_0 - C_e)/C_0 \times 100 \quad (1)$$

$$q_e = (C_o - C_e) \times V/M \quad (2)$$

Where, C_0 and C_e are the initial and final concentration respectively. V and M are the volume of the solution (in liters) and weight of adsorbent (in grams) respectively.

7.2.9 Isotherm and kinetic studies: Different flasks containing 100 mg adsorbent and Cr (VI) solution (concentration 10, 20, 30, 40, 50 mg/L) were incubated at 25°C, and rotated at 150 rpm for 10 h. Cr adsorption at equilibrium was studied using Langmuir, Fruendlich, and Dubinin–Radushkevich isotherm model. The rate of adsorption was studied by pseudo-first-order, pseudo-second-order kinetics and intraparticle diffusion.

7.2.9.1 Isotherm studies: The Langmuir isotherm model is based on the assumption of monolayer coverage of adsorbate over a homogeneous adsorbent surface. It is described as homogenous adsorption assuming that all the adsorption site has equal affinity, and adsorption at one site does not affect the adsorption at an adjacent site.[370] It is used to describe monolayer adsorption onto the surface of an adsorbent, and is expressed as follows

$$\frac{C_e}{q_e} = \frac{1}{Q_0 b} + \frac{C_e}{Q_0} \quad (3)$$

Where C_e and q_e are the concentrations (mg/L) and amount of Cr (mg/g) at equilibrium. Q_0 (mg/g) and b (L/mg) are Langmuir constants and related to the adsorption capacity and energy of adsorption, respectively.[371] The intercept and slope of plot C_e/q_e against C_e were used to evaluate the values of b and Q_0.

The significant characteristics of Langmuir isotherm can be expressed in terms of separation factor or equilibrium parameter, R_L. It is expressed by the following equation:

$$R_L = \frac{1}{(1 + bC_i)} \quad (4)$$

Where C_i (mg/L) represents initial metal concentration, and b represents Langmuir constant. R_L gives the information about the nature of the adsorption process. It is considered unfavorable if $R_L > 1$, linear if $R_L = 1$, and favorable if $0 < R_L < 1$, and irreversible if $RL = 0$. [372]

The Freundlich isotherm model equation is employed to determine the adsorption on heterogeneous surfaces, and is characterized by the heterogeneity factor (n).[373] The isotherm is expressed as:

$$\log q_e = \log K_F + \frac{1}{n_F} \log C_e \quad (5)$$

Where q_e is adsorption capacity at equilibrium (mg/g) and C_e is the equilibrium concentration of Cr (VI). K_F and n_F are Freundlich constants where K_F (L/g) is adsorption coefficient and n_F indicates adsorption intensity (dimensionless).[374] The value of 1/n between 0 and 1 indicates a favorable condition for Cr (VI) adsorption onto adsorbent surface.

The Dubinin-Radushkevich isotherm model (D-R isotherm) does not assume a homogeneous surface or a constant biosorption process. D-R isotherm model represents the micro-pore filling.[375] This model predicts the adsorption process as either physisorption or chemisorption. D–R isotherm is expressed as:

$$lnq_e = lnQ_m - K\varepsilon^2 \quad (6)$$

Where Q_m is maximum adsorption capacity (mg/g), K is adsorption energy (mol^2/J^2). ε represents Polanyi potential, calculated using the following equation:

$$\varepsilon = RTln(1 + \frac{1}{C_e}) \quad (7)$$

Where R is gas constant (8.314 J/mol/K), and T is temperature. The values of Q_m and K were determined by plotting log (q_e) versus ε^2. The mean adsorption energy, E (kJ/mol), was calculated by the equation:

$$E = \frac{1}{\sqrt{2K}} \quad (8)$$

7.2.9.2 Adsorption Kinetics: The dynamics of the adsorption process in terms of the order and the rate constant can be evaluated using the kinetic adsorption data. The kinetics of Cr (VI) removal is explained by using pseudo-first-order, pseudo-second-order, and intraparticle diffusion model.

According to pseudo-first order kinetic model, the rate of occupied adsorbed sites is proportional to the rate of unoccupied sites. The pseudo-first-order kinetic equation is given as follows:

$$\log\ (q_e - q_t) = log\ q_e - \frac{K_1}{2.303} t \qquad (9)$$

Where q_t and q_e are adsorption capacities at equilibrium (mg/g) and K_1 is the pseudo-first-order rate constant (min^{-1}). The values of equilibrium metal concentration q_e, rate constant k_1, and coefficient of determination (R^2) can be obtained by plotting log ($q_e - q_t$) against t.

The pseudo-second-order kinetic model implies chemisorption during the adsorption process. It is expressed as follows:

$$\frac{t}{q_t} = \frac{1}{K_2 q_e^2} + \frac{t}{q_e} \qquad (10)$$

Where K_2 is the pseudo-second order rate constant (g/mL min). Values of k_2 and q_e were calculated from the plot of t/q_t against t.

In addition to the pseudo-first and pseudo-second-order, the intraparticle diffusion model was used to understand the mass transfer mechanism. Intraparticle diffusion is expressed as follows

$$q_t = K_{id} t^{1/2} + C \qquad (11)$$

Where k_{id} is the intraparticle diffusion rate constant ($mg/g/min^{1/2}$) and C is the intercept which represents the thickness of the boundary layer effect.

7.2.10 Desorption and Regeneration Study: Desorption studies were conducted in batch experiments. 50 mg/L of Cr (VI) saturated adsorbents were treated with 50 mL water at pH 12, for 6 h.[376] Human hairs were then separated from the solution, and washed with distilled water. Washed human hairs were further regenerated with 1N HCl. Regenerated human hairs were washed with distilled water and dried at room temperature. Desorption percentage was calculated using the equation:

$$\% \text{ Desorption} = \frac{\text{Concentration after elution}}{\text{Concentration before elution}} \times 100 \quad (12)$$

7.2.11 Column Study for Cr (VI) Adsorption: Continuous column experiments for Cr (VI) adsorption were carried out with RH packed as bed in glass column of dimensions of internal diameter 2 cm and length 30 cm. The packed column was washed several times with deionized water, and loaded with glass wool. Glass beads were loaded next to the glass wool. Breakthrough curve was obtained with variable bed height (5, 10, 20 cm). 50 mg/L of Cr (VI) solution was passed through the packed bed column by a peristaltic pump (PP-20-EX, Miclins, India) at the flow rate of 5 mL/min. Sample from the outlet was collected at certain time intervals and Cr (VI) concentration was estimated. Different parameters of column study were evaluated by using the following equations:

Total column capacity for Cr adsorption was calculated by (13)

$$q_{total} = \frac{Q}{1000} \int_{t=0}^{t=total} C_{ads} dt$$

Where t_{total} is the total time of flow (min), Q is flow rate (mL/min)

Equilibrium adsorption capacity $q_{e(exp)}$ was calculated by using the formula: (14)

$$q_{e(exp)} = \frac{q_{total}}{M}$$

Where M is mass (in g) of adsorbent packed in the column.

Total amount of Cr (VI) delivered to the column was calculated by: (15)

$$m_{total} = \frac{C_0 \times Q \times t_{total}}{1000}$$

Where, C_0 is initial Cr (VI) concentration, Q is the flow rate (mL/min).

Total Cr (VI) removal capacity of column was calculated by using the equation: (16)

$$Y(\%) = \frac{q_{total}}{m_{total}} \times 100$$

Total treated volume (in mL) was calculated by using the equation: (17)

$$V_{eff} = Q \times t$$

7.3 Results and Discussion

7.3.1 Synthesis and characterization of 1, 2-bis(tritylthio)ethane crystals and magnetite nanoparticles: The reaction steps of the synthesized 1, 2-bis(tritylthio)ethane crystals are shown in Figure 7.1. Tri-phenyl methyl (trityl) group is a stable radical, first reported by M. Gomberg in 1900.[377] The positive charge on the α- carbon atom is 'resonance stabilized' by three aromatic rings. In the presence of acid (TFA), trityl chloride generates free radicals which interact with EDT to form 1, 2-bis(tritylthio)ethane.

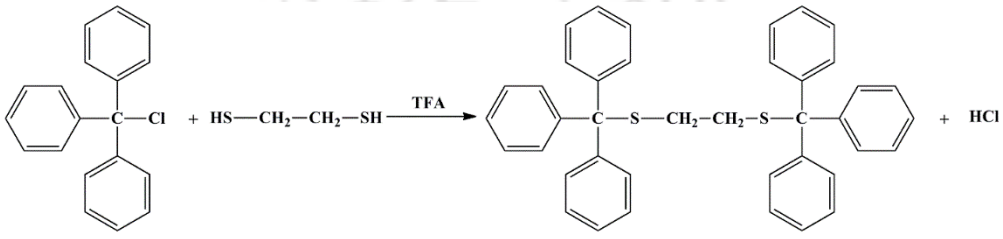

Figure 7.1. Synthesis of 1, 2-bis(tritylthio)ethane crystals. Trityl chloride salt was incubated with 1, 2-Ethane dithiol in the presence of Tri-fluoro acetic acid for 24 h. After 24 h, the obtained crystals were washed with diethyl ether

7.3.2 Characterization of 1, 2-bis(tritylthio)ethane crystals and magnetite nanoparticles:

FESEM image of 1, 2-bis(tritylthio)ethane crystal and FETEM image of magnetite nanoparticles are shown in Figure 7.2. As shown in the figure 7.2 magnetite nanoparticles formed nanosphere like structure.

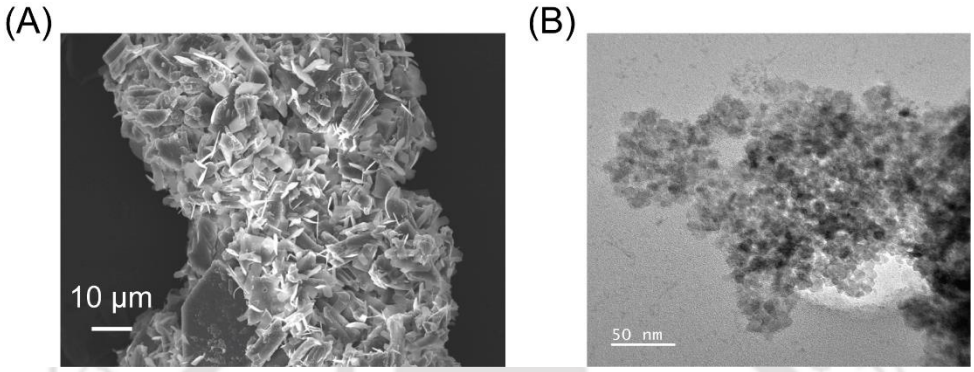

Figure 7.2 (A) FESEM image of 1, 2-bis(tritylthio)ethane crystals, and (B) FETEM image of magnetite nanoparticles.

7.3.3 pH stability of 1,2-bis(tritylthio)ethane crystals: FESEM image of 1, 2-bis(tritylthio)ethane crystals at different pH conditions showed no significant difference in the morphology of the crystal structure. This confirms the stability of 1, 2-bis(tritylthio)ethane under different pH conditions, so that it can be used as an adsorbents at extreme pH conditions (Figure 7.3).

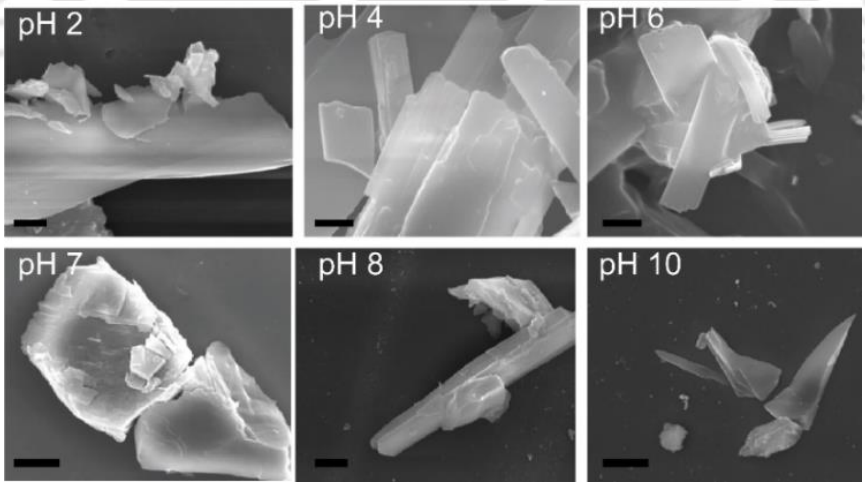

Figure 7.3 Stability of 1, 2-bis(tritylthio)ethane crystals at different pH conditions. FESEM image of 1,2 bis(tritylthio) ethane crystals at different pH, showed no significant difference in the morphology of the crystal structure. Scale bar represents 1µm scale.

7.3.4 Cr removal by adsorbent systems: In a set of preliminary experiments, we screened the Cr (VI) removal efficacy of various adsorbents such as glass wools, 1, 2-bis(tritylthio)ethane crystals, hair, and couple of hybrid materials (Figure 7.4). Results showed that the maximum adsorption was observed in experiments with human hair, followed by hybrid material packed with hair. Compared to human hair, adsorption of other adsorbent systems were not appreciable. We observed relatively low Cr (VI) removal by 1, 2-bis(tritylthio)ethane crystals and other adsorbents. This prompted us to perform a series of experiments to verify the utility of human hair as Cr (VI) adsorbent, so as to develop it as an adsorbent system at commercial scale.

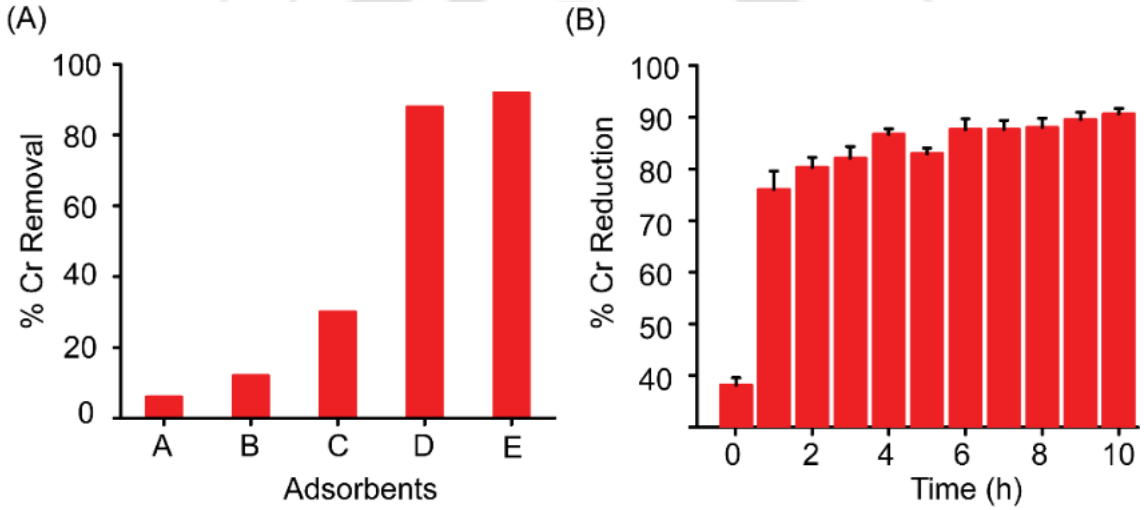

Figure 7.4 (A) Pilot experiment to verify Cr removal by different adsorbent systems, A: glass wool, B: 1,2-bis(tritylthio)ethane, C: Trityl-Magnetite hybrid, D: hybrid materials with human hair, and E: human hair. (B) Reduction of Cr (VI) by hybrid material. Hybrid material reduced up to 90% toxic Cr (VI) to nontoxic Cr (III) form

7.3.5 Determination of Cr (VI) reduction by Trityl-Magnetite Hybrid material: We evaluated the Cr (VI) reduction efficiency of magnetite coated 1, 2-bis(tritylthio)ethane crystals (hybrid materials), which reduced Cr (VI) to Cr (III) with 90% efficiency (Figure 7.4 B). It is reported that Fe (II) in magnetite nanoparticles facilitates the reduction of Cr (VI) to Cr (III).[378] As the reaction progresses, Cr (III) hydroxide or Cr (III)-Fe (III) complex were formed (reaction (i)).[379,380,381] Parks and

co-workers have reported that the sorption of Cr (VI) follows a two-step process; (i) electrostatic attraction of Cr (VI) ion, followed by (ii) electron transfer between Cr (VI) and Fe (II).[382,383]

$$CrO_4^{2-} + 3Fe^{2+} + 3H_2O + H^+ = CrOH^{2+} + 3Fe(OH)_2^+ \quad \text{(i)}$$

7.3.6 Characterization of human hair: Morphology of adsorbents before and after Cr adsorption study was observed by FESEM showing no significant structural change at the surface (Figure 7.5). The Adsorption of Cr (VI) on hair is evident from the FESEM-EDX analysis, suggesting adsorption of Cr on the surface of hair.

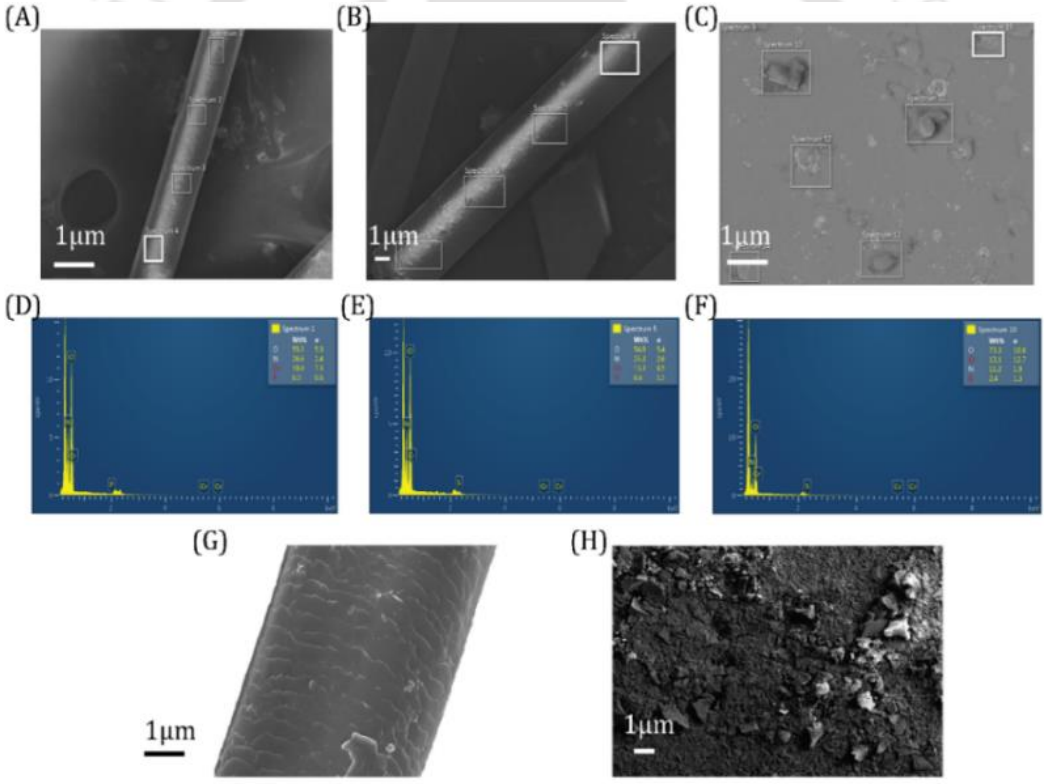

Figure 7.5 FESEM analysis of adsorbents (A), PH (B) RH and (C) HP after Cr (VI) adsorption with EDX plot in D, E, F for PH, RH and HP respectively confirming Cr (VI) adsorption. Image (G) and (H) are the surface of human hair and hair powder before Cr (VI) adsorption.

FT-IR analysis was carried out to characterize the functional groups involved in the binding of Cr (VI), and analyzed by the deviation in the vibrational frequency [384] (Figure 7.6). Main components of human hairs are proteins, water, and lipids. IR spectrum of unprocessed hair, has characteristic peaks due to the vibration of amide bonds in the peptide linkage of proteins in the range 1700-1590 cm^{-1}, 1580-1500 cm^{-1}, and 1320-1210 cm^{-1}. The prominent peak at 1637 cm^{-1} in all adsorbents is due to the amide I bond involving C=O stretching. We have observed no deviation of 1637 cm^{-1} absorption peak, in any adsorbents. The absorption peak in the range of 1510-1520 cm^{-1} are typical of amide II absorption. The absorption peak at 1449 cm^{-1} corresponds to the C-H stretching. The absorption peak at 1234 cm^{-1} corresponds to the amide III band which involves C-H stretching and N-H bending modes of vibrations. Absorption peaks due to the weak dioxide band (S=O_2) at 1114 cm^{-1}, mono-oxide band at 1071 cm^{-1} (S-S=O), and cysteic acid band at 1171 cm^{-1} were also observed.[385]

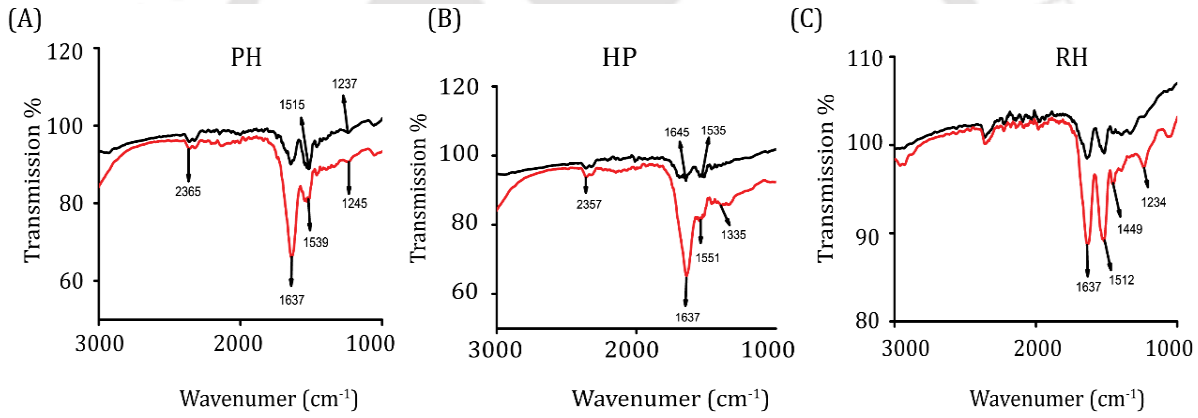

Figure 7.6 FTIR analysis of (A) PH, (B) HP and (C) RH before and after Cr adsorption. Black solid line represents IR spectral peaks before Cr (VI) adsorption and red solid line represents after Cr (VI) adsorption

7.3.7 Effect of dose, pH and time on adsorption capacity: The Cr (VI) removal efficiency of human hair at different pH was observed at an initial concentration of 50 mg/L. Increase in Cr (VI) adsorption was observed with time and reached equilibrium in 3h. The adsorption capacity of different adsorbents were found to be different at different pH conditions. At pH 2, the calculated adsorption capacity of PH was 15.14 mg/g, 13.27 mg/g for RH and 10.5 mg/g for HP (Figure 7.7 A). With increase

in pH, the adsorption capacity was found to be decreased. Higher absorption at low pH is due to the change in polarity of the adsorbents' surface, due to change in pH of Cr solution. Cr (VI) exists in different forms such as H_2CrO_4, $HCrO_4^-$, CrO_4^{2-} and $Cr_2O_7^{2-}$ in aqueous solution and the stability of these forms is pH dependent. The active form of Cr (VI) adsorbed is $HCrO_4^-$, which is stable at only low pH, but the concentration of $HCrO_4^-$ decreases with increase in pH. Adsorbents get protonated at lower pH. Electrostatic attraction between $HCrO_4^-$ and protonated adsorbent surface, promotes adsorption of Cr (VI).[386]

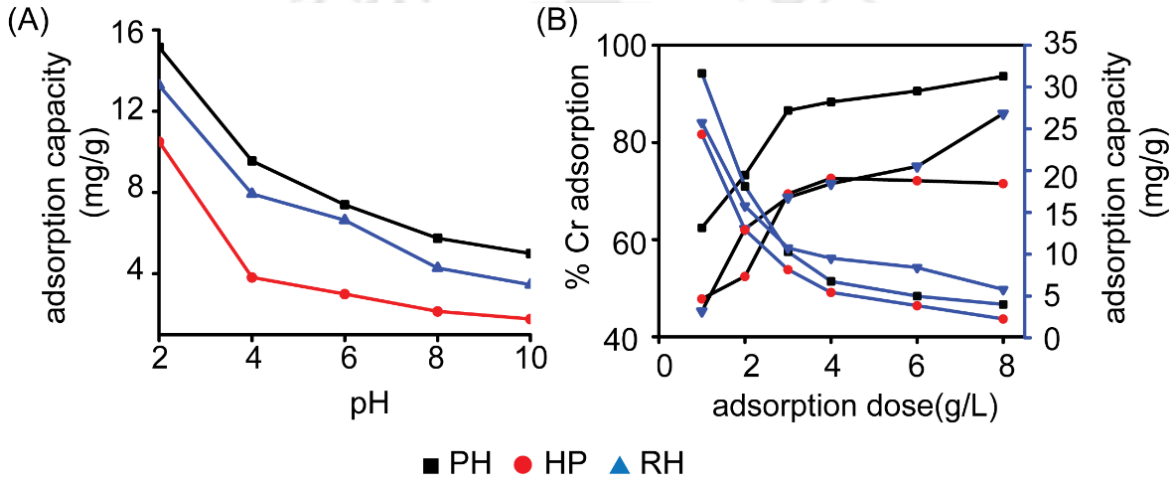

Figure 7.7 Chromium adsorption: Effect of pH (A) and adsorbent dose (B). Adsorption capacity (q_e) is calculated from the initial and final concentrations, volume of the solution and weight of the adsorbent (equation 2). Percentage adsorption (black) increases with increase in adsorption dose, while adsorption capacity (blue) decreases.

The effect of adsorbent dose on the adsorption of Cr at 25°C is shown in Figure 7.7 B. Results suggest that, percentage removal of chromium increases with adsorbent dose, whereas adsorption capacity decreases. On increasing the adsorbent dose from 0.5 to 8 g/L, the percentage Cr removal increased from 63% to approximately 94% for PH, 49 to 72% for HP and 47 to 86% for RH. This is due to the availability of active binding sites with increased adsorbent dose.[387] Earlier reported observations suggest that decrease in adsorbent capacity is likely due to the aggregation of adsorbent particles and unsaturated sites

present in adsorbents. Consequently, the active sites are deprived from being bound by metal ions.[388] Effect of initial Cr concentration with respect to time is shown in Figure 7.8. Cr adsorption efficiency of PH was found to be higher than HP and RH. This may be attributed to the higher surface area of PH, compared to RH. The lower Cr adsorption by HP may be attributed to the loss of active sites during pyrolysis in the muffle furnace. After 3h, no significant increase in the Cr (VI) adsorption was observed. This may be because of the non-availability of active sites of adsorption. Therefore, in all subsequent experiments, 3 hours was considered as the optimum contact time for adsorption of Cr.

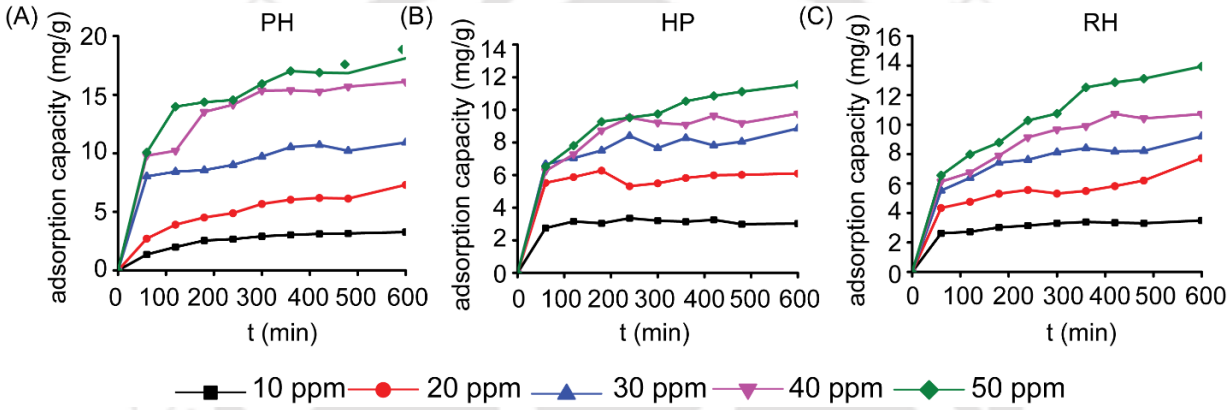

Figure 7.8 Change in adsorption capacity with time. Adsorption capacity increases with time, reaches saturation in 3 hours.

7.3.8 Adsorption Isotherm and adsorption kinetics: Adsorption isotherm and adsorption kinetics studies can provide significant insights while modelling specific treatment process. The equilibrium constant and adsorption isotherm were measured at a constant adsorbent dose (100 mg), with varying initial Cr (VI) concentration from 10 to 50 mg/L. The adsorption equilibrium was achieved by shaking Cr solution with adsorbents at 200 rpm. The Langmuir, Freundlich, and D-R isotherm models were employed to determine the adsorption capacity of the adsorbents (Figure 7.9). Parameters of the isotherm models are summarized in Table 7.1. The data suggests that the adsorption follows Freundlich isotherm model (R^2=0.99). The value of adsorption intensity (n=1.80) lying in the range of 1-10 confirms the

favorable conditions for adsorption.[376] The mean biosorption energy (E) was evaluated by D-R isotherm which gives crucial information on predicting the type of biosorption process. If E is less than 8 kJ/mol, the biosorption process is controlled by physisorption, whereas if E > 16 kJ/mol, chemisorption process is followed. When value of E lies between 8 and 16 kJ/mol, ion exchange process is followed.[389] In this study the value of E for PH, HP, and RH was calculated to be 0.955, 0.479 and 0.763 respectively. The mean free energy obtained for this study is significantly less than 8 kJ/mol in all the three cases. Though this data supports physisorption, the correlation with D-R isotherm is relatively poor. From Table 7.1, it may be observed that adsorption data fits well with Freundlich isotherm model (R^2=0.99), compared to Langmuir isotherm (R^2=0.94) and D-R isotherm (R^2=0.80). So, the Freundlich model can describe the adsorption equilibrium more precisely. The adsorption data of all the three adsorbents PH, HP and RH, did not fit well with the pseudo-first-order kinetic model, instead it is clearly following pseudo-second-order kinetics (R^2>0.98) (Figure 7.10, Table 7.2). Results therefore, indicates that the adsorption occurs through chemisorption process. The kinetic data were also analyzed using an intraparticle diffusion model indicating that the Cr (VI) adsorption occurs in two phases: the surface adsorption and intraprticle diffusion.[390] But the kinetic data was not supportive of this assumption.

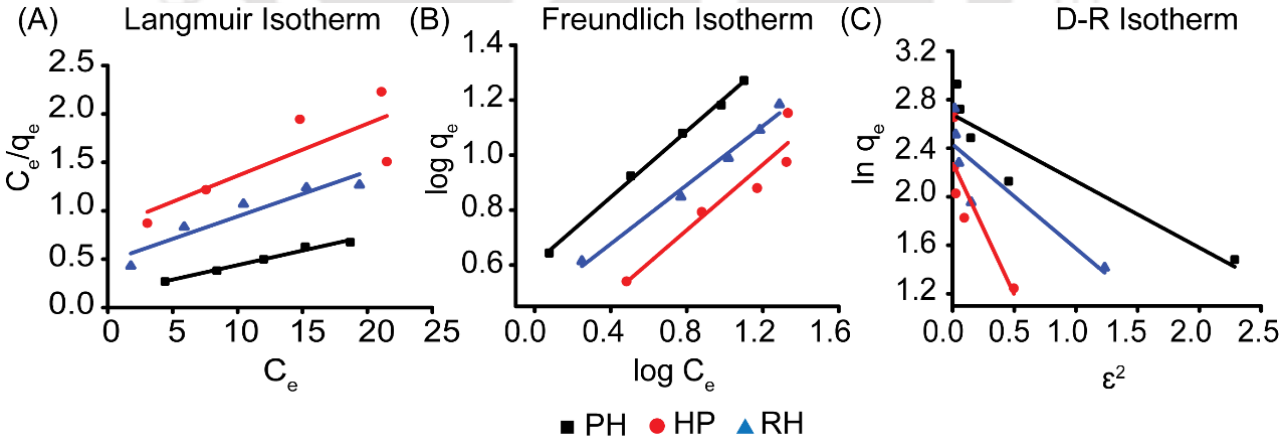

Figure 7.9 Adsorption Isotherm during chromium adsorption. (A) Langmuir Isotherm and (B) Freundlich Isotherm, and (C) Dubinin–Radushkevich Isotherm, suggesting the possible mechanism of adsorption at equilibrium.

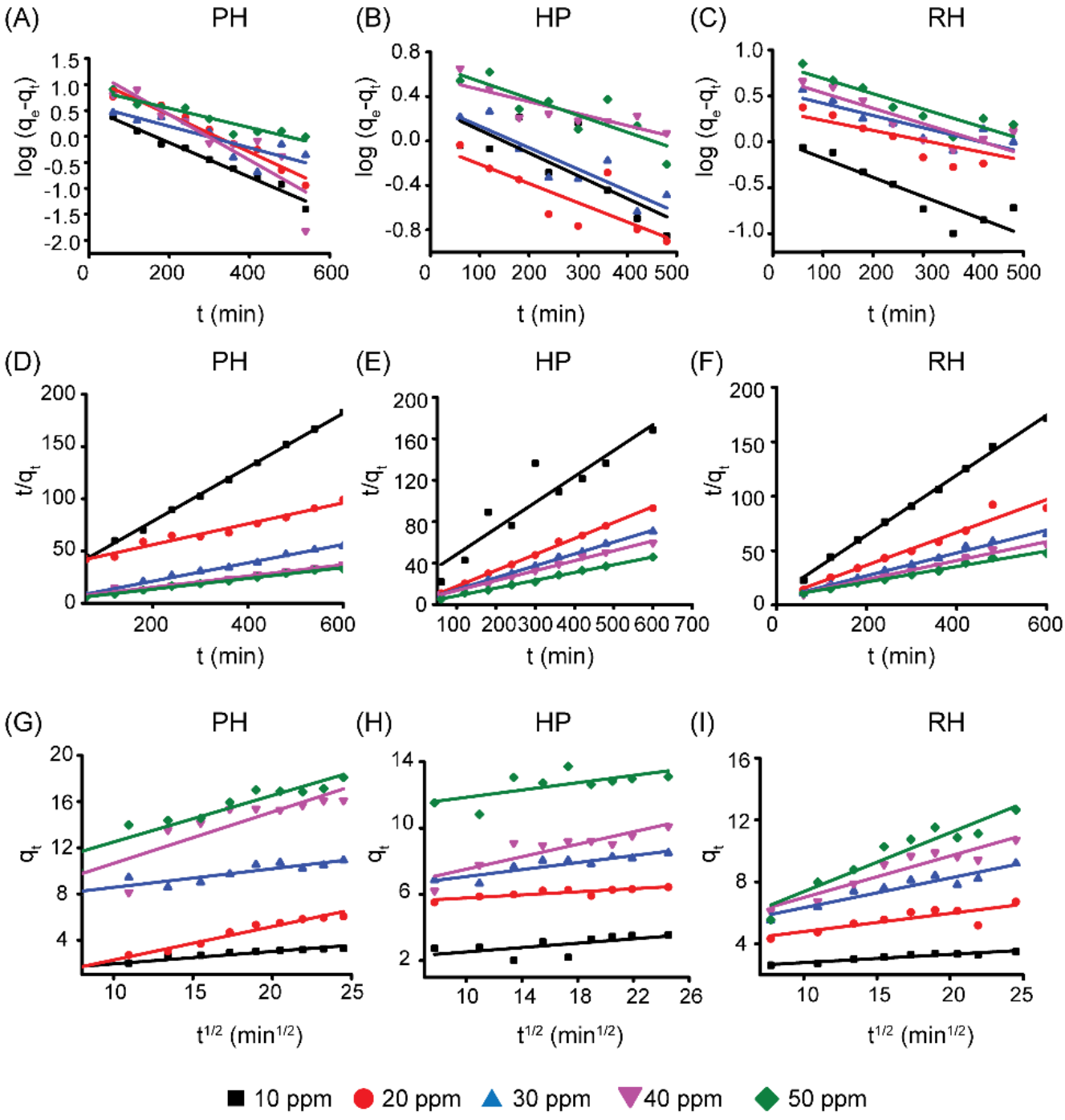

Figure 7.10 Adsorption kinetics during chromium adsorption. Graph A, B and C represents Pseudo-first order; graph D, E and F represents Pseudo-second order, and graph G, H and I represents intra-particle diffusion plot for three hair samples (PH, HP and RH respectively). The adsorption data follows pseudo second order kinetics, suggesting the possibility of chemisorption.

Table 7.1. Estimated values of parameters for different Isotherm models

Isotherm model	Parameters	PH	HP	RH
Langmuir	Q_0	27.94	18.60	21.52
	b	0.138	0.065	0.097
	R_L	0.42	0.60	0.51
	R^2	0.94	0.80	0.86
Freundlich	K_F	1.83	1.28	1.58
	$1/n_F$	0.60	0.59	0.53
	R^2	0.99	0.86	0.98
Dubinin–Radushkevich	Q	14.53	9.78	11.37
	E	0.955	0.479	0.763
	K	5.49E-07	2.18E-06	8.58E-07
	R^2	0.80	0.67	0.69

Table 7.2. Estimated values of parameters for different kinetic models

Adsorbents	**C_o**	**Pseudo-First-Order**			**Pseudo-Second-Order**			**Intraparticle Diffusion**		
	(mg/L)	**K_1 (min^{-1})**	**q_e (mg/g)**	**R^2**	**K_2 (g/mg/min)**	**q_e (mg/g)**	**R^2**	**C (mg/g)**	**K_{id} (mg/g/$min^{1/2}$)**	**R^2**
PH	10	0.457	1.719	0.974	0.04	3.87	0.997	0.868	0.107	0.89
	20	0.495	3.113	0.962	0.016	9.98	0.950	0.102	0.289	0.96
	30	0.270	1.754	0.615	0.046	11.38	0.985	6.954	0.161	0.78
	40	0.604	3.652	0.763	0.025	18.54	0.985	6.199	0.445	0.74
	50	0.255	2.489	0.885	0.029	19.31	0.985	8.469	0.403	0.87
HP	10	0.284	1.354	0.530	0.051	3.99	0.834	1.867	0.066	0.30
	20	0.275	0.963	0.596	0.102	6.50	0.997	5.317	0.046	0.72
	30	0.267	1.386	0.755	0.064	8.75	0.997	6.016	0.105	0.79

	40	0.149	1.76	0.665	0.048	10.44	0.982	5.635	0.188	0.76
	50	0.210	1.98	0.668	0.078	13.35	0.986	10.75	0.110	0.37
RH	10	0.004	1.032	0.760	0.091	3.628	0.997	2.256	0.053	0.88
	20	0.002	1.408	0.326	0.0059	6.63	0.950	3.161	0.117	0.65
	30	0.003	1.741	0.716	0.043	9.53	0.985	4.41	0.192	0.87
	40	0.038	2.018	0.173	0.035	11.50	0.985	4.302	0.268	0.87
	50	0.003	2.36	0.794	0.027	14.06	0.985	3.561	0.380	0.89

7.3.9 Desorption and Regeneration of hair samples: Repeated batch experiments have been performed to evaluate the reusability of the adsorbents. The reusability of adsorbents were tested by performing adsorption–desorption cycles of Cr (VI) up to three times using the same chromium solutions. The percentage Cr removal after regeneration was reduced to 40.12 % for PH, 25.34 % for HP, and 36.67 % for RH (Table 7.3).The significant decrease in the removal percentage may due to the non-availability of binding sites for chromium ions. The data however reaffirms the importance of pulverization, while preparing hair as a possible adsorbent in commercially usable chromium purification systems.

Table 7.3 Percentage Cr removal after Regeneration

Cycles	PH	HP	RH
1	75.21	56.68	45.34
2	59.41	43.43	48.23
3	40.12	25.34	36.67

7.3.10 Continuous Column Experiment: The batch adsorption study of Cr (VI) removal by different forms of hairs revealed that the PH and RH adsorb Cr (VI) at appreciable levels. Further application of RH for Cr (VI) removal was evaluated through continuous column operations. The two predominant parameters which affect the breakthrough curve are column height and flow rate. Here, we have tested the effect of different column heights at a flow rate of 5 mL/min, and obtained breakthrough a curve is illustrated in Figure 7.11. The different values from column experiments are shown in table 7.4. The results showed that on increasing column height from 5 to 20 cm, the Cr removal capacity of column increased from 47.67mg/g to 57.80 mg/g. The breakthrough time increased from 1.3 h (for 5 cm bed height) to 80 h (20 cm bed height) resulting in more adsorption efficiency of the column and more Cr removal from the passing solution.[391] At the completion of continuous column experiment, total Cr removed by column was observed to be enhanced from 240 mg (at 5cm bed height) to 1200 mg (at 20 cm bed height). It allows solution to get sufficient time to diffuse into the adsorbents, thus staying in the column for longer time, thus treating a larger volume of effluents. In the initial phase of the experiment, adsorption sites of the adsorbent are freely available to bind with Cr; resulting in negligible Cr

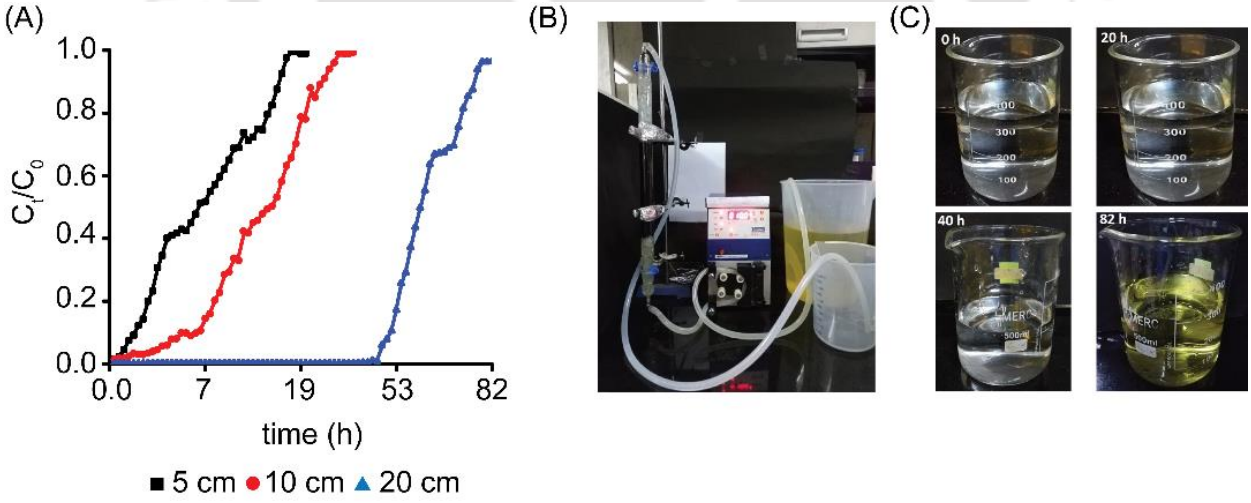

Figure 7.11 (A) Effect of bed height on breakthrough curve for Cr (VI) ion adsorption on human hair (C_0 = 50 ppm, flow rate = 5 mL/min). (B) Set-up of continuous column experiment, (C) Elution of Cr (VI) solution at different time

concentration in eluting solution. Gradually due to binding of Cr with the adsorbent, bottom part of the column bed was getting saturated, thus the adsorption zone gradually shifts towards the upper unsaturated part. As the column bed getting saturated, Cr concentration in eluting solution increases gradually. Cr concentration in eluting solution increases till the entire column bed (adsorption zone) gets saturated (breakthrough time), resulting in the increased breakthrough time (T_b) from 80 min (at 5cm bed height) to 2640 min (at 20 cm bed height). Increase in bed height therefore results in relatively more Cr (VI) removal and increased column efficiency.

Table 7.4. Breakthrough parameters at different bed height

Bed Height (cm)	**C_0 (mg/L)**	**M (g)**	**Q (mL/ min)**	**T_b (h)**	**t_{total} (h)**	**q_{total} (mg)**	**$Q_{e(exp)}$ (mg/g)**	**m_{total} (mg)**	**Y (%)**	**V_{eff} (mL)**
5	50	4	5	1.3	16	190.70	47.67	240	96	4800
10	50	9	5	2.5	30	447.3	49.7	450	97	9000
20	50	20	5	44	80	1156	57.80	1200	98	24000

7.4 Conclusions

This study focuses on the removal and reduction of Cr (VI) from wastewater. In this study, we have validated the Cr (VI) reduction efficiency of hybrid materials synthesized by magnetite and by 1,2-bis(tritylthio)ethane crystals. We observed that synthesized hybrid materials could reduce toxic Cr (VI) into non-toxic Cr (III) form up to 90%. While screening the adsorption capacity of different adsorbents for Cr (VI) removal, we found that hybrid materials and 1,2-bis(tritylthio)ethane crystals have relatively low Cr (VI) removal efficiency, compared to human hair. This directed us to investigate the capacity of human hair as a heavy metal adsorbent. We investigated the three forms of human hair, PH, HP, and RH as Cr adsorbent, and performed a series of experiments to validate their adsorption capacity. Various

parameters were investigated to understand the mechanism and kinetics of Cr (VI) removal. The adsorption capacity of PH was observed to be maximum (15.14 mg/g), followed by RH (13.27 mg/g) and HP (10.5 mg/g). The adsorption process was influenced by pH, and the maximum adsorption was observed at pH 2. Adsorption of Cr (VI) increases with an increase in the concentration of Cr (VI), and no significant increase in adsorption was observed after 3h, indicating an optimum time of 3 hours for typical Cr (VI) adsorption experimental cycles. An adsorption and desorption experiment was performed to validate the reusability of the adsorbent systems. The results suggest that for PH, efficiency of Cr (VI) removal decreased significantly from 75% to 40%, after three cycles. Kinetic studies were also performed to understand the adsorption process. Cr (VI) adsorption on human hair follows pseudo-second-order kinetic model, suggesting chemisorption. From the adsorption study, it is clear that the use of a bio-waste like hair, can be a simple, cost-effective, and efficient method for chromium removal can be used in large-scale applications. Table A1 shows the adsorbent capacity of some already reported bio-adsorbents, and our designed adsorbent system with pulverised hair (Appendix 2). Prototype of a possible device for chromium removal is in Appendix 3.

8

Conclusions and Future Directions

8.1 Conclusions

Fabrication of bioinspired molecules is opening up new possibilities in the field of medical technology. In recent years, peptide-based smart materials have attracted attention for fabrication of *de novo* designed functional molecules, owing to their biocompatibility, self-assembling property, and ease of synthesis. The development of new computational tools has increased our ability to design new peptide molecules for various applications. Although such systems have a vast application range and utility in every field, biological applications are of particular interest. This thesis explored the possibility of designing bio-inspired molecules, primarily focused on peptides, for four different applications, ranging from fluorescent mini-protein to antimicrobial peptide hydrogels for wound healing.

In chapter 4, we have designed the fluorescent molecule to overcome the limitations of intrinsic aromatic amino acid, tryptophan which is mainly responsible for fluorescence in proteins. Tryptophan needs to be excited at 280 nm, and emit in 340-350 nm range, and not in the visible region. To overcome this limitation, we have designed a self-folding hetero-chiral artificial protein, which was further examined to be adapted as fully functional molecule for sensing and imaging applications. The *de novo* designed fluorescent mini-protein has an unnatural amino acid, β-(1-Azulenyl)-L-Alanine, impregnated in the hydrophobic core, which allows a spectral separation from the native tryptophan signal. β-(1-Azulenyl)-L-Alanine can be selectively excited at 342 nm which emits in the visible region. *De novo* Designed proteins were synthesized by solid phase peptide synthesis and characterized by HPLC and mass spectrometry. Structure and stability were examined by spectroscopic and calorimetric methods. The work presented in this chapter opens- up the possibility of developing new molecules that can be adapted in imaging tools.

In chapter 5, we have explored the quantum confinement in peptide nanoassemblies. Phenylalanine dipeptides (FF) was reported to form nanotubes, which leads the creation of crystalline structures in the sub-nanometer scale. We have extended the molecular complexity, and *de novo* designed the syndiotactic phenylalanine hexamer peptide, FfFfFf-OH, which folds into a helical architecture, facilitating an extended phenylalanine network forming quantum confinement. The radius of the quantum dots was

estimated to be 1.07 nm. The utility of such peptide quantum dots can be further explored in electronics, semiconductors, imaging molecules, and drug delivery.

In chapter 6, we have designed three ultrashort peptide hydrogels and validated their antimicrobial potency. In this work, we have synthesized Fmoc-tripeptide hydrogels. The hydrogel characterization was performed by measuring visco-elasticity, in a typical frequency sweep and amplitude sweep analysis. The storage modulus (G') and loss modulus (G") were measured as a function of angular frequency. The designed hydrogels are also verified for their self-healing property, which has promising applications in tissue engineering. The synthesized hydrogels were further investigated as a potential antimicrobial hydrogel against both Gram-positive and Gram-negative bacteria. The mechanism of action of peptide hydrogels were investigated by measuring the reactive oxygen species (ROS) generation and outer membrane permeabilization assay. Results showed that peptide hydrogels enhanced ROS generation in the Gram-positive bacteria. More ROS level in the bacterial cells leads to increased osmotic and oxidative cellular stress inside the cells, resulting in bacterial cell death. We observed no significant increase in the ROS levels in Gram-negative bacteria. To investigate the reason of antibacterial activity in Gram-negative bacteria, we performed membrane permeabilization assay using NPN fluorophore, which gives enhancement in the fluorescence intensity on membrane disruption. Fmoc-FFH and Fmoc-FHF hydrogel treated *Pseudomonas aeruginosa* bacterial colonies showed enhanced NPN fluorescence, confirming outer membrane disruption. Our experiments have confirmed that the designed peptide hydrogels have good intrinsic antibacterial potency, against both Gram-positive and Gram-negative bacteria, which can be further validated as an antibacterial drug for topical applications. The work done in this chapter may lead to the fabrication of hydrogel molecules with inherent antimicrobial properties and can be exploited as a dressing material.

In chapter 7, we have investigated the issue of chromium (Cr) removal of a newly synthesized crystals of 1,2-bis(tritylthio)ethane, already reported from our laboratory. In this work, we have synthesized magnetite impregnated 1, 2-bis(tritylthio)ethane hybrid material (trityl-magnetite hybrid). The trityl-magnetite hybrid was investigated for its efficiency in reducing toxic Cr (VI) to Cr (III); and it showed 90% efficiency in reduction. In order to get a cost effective heavy metal adsorbents, we have compared the metal removal capacity of glass wools, human hair, 1, 2-bis(tritylthio)ethane crystals, trityl-magnetite

hybrid materials, and trityl-hair hybrid materials. We observed that human hair exhibited higher Cr removal efficiency as compared to other adsorbents. This prompted us to further investigate the human hair as potential Cr adsorbents. We have compared the three physical forms of human hair; pulverized hair (PH), hair powder (HP), and raw hair (RH) for their Cr removing ability by evaluating control parameters such as , effect of pH, effect of initial Cr concentration, and contact time. Among different human hair forms, PH showed more than that 92% Cr removal efficiency, and an adsorption capacity of 15.14 mg/g. Kinetic studies were performed to understand the adsorption process, which showed that the Cr (VI) adsorption on human hair follows pseudo-second-order kinetics, suggesting chemisorption. This work presented in this chapter gives a practical solution in developing cost-effective chromium removing device by utilizing bio-waste materials. This project is especially important, because it directly addresses the need of larger population in this geographic area. Eastern states of India, western regions of China and Bangladesh have been suffering from contamination of heavy metals in drinking water for a very long time.

8.2 Future Directions

De novo designed peptide molecules have broad range of applications, and ultrashort peptides opens up new possibilities of fabricating smart materials. The designed peptide molecules in this thesis lead the following objectives and opportunities for future exploration;

- Development of fluorescent molecular probes as imaging tools for biological applications
- Translation of peptide quantum dots for optical, electrical, and semiconductor applications
- *In vivo* investigation of antimicrobial peptide hydrogels for topical application primarily focused on diabetic foot ulcers and wound healing
- Fabrication of a cost-effective chromium removing device

References

1. McConney, M. E.; Anderson, K. D.; Brott, L. L.; Naik, R. R.; Tsukruk, V. V., Bioinspired material approaches to sensing. *Advanced Functional Materials* **2009,** *19* (16), 2527-2544.
2. Bromley, E. H.; Channon, K.; Moutevelis, E.; Woolfson, D. N., Peptide and protein building blocks for synthetic biology: from programming biomolecules to self-organized biomolecular systems. *ACS chemical biology* **2008,** *3* (1), 38-50.
3. Whitesides, G. M.; Grzybowski, B., Self-assembly at all scales. *Science* **2002,** *295* (5564), 2418-2421.
4. Boyle, A. L.; Woolfson, D. N., Rational Design of Peptide-Based Biosupramolecular Systems. *Supramolecular Chemistry: From Molecules to Nanomaterials* **2012**.
5. Jayawickramarajah, J.; Wilson, A., Volume 5: Supramolecular Medicinal Chemistry and Chemical Biology. **2017**.
6. Stephanopoulos, N.; Ortony, J. H.; Stupp, S. I., Self-assembly for the synthesis of functional biomaterials. *Acta materialia* **2013,** *61* (3), 912-930.
7. Stupp, S. I., Self-assembly and biomaterials. *Nano letters* **2010,** *10* (12), 4783-4786.
8. Baker, E. G.; Bartlett, G. J.; Porter Goff, K. L.; Woolfson, D. N., Miniprotein design: Past, present, and prospects. *Accounts of chemical research* **2017,** *50* (9), 2085-2092.
9. Qiu, L.; Pabit, S. A.; Roitberg, A. E.; Hagen, S. J., Smaller and faster: The 20-residue Trp-cage protein folds in 4 μs. *Journal of the American Chemical Society* **2002,** *124* (44), 12952-12953.
10. Craven, T. W.; Cho, M.-K.; Traaseth, N. J.; Bonneau, R.; Kirshenbaum, K., A miniature protein stabilized by a cation− π interaction network. *Journal of the American Chemical Society* **2016,** *138* (5), 1543-1550.
11. McKnight, C. J.; Matsudaira, P. T.; Kim, P. S., NMR structure of the 35-residue villin headpiece subdomain. *Nature structural biology* **1997,** *4* (3), 180-184.
12. Baker, E. G.; Williams, C.; Hudson, K. L.; Bartlett, G. J.; Heal, J. W.; Goff, K. L. P.; Sessions, R. B.; Crump, M. P.; Woolfson, D. N., Engineering protein stability with atomic precision in a monomeric miniprotein. *Nature chemical biology* **2017,** *13* (7), 764-770.
13. Ulijn, R. V.; Smith, A. M., Designing peptide based nanomaterials. *Chemical Society Reviews* **2008,** *37* (4), 664-675.
14. Mazumdar, A.; Haddad, Y.; Milosavljevic, V.; Michalkova, H.; Guran, R.; Bhowmick, S.; Moulick, A., Peptide-carbon quantum dots conjugate, derived from human retinoic acid receptor responder protein 2, against antibiotic-resistant gram positive and gram negative pathogenic bacteria. *Nanomaterials* **2020,** *10* (2), 325.
15. Liu, B. R.; Huang, Y.-W.; Chiang, H.-J.; Lee, H.-J., Cell-penetrating peptide-functionized quantum dots for intracellular delivery. *Journal of nanoscience and nanotechnology* **2010,** *10* (12), 7897-7905.
16. Handelman, A.; Beker, P.; Amdursky, N.; Rosenman, G., Physics and engineering of peptide supramolecular nanostructures. *Physical Chemistry Chemical Physics* **2012,** *14* (18), 6391-6408.
17. Gan, Z.; Wu, X.; Zhu, X.; Shen, J., Light-Induced Ferroelectricity in Bioinspired Self-Assembled Diphenylalanine Nanotubes/Microtubes. *Angewandte Chemie International Edition* **2013,** *52* (7), 2055-2059.
18. Kholkin, A.; Amdursky, N.; Bdikin, I.; Gazit, E.; Rosenman, G., Strong piezoelectricity in bioinspired peptide nanotubes. *ACS nano* **2010,** *4* (2), 610-614.
19. Amdursky, N.; Molotskii, M.; Gazit, E.; Rosenman, G., Elementary building blocks of self-assembled peptide nanotubes. *Journal of the American Chemical Society* **2010,** *132* (44), 15632-15636.

20. Salick, D. A.; Kretsinger, J. K.; Pochan, D. J.; Schneider, J. P., Inherent antibacterial activity of a peptide-based β-hairpin hydrogel. *Journal of the American Chemical Society* **2007,** *129* (47), 14793-14799.
21. Cao, F.; Mei, L.; Zhu, G.; Song, M.; Zhang, X., An injectable molecular hydrogel assembled by antimicrobial peptide PAF26 for antimicrobial application. *RSC advances* **2019,** *9* (53), 30803-30808.
22. Gahane, A. Y.; Ranjan, P.; Singh, V.; Sharma, R. K.; Sinha, N.; Sharma, M.; Chaudhry, R.; Thakur, A. K., Fmoc-phenylalanine displays antibacterial activity against Gram-positive bacteria in gel and solution phases. *Soft matter* **2018,** *14* (12), 2234-2244.
23. Lehn, J.-M., Supramolecular chemistry. *Science* **1993,** *260* (5115), 1762-1764.
24. Yadav, S.; Sharma, A. K.; Kumar, P., Nanoscale self-assembly for therapeutic delivery. *Frontiers in bioengineering and biotechnology* **2020,** *8*, 127.
25. Trasatti, J. P.; Woo, J.; Ladiwala, A.; Cramer, S.; Karande, P., Rational design of peptide affinity ligands for the purification of therapeutic enzymes. *Biotechnology progress* **2018,** *34* (4), 987-998.
26. Tran, N. H.; Zhang, X.; Xin, L.; Shan, B.; Li, M., De novo peptide sequencing by deep learning. *Proceedings of the National Academy of Sciences* **2017,** *114* (31), 8247-8252.
27. Ramakrishnan, V.; Ranbhor, R.; Durani, S., Simulated folding in polypeptides of diversified molecular tacticity: implications for protein folding and de novo design. *Biopolymers: Original Research on Biomolecules* **2005,** *78* (2), 96-105.
28. Ramakrishnan, V.; Ranbhor, R.; Kumar, A.; Durani, S., The link between sequence and conformation in protein structures appears to be stereochemically established. *The Journal of Physical Chemistry B* **2006,** *110* (18), 9314-9323.
29. Urry, D.; Goodall, M.; Glickson, J.; Mayers, D., The gramicidin A transmembrane channel: characteristics of head-to-head dimerized π (L, D) helices. *Proceedings of the National Academy of Sciences* **1971,** *68* (8), 1907-1911.
30. Aravinda, S.; Shamala, N.; Roy, R. S.; Balaram, P., Non-protein amino acids in peptide design. *Journal of Chemical Sciences* **2003,** *115* (5-6), 373-400.
31. Zhai, C.; Schreiber, C. L.; Padilla-Coley, S.; Oliver, A. G.; Smith, B. D., Fluorescent Self-Threaded Peptide Probes for Biological Imaging. *Angewandte Chemie International Edition* **2020,** *59* (52), 23740-23747.
32. Walport, L. J.; Obexer, R.; Suga, H., Strategies for transitioning macrocyclic peptides to cell-permeable drug leads. *Current Opinion in Biotechnology* **2017,** *48*, 242-250.
33. Nair, R. V.; Baravkar, S. B.; Ingole, T. S.; Sanjayan, G. J., Synthetic turn mimetics and hairpin nucleators: Quo Vadimus? *Chemical Communications* **2014,** *50* (90), 13874-13884.
34. Fan, Z.; Chang, Y.; Cui, C.; Sun, L.; Wang, D. H.; Pan, Z.; Zhang, M., Near infrared fluorescent peptide nanoparticles for enhancing esophageal cancer therapeutic efficacy. *Nature Communications* **2018,** *9* (1), 2605.
35. Wang, J.; Zhang, J.; Wang, J.; Fang, G.; Liu, J.; Wang, S., Fluorescent peptide probes for organophosphorus pesticides detection. *Journal of Hazardous Materials* **2020,** *389*, 122074.
36. Siepi, M.; Oliva, R.; Petraccone, L.; Del Vecchio, P.; Ricca, E.; Isticato, R.; Lanzilli, M.; Maglio, O.; Lombardi, A.; Leone, L., Fluorescent peptide dH3w: A sensor for environmental monitoring of mercury (II). *PloS one* **2018,** *13* (10), e0204164.
37. Masters, B. R., Molecular fluorescence: principles and applications. *Journal of Biomedical Optics* **2013,** *18* (3), 039901.
38. Fan, Z.; Sun, L.; Huang, Y.; Wang, Y.; Zhang, M., Bioinspired fluorescent dipeptide nanoparticles for targeted cancer cell imaging and real-time monitoring of drug release. *Nature Nanotechnology* **2016,** *11* (4), 388-394.

39. Tao, K.; Fan, Z.; Sun, L.; Makam, P.; Tian, Z.; Ruegsegger, M.; Shaham-Niv, S.; Hansford, D.; Aizen, R.; Pan, Z., Quantum confined peptide assemblies with tunable visible to near-infrared spectral range. *Nature communications* **2018,** *9* (1), 1-11.
40. Prakash, V.; Ranbhor, R.; Ramakrishnan, V., De Novo Designed Heterochiral Blue Fluorescent Protein. *ACS Omega* **2020,** *5* (41), 26382-26388.
41. Bishop, J. L.; Finlay, B. B., Friend or foe? Antimicrobial peptides trigger pathogen virulence. *Trends in molecular medicine* **2006,** *12* (1), 3-6.
42. Boman, H. G., Peptide antibiotics and their role in innate immunity. *Annual review of immunology* **1995,** *13*, 61-92.
43. Hazam, P. K.; Singh, A.; Chaudhary, N.; Ramakrishnan, V., Bactericidal potency and extended serum life of stereo-chemically engineered peptides against Mycobacterium. *International Journal of Peptide Research and Therapeutics* **2019,** *25* (2), 465-472.
44. Hazam, P. K.; Akhil, R.; Jerath, G.; Saikia, J.; Ramakrishnan, V., Topological effects on the designability and bactericidal potency of antimicrobial peptides. *Biophysical chemistry* **2019,** *248*, 1-8.
45. Hazam, P. K.; Jerath, G.; Chaudhary, N.; Ramakrishnan, V., Peptido-mimetic Approach in the Design of Syndiotactic Antimicrobial Peptides. *International Journal of Peptide Research and Therapeutics* **2018,** *24* (2), 299-307.
46. Hazam, P. K.; Phukan, C.; Akhil, R.; Singh, A.; Ramakrishnan, V., Antimicrobial effects of syndiotactic polypeptides. *Scientific reports* **2021,** *11* (1), 1-10.
47. Langel, U., *Cell-penetrating peptides: processes and applications*. CRC press: 2002.
48. Pujals, S.; Fernández-Carneado, J.; Ludevid, M. D.; Giralt, E., D-SAP: a new, noncytotoxic, and fully protease resistant cell-penetrating peptide. *ChemMedChem: Chemistry Enabling Drug Discovery* **2008,** *3* (2), 296-301.
49. Jerath, G.; Goyal, R.; Trivedi, V.; Santhoshkumar, T.; Ramakrishnan, V., Syndiotactic peptides for targeted delivery. *Acta biomaterialia* **2019,** *87*, 130-139.
50. Goyal, R.; Jerath, G.; Akhil, R.; Chandrasekharan, A.; Puppala, E. R.; Ponneganti, S.; Sarma, A.; Naidu, V.; Santhoshkumar, T.; Ramakrishnan, V., Geometry encoded functional programming of tumor homing peptides for targeted drug delivery. *Journal of Controlled Release* **2021,** *333*, 16-27.
51. Goyal, R.; Jerath, G.; Chandrasekharan, A.; Christian, Y.; Kumar, T.; Ramakrishnan, V., Molecular hybridization combining tumor homing and penetrating peptide domains for cellular targeting. *Drug delivery and translational research* **2021**, 1-8.
52. Damborsky, J.; Brezovsky, J., Computational tools for designing and engineering biocatalysts. *Current Opinion in Chemical Biology* **2009,** *13* (1), 26-34.
53. Garcia-Viloca, M.; Gao, J.; Karplus, M.; Truhlar, D. G., How Enzymes Work: Analysis by Modern Rate Theory and Computer Simulations. *Science* **2004,** *303* (5655), 186-195.
54. Hellinga, H. W.; Richards, F. M., Construction of new ligand binding sites in proteins of known structure. I. Computer-aided modeling of sites with pre-defined geometry. *Journal of molecular biology* **1991,** *222* (3), 763-85.
55. Dahiyat, B. I.; Mayo, S. L., Protein design automation. *Protein science : a publication of the Protein Society* **1996,** *5* (5), 895-903.
56. Zanghellini, A.; Jiang, L.; Wollacott, A. M.; Cheng, G.; Meiler, J.; Althoff, E. A.; Röthlisberger, D.; Baker, D., New algorithms and an in silico benchmark for computational enzyme design. *Protein science : a publication of the Protein Society* **2006,** *15* (12), 2785-2794.
57. Kolundzic, F.; Noshi, M. N.; Tjandra, M.; Movassaghi, M.; Miller, S. J., Chemoselective and enantioselective oxidation of indoles employing aspartyl peptide catalysts. *Journal of the American Chemical Society* **2011,** *133* (23), 9104-9111.

58. Cherny, I.; Gazit, E., Amyloids: not only pathological agents but also ordered nanomaterials. *Angewandte Chemie International Edition* **2008,** *47* (22), 4062-4069.
59. Fichman, G.; Gazit, E., Self-assembly of short peptides to form hydrogels: Design of building blocks, physical properties and technological applications. *Acta biomaterialia* **2014,** *10* (4), 1671-1682.
60. Woolfson, D. N., The design of coiled-coil structures and assemblies. *Advances in protein chemistry* **2005,** *70*, 79-112.
61. Fishwick, C. W.; Beevers, A. J.; Carrick, L. M.; Whitehouse, C. D.; Aggeli, A.; Boden, N., Structures of helical β-tapes and twisted ribbons: the role of side-chain interactions on twist and bend behavior. *Nano letters* **2003,** *3* (11), 1475-1479.
62. Pires, M. M.; Przybyla, D. E.; Chmielewski, J., A metal–collagen peptide framework for three-dimensional cell culture. *Angewandte Chemie International Edition* **2009,** *48* (42), 7813-7817.
63. Cui, H.; Muraoka, T.; Cheetham, A. G.; Stupp, S. I., Self-assembly of giant peptide nanobelts. *Nano letters* **2009,** *9* (3), 945-951.
64. Johnsson, K.; Allemann, R. K.; Widmer, H.; Benner, S. A., Synthesis, structure and activity of artificial, rationally designed catalytic polypeptides. *Nature* **1993,** *365* (6446), 530-532.
65. Broo, K. S.; Brive, L.; Ahlberg, P.; Baltzer, L., Catalysis of hydrolysis and transesterification reactions of p-nitrophenyl esters by a designed helix− loop− helix dimer. *Journal of the American Chemical Society* **1997,** *119* (47), 11362-11372.
66. Allert, M.; Baltzer, L., Noncovalent Binding of a Reaction Intermediate by a Designed Helix-Loop-Helix Motif—Implications for Catalyst Design. *ChemBioChem* **2003,** *4* (4), 306-318.
67. Tanaka, K.; Mori, A.; Inoue, S., The cyclic dipeptide cyclo [(S)-phenylalanyl-(S)-histidyl] as a catalyst for asymmetric addition of hydrogen cyanide to aldehydes. *The Journal of organic chemistry* **1990,** *55* (1), 181-185.
68. Reja, A.; Afrose, S. P.; Das, D., Aldolase Cascade Facilitated by Self-Assembled Nanotubes from Short Peptide Amphiphiles. *Angewandte Chemie* **2020,** *132* (11), 4359-4364.
69. Babaei, P.; Safaei-Ghomi, J., L-proline covered N doped graphene quantum dots modified CuO/ZnO hexagonal nanocomposite as a robust retrievable catalyst in synthesis of substituted chiral 2-amino-4H-chromenes. *Materials Chemistry and Physics* **2021**, 124668.
70. Eder, U.; Sauer, G.; Wiechert, R., New type of asymmetric cyclization to optically active steroid CD partial structures. *Angewandte Chemie International Edition in English* **1971,** *10* (7), 496-497.
71. Fuentes, J. A.; Lebl, T.; Slawin, A. M.; Clarke, M. L., Synthesis of organocatalysts using non-covalent chemistry; understanding the reactivity of ProNap, an enamine-type organocatalyst that can self assemble with complementary co-catalysts. *Chemical Science* **2011,** *2* (10), 1997-2005.
72. Rodríguez-Llansola, F.; Escuder, B.; Hamley, I. W.; Hayes, W.; Miravet, J. F., Structural and morphological studies of the dipeptide based L-Pro-L-Val organocatalytic gels and their rheological behaviour. *Soft Matter* **2012,** *8* (34), 8865-8872.
73. Rodríguez-Llansola, F.; Escuder, B.; Miravet, J. F., Remarkable increase in basicity associated with supramolecular gelation. *Organic & Biomolecular Chemistry* **2009,** *7* (15), 3091-3094.
74. Pelin, J. N.; Gerbelli, B. B.; Edwards-Gayle, C. J.; Aguilar, A. M.; Castelletto, V.; Hamley, I. W.; Alves, W. A., Amyloid Peptide Mixtures: Self-Assembly, Hydrogelation, Nematic Ordering, and Catalysts in Aldol Reactions. *Langmuir* **2020,** *36* (11), 2767-2774.
75. Guler, M. O.; Stupp, S. I., A self-assembled nanofiber catalyst for ester hydrolysis. *Journal of the American Chemical Society* **2007,** *129* (40), 12082-12083.
76. Huang, Z.; Guan, S.; Wang, Y.; Shi, G.; Cao, L.; Gao, Y.; Dong, Z.; Xu, J.; Luo, Q.; Liu, J., Self-assembly of amphiphilic peptides into bio-functionalized nanotubes: a novel hydrolase model. *Journal of Materials Chemistry B* **2013,** *1* (17), 2297-2304.

77. Wang, M.; Lv, Y.; Liu, X.; Qi, W.; Su, R.; He, Z., Enhancing the activity of peptide-based artificial hydrolase with catalytic Ser/His/Asp triad and molecular imprinting. *ACS applied materials & interfaces* **2016,** *8* (22), 14133-14141.
78. Bélières, M.; Chouini-Lalanne, N.; Déjugnat, C., Synthesis, self-assembly, and catalytic activity of histidine-based structured lipopeptides for hydrolysis reactions in water. *RSC Advances* **2015,** *5* (45), 35830-35842.
79. Yamashita, M. M.; Wesson, L.; Eisenman, G.; Eisenberg, D., Where metal ions bind in proteins. *Proceedings of the National Academy of Sciences* **1990,** *87* (15), 5648-5652.
80. Sovago, I.; Kallay, C.; Varnagy, K., Peptides as complexing agents: Factors influencing the structure and thermodynamic stability of peptide complexes. *Coordination Chemistry Reviews* **2012,** *256* (19-20), 2225-2233.
81. Marsh, E. N. G.; DeGrado, W. F., Noncovalent self-assembly of a heterotetrameric diiron protein. *Proceedings of the National Academy of Sciences* **2002,** *99* (8), 5150-5154.
82. Al-Garawi, Z. S.; McIntosh, B. A.; Neill-Hall, D.; Hatimy, A. A.; Sweet, S. M.; Bagley, M. C.; Serpell, L. C., The amyloid architecture provides a scaffold for enzyme-like catalysts. *Nanoscale* **2017,** *9* (30), 10773-10783.
83. Laungani, A. C.; Slattery, J. M.; Krossing, I.; Breit, B., Supramolecular Bidentate Ligands by Metal-Directed in situ Formation of Antiparallel β-Sheet Structures and Application in Asymmetric Catalysis. *Chemistry–A European Journal* **2008,** *14* (15), 4488-4502.
84. Rajagopal, K.; Schneider, J. P., Self-assembling peptides and proteins for nanotechnological applications. *Current opinion in structural biology* **2004,** *14* (4), 480-486.
85. Zhang, S.; Rich, A., Direct conversion of an oligopeptide from a β-sheet to an α-helix: a model for amyloid formation. *Proceedings of the National Academy of Sciences* **1997,** *94* (1), 23-28.
86. Ghadiri, M. R.; Soares, C.; Choi, C., A convergent approach to protein design. Metal ion-assisted spontaneous self-assembly of a polypeptide into a triple-helix bundle protein. *Journal of the American Chemical Society* **1992,** *114* (3), 825-831.
87. Wu, L.; Lin, B.; Yang, H.; Chen, J.; Mao, Z.; Wang, W.; Gao, C., Enzyme-responsive multifunctional peptide coating of gold nanorods improves tumor targeting and photothermal therapy efficacy. *Acta biomaterialia* **2019,** *86*, 363-372.
88. Meyer, D. E.; Chilkoti, A., Quantification of the effects of chain length and concentration on the thermal behavior of elastin-like polypeptides. *Biomacromolecules* **2004,** *5* (3), 846-851.
89. Prabhukumar, G.; Matsumoto, M.; Mulchandani, A.; Chen, W., Cadmium removal from contaminated soil by tunable biopolymers. *Environmental science & technology* **2004,** *38* (11), 3148-3152.
90. Sreekumar, P. G.; Li, Z.; Wang, W.; Spee, C.; Hinton, D. R.; Kannan, R.; MacKay, J. A., Intra-vitreal αB crystallin fused to elastin-like polypeptide provides neuroprotection in a mouse model of age-related macular degeneration. *Journal of Controlled Release* **2018,** *283*, 94-104.
91. Anelli, P. L.; Asakawa, M.; Ashton, P. R.; Bissell, R. A.; Clavier, G.; Górski, R.; Kaifer, A. E.; Langford, S. J.; Mattersteig, G.; Menzer, S., Toward controllable molecular shuttles. *Chemistry–A European Journal* **1997,** *3* (7), 1113-1135.
92. Cárdenas, D. J.; Livoreil, A.; Sauvage, J.-P., Redox control of the ring-gliding motion in a Cu-complexed catenane: A process involving three distinct geometries. *Journal of the American Chemical Society* **1996,** *118* (47), 11980-11981.
93. Collin, J.-P.; Gavinã, P.; Sauvage, J.-P., Electrochemically induced molecular motions in a copper (I) complex pseudorotaxane. *Chemical Communications* **1996,** (17), 2005-2006.
94. Villalva, J.; Nieto-Ortega, B.; Melle-Franco, M.; Perez, E. M., Quasi-Barrierless Submolecular Motion in Mechanically Interlocked Carbon Nanotubes. *The Journal of Physical Chemistry C* **2020,** *124* (28), 15541-15546.

95. Qiu, Y.; Song, B.; Pezzato, C.; Shen, D.; Liu, W.; Zhang, L.; Feng, Y.; Guo, Q.-H.; Cai, K.; Li, W., A precise polyrotaxane synthesizer. *Science* **2020,** *368* (6496), 1247-1253.
96. Singh, D.; Bisland, S. K.; Kawamura, K.; Gariépy, J., Peptide-based intracellular shuttle able to facilitate gene transfer in mammalian cells. *Bioconjugate chemistry* **1999,** *10* (5), 745-754.
97. Chen, S.; Wang, Y.; Nie, T.; Bao, C.; Wang, C.; Xu, T.; Lin, Q.; Qu, D.-H.; Gong, X.; Yang, Y., An artificial molecular shuttle operates in lipid bilayers for ion transport. *Journal of the American Chemical Society* **2018,** *140* (51), 17992-17998.
98. Garcia, J.; Arranz-Gibert, P.; Sánchez-Navarro, M.; Giralt, E.; Teixidó, M., Peptide Shuttle-Mediated Delivery for Brain Gene Therapies. *Current Topics in Medicinal Chemistry* **2020**.
99. Bukchin, A.; Sanchez-Navarro, M.; Carrera, A.; Resa-Pares, C.; Castillo-Ecija, H.; Balaguer-Lluna, L.; Teixidó, M.; Olaciregui, N. G.; Giralt, E.; Carcaboso, A. M., Amphiphilic polymeric nanoparticles modified with a protease-resistant peptide shuttle for the delivery of SN-38 in diffuse intrinsic pontine glioma. *ACS Applied Nano Materials* **2021,** *4* (2), 1314-1329.
100. Farha, O. K.; Yazaydın, A. Ö.; Eryazici, I.; Malliakas, C. D.; Hauser, B. G.; Kanatzidis, M. G.; Nguyen, S. T.; Snurr, R. Q.; Hupp, J. T., De novo synthesis of a metal–organic framework material featuring ultrahigh surface area and gas storage capacities. *Nature chemistry* **2010,** *2* (11), 944-948.
101. Lee, J.; Farha, O. K.; Roberts, J.; Scheidt, K. A.; Nguyen, S. T.; Hupp, J. T., Metal–organic framework materials as catalysts. *Chemical Society Reviews* **2009,** *38* (5), 1450-1459.
102. Qiu, S.; Xue, M.; Zhu, G., Metal–organic framework membranes: from synthesis to separation application. *Chemical Society Reviews* **2014,** *43* (16), 6116-6140.
103. Horcajada, P.; Serre, C.; Vallet-Regí, M.; Sebban, M.; Taulelle, F.; Férey, G., Metal–organic frameworks as efficient materials for drug delivery. *Angewandte chemie* **2006,** *118* (36), 6120-6124.
104. Cui, R.; Zhao, P.; Yan, Y.; Bao, G.; Damirin, A.; Liu, Z., Outstanding Drug-Loading/Release Capacity of Hollow Fe-Metal–Organic Framework-Based Microcapsules: A Potential Multifunctional Drug-Delivery Platform. *Inorganic Chemistry* **2021,** *60* (3), 1664-1671.
105. Wang, X.-G.; Dong, Z.-Y.; Cheng, H.; Wan, S.-S.; Chen, W.-H.; Zou, M.-Z.; Huo, J.-W.; Deng, H.-X.; Zhang, X.-Z., A multifunctional metal–organic framework based tumor targeting drug delivery system for cancer therapy. *Nanoscale* **2015,** *7* (38), 16061-16070.
106. Teplensky, M. H.; Fantham, M.; Poudel, C.; Hockings, C.; Lu, M.; Guna, A.; Aragones-Anglada, M.; Moghadam, P. Z.; Li, P.; Farha, O. K., A highly porous metal-organic framework system to deliver payloads for gene knockdown. *Chem* **2019,** *5* (11), 2926-2941.
107. Horcajada, P.; Gref, R.; Baati, T.; Allan, P. K.; Maurin, G.; Couvreur, P.; Ferey, G.; Morris, R. E.; Serre, C., Metal–organic frameworks in biomedicine. *Chemical reviews* **2012,** *112* (2), 1232-1268.
108. Sun, Z.; Wu, S.; Peng, Y.; Wang, M.; Jalalah, M.; Al-Assiri, M.; Harraz, F. A.; Yang, J.; Li, G., Sensor array for rapid pathogens identification fabricated with peptide-conjugated 2D metal-organic framework nanosheets. *Chemical Engineering Journal* **2021,** *405*, 126707.
109. Skwarczynski, M.; Toth, I., Peptide-based synthetic vaccines. *Chemical science* **2016,** *7* (2), 842-854.
110. Sesardic, D., Synthetic peptide vaccines. *Journal of medical microbiology* **1993,** *39* (4), 241-242.
111. Bijker, M. S.; Melief, C. J.; Offringa, R.; Van Der Burg, S. H., Design and development of synthetic peptide vaccines: past, present and future. *Expert review of vaccines* **2007,** *6* (4), 591-603.
112. Steele, J. T.; ALLEN, S. D.; KAUMAYA, P. T., Cancer Immunotherapy with Rationally Designed Synthetic Peptides. In *Handbook of Biologically Active Peptides*, Elsevier: 2006; pp 491-498.
113. Purcell, A. W.; McCluskey, J.; Rossjohn, J., More than one reason to rethink the use of peptides in vaccine design. *Nature reviews Drug discovery* **2007,** *6* (5), 404-414.

114. Liu, Y.; McNevin, J.; Zhao, H.; Tebit, D. M.; Troyer, R. M.; McSweyn, M.; Ghosh, A. K.; Shriner, D.; Arts, E. J.; McElrath, M. J., Evolution of human immunodeficiency virus type 1 cytotoxic T-lymphocyte epitopes: fitness-balanced escape. *Journal of virology* **2007,** *81* (22), 12179-12188.
115. Epstein, J. E.; Giersing, B.; Mullen, G.; Moorthy, V.; Richie, T. L., Malaria vaccines: are we getting closer? *Current opinion in molecular therapeutics* **2007,** *9* (1), 12-24.
116. Greten, T. F.; Forner, A.; Korangy, F.; N'Kontchou, G.; Barget, N.; Ayuso, C.; Ormandy, L. A.; Manns, M. P.; Beaugrand, M.; Bruix, J., A phase II open label trial evaluating safety and efficacy of a telomerase peptide vaccination in patients with advanced hepatocellular carcinoma. *BMC cancer* **2010,** *10* (1), 1-7.
117. Zhao, X.; Pan, F.; Xu, H.; Yaseen, M.; Shan, H.; Hauser, C. A.; Zhang, S.; Lu, J. R., Molecular self-assembly and applications of designer peptide amphiphiles. *Chemical Society Reviews* **2010,** *39* (9), 3480-3498.
118. Blanco, F. J.; Rivas, G.; Serrano, L., A short linear peptide that folds into a native stable β-hairpin in aqueous solution. *Nature structural biology* **1994,** *1* (9), 584-590.
119. Zorzi, A.; Deyle, K.; Heinis, C., Cyclic peptide therapeutics: past, present and future. *Current opinion in chemical biology* **2017,** *38*, 24-29.
120. Guler, M. O.; Soukasene, S.; Hulvat, J. F.; Stupp, S. I., Presentation and recognition of biotin on nanofibers formed by branched peptide amphiphiles. *Nano letters* **2005,** *5* (2), 249-252.
121. Ghadiri, M. R.; Granja, J. R.; Milligan, R. A.; McRee, D. E.; Khazanovich, N., Self-assembling organic nanotubes based on a cyclic peptide architecture. *Nature* **1993,** *366* (6453), 324-327.
122. Hauser, C. A.; Zhang, S., Peptides as biological semiconductors. *Nature* **2010,** *468* (7323), 516-517.
123. Amdursky, N.; Molotskii, M.; Aronov, D.; Adler-Abramovich, L.; Gazit, E.; Rosenman, G., Blue Luminescence Based on Quantum Confinement at Peptide Nanotubes. *Nano Letters* **2009,** *9* (9), 3111-3115.
124. Bosne, E.; Heredia, A.; Kopyl, S.; Karpinsky, D.; Pinto, A.; Kholkin, A., Piezoelectric resonators based on self-assembled diphenylalanine microtubes. *Applied Physics Letters* **2013,** *102* (7), 073504.
125. Bucak, S.; Cenker, C.; Nasir, I.; Olsson, U.; Zackrisson, M., Peptide Nanotube Nematic Phase. *Langmuir* **2009,** *25* (8), 4262-4265.
126. Hamley, I. W.; Dehsorkhi, A.; Castelletto, V., Self-assembled arginine-coated peptide nanosheets in water. *Chemical Communications* **2013,** *49* (18), 1850-1852.
127. da Silva, E. R.; Walter, M. N. M.; Reza, M.; Castelletto, V.; Ruokolainen, J.; Connon, C. J.; Alves, W. A.; Hamley, I. W., Self-assembled arginine-capped peptide bolaamphiphile nanosheets for cell culture and controlled wettability surfaces. *Biomacromolecules* **2015,** *16* (10), 3180-3190.
128. Dai, B.; Li, D.; Xi, W.; Luo, F.; Zhang, X.; Zou, M.; Cao, M.; Hu, J.; Wang, W.; Wei, G., Tunable assembly of amyloid-forming peptides into nanosheets as a retrovirus carrier. *Proceedings of the National Academy of Sciences* **2015,** *112* (10), 2996-3001.
129. Fernandez-Lopez, S.; Kim, H.-S.; Choi, E. C.; Delgado, M.; Granja, J. R.; Khasanov, A.; Kraehenbuehl, K.; Long, G.; Weinberger, D. A.; Wilcoxen, K. M., Antibacterial agents based on the cyclic D, L-α-peptide architecture. *Nature* **2001,** *412* (6845), 452-455.
130. Bélanger, D.; Tong, X.; Soumaré, S.; Dory, Y. L.; Zhao, Y., Cyclic Peptide–Polymer Complexes and Their Self-Assembly. *Chemistry–A European Journal* **2009,** *15* (17), 4428-4436.
131. Colgrave, M. L.; Korsinczky, M. J.; Clark, R. J.; Foley, F.; Craik, D. J., Sunflower trypsin inhibitor-1, proteolytic studies on a trypsin inhibitor peptide and its analogs. *Peptide Science* **2010,** *94* (5), 665-672.
132. Oba, M.; Fukushima, S.; Kanayama, N.; Aoyagi, K.; Nishiyama, N.; Koyama, H.; Kataoka, K., Cyclic RGD peptide-conjugated polyplex micelles as a targetable gene delivery system directed to cells possessing αvβ3 and αvβ5 integrins. *Bioconjugate chemistry* **2007,** *18* (5), 1415-1423.
133. Ardoña, H. A. M.; Tovar, J. D., Peptide π-electron conjugates: organic electronics for biology? *Bioconjugate chemistry* **2015,** *26* (12), 2290-2302.

134. Brown, P.; Abdulle, O.; Boakes, S.; Duperchy, E.; Moss, S.; Simonovic, M.; Stanway, S.; Wilson, A.; Dawson, M. J., Direct modifications of the cyclic peptide polymyxin B leading to analogues with enhanced in vitro antibacterial activity. *Bioorganic & medicinal chemistry letters* **2020,** *30* (11), 127163.
135. Zhang, Y.; Ouyang, H.; Lim, C. T.; Ramakrishna, S.; Huang, Z. M., Electrospinning of gelatin fibers and gelatin/PCL composite fibrous scaffolds. *Journal of Biomedical Materials Research Part B: Applied Biomaterials: An Official Journal of The Society for Biomaterials, The Japanese Society for Biomaterials, and The Australian Society for Biomaterials and the Korean Society for Biomaterials* **2005,** *72* (1), 156-165.
136. Sasidharan, S.; Hazam, P. K.; Ramakrishnan, V., Symmetry-directed self-organization in peptide nanoassemblies through aromatic π–π interactions. *The Journal of Physical Chemistry B* **2017,** *121* (2), 404-411.
137. Xiao, S.; Xiao, S.; Gräter, F., Dissecting the structural determinants for the difference in mechanical stability of silk and amyloid beta-sheet stacks. *Physical Chemistry Chemical Physics* **2013,** *15* (22), 8765-8771.
138. Bortolini, C.; Jones, N.; Hoffmann, S.; Wang, C.; Besenbacher, F.; Dong, M., Mechanical properties of amyloid-like fibrils defined by secondary structures. *Nanoscale* **2015,** *7* (17), 7745-7752.
139. Bahram, M.; Mohseni, N.; Moghtader, M., An introduction to hydrogels and some recent applications. In *Emerging concepts in analysis and applications of hydrogels*, IntechOpen: 2016.
140. Du, X.; Zhou, J.; Shi, J.; Xu, B., Supramolecular hydrogelators and hydrogels: from soft matter to molecular biomaterials. *Chemical reviews* **2015,** *115* (24), 13165-13307.
141. Chakraborty, P.; Gazit, E., Amino Acid Based Self-assembled Nanostructures: Complex Structures from Remarkably Simple Building Blocks. *ChemNanoMat* **2018,** *4* (8), 730-740.
142. Ryan, D. M.; Anderson, S. B.; Nilsson, B. L., The influence of side-chain halogenation on the self-assembly and hydrogelation of Fmoc-phenylalanine derivatives. *Soft Matter* **2010,** *6* (14), 3220-3231.
143. Ryan, D. M.; Doran, T. M.; Nilsson, B. L., Stabilizing self-assembled Fmoc–F 5–Phe hydrogels by co-assembly with PEG-functionalized monomers. *Chemical Communications* **2011,** *47* (1), 475-477.
144. Nanda, J.; Biswas, A.; Banerjee, A., Single amino acid based thixotropic hydrogel formation and pH-dependent morphological change of gel nanofibers. *Soft Matter* **2013,** *9* (16), 4198-4208.
145. Garcia, A. M.; Lavendomme, R.; Kralj, S.; Kurbasic, M.; Bellotto, O.; Cringoli, M. C.; Semeraro, S.; Bandiera, A.; De Zorzi, R.; Marchesan, S., Self-assembly of an amino acid derivative into an antimicrobial hydrogel biomaterial. *Chemistry–A European Journal* **2020,** *26* (8), 1880-1886.
146. Seow, W. Y.; Hauser, C. A., Short to ultrashort peptide hydrogels for biomedical uses. *Materials Today* **2014,** *17* (8), 381-388.
147. Zhang, S.; Holmes, T.; Lockshin, C.; Rich, A., Spontaneous assembly of a self-complementary oligopeptide to form a stable macroscopic membrane. *Proceedings of the National Academy of Sciences* **1993,** *90* (8), 3334-3338.
148. Yokoi, H.; Kinoshita, T.; Zhang, S., Dynamic reassembly of peptide RADA16 nanofiber scaffold. *Proceedings of the National Academy of Sciences* **2005,** *102* (24), 8414-8419.
149. Marchesan, S.; Vargiu, A. V.; Styan, K. E., The Phe-Phe motif for peptide self-assembly in nanomedicine. *Molecules* **2015,** *20* (11), 19775-19788.
150. Orbach, R.; Mironi-Harpaz, I.; Adler-Abramovich, L.; Mossou, E.; Mitchell, E. P.; Forsyth, V. T.; Gazit, E.; Seliktar, D., The rheological and structural properties of Fmoc-peptide-based hydrogels: the effect of aromatic molecular architecture on self-assembly and physical characteristics. *Langmuir* **2012,** *28* (4), 2015-2022.
151. Laverty, G.; McCloskey, A. P.; Gilmore, B. F.; Jones, D. S.; Zhou, J.; Xu, B., Ultrashort cationic naphthalene-derived self-assembled peptides as antimicrobial nanomaterials. *Biomacromolecules* **2014,** *15* (9), 3429-3439.

152. Kubiak, P. S.; Awhida, S.; Hotchen, C.; Deng, W.; Alston, B.; McDonald, T. O.; Adams, D. J.; Cameron, P. J., Polymerization of low molecular weight hydrogelators to form electrochromic polymers. *Chemical Communications* **2015,** *51* (52), 10427-10430.
153. Martin, A. D.; Robinson, A. B.; Mason, A. F.; Wojciechowski, J. P.; Thordarson, P., Exceptionally strong hydrogels through self-assembly of an indole-capped dipeptide. *Chemical Communications* **2014,** *50* (98), 15541-15544.
154. Aldilla, V. R.; Chen, R.; Martin, A. D.; Marjo, C. E.; Rich, A. M.; Black, D. S.; Thordarson, P.; Kumar, N., Anthranilamide-based short peptides self-assembled hydrogels as antibacterial agents. *Scientific reports* **2020,** *10* (1), 1-12.
155. Huang, Y.; Qiu, Z.; Xu, Y.; Shi, J.; Lin, H.; Zhang, Y., Supramolecular hydrogels based on short peptides linked with conformational switch. *Organic & biomolecular chemistry* **2011,** *9* (7), 2149-2155.
156. Yoshii, T.; Onogi, S.; Shigemitsu, H.; Hamachi, I., Chemically reactive supramolecular hydrogel coupled with a signal amplification system for enhanced analyte sensitivity. *Journal of the American Chemical Society* **2015,** *137* (9), 3360-3365.
157. Echeverria, C.; Fernandes, S. N.; Godinho, M. H.; Borges, J. P.; Soares, P. I., Functional stimuli-responsive gels: Hydrogels and microgels. *Gels* **2018,** *4* (2), 54.
158. Ikeda, M.; Tanida, T.; Yoshii, T.; Hamachi, I., Rational molecular design of stimulus-responsive supramolecular hydrogels based on dipeptides. *Advanced Materials* **2011,** *23* (25), 2819-2822.
159. Mei, L.; Xu, K.; Zhai, Z.; He, S.; Zhu, T.; Zhong, W., Doxorubicin-reinforced supramolecular hydrogels of RGD-derived peptide conjugates for pH-responsive drug delivery. *Organic & biomolecular chemistry* **2019,** *17* (15), 3853-3860.
160. Raza, F.; Zhu, Y.; Chen, L.; You, X.; Zhang, J.; Khan, A.; Khan, M. W.; Hasnat, M.; Zafar, H.; Wu, J., Paclitaxel-loaded pH responsive hydrogel based on self-assembled peptides for tumor targeting. *Biomaterials science* **2019,** *7* (5), 2023-2036.
161. Tang, J. D.; Mura, C.; Lampe, K. J., Stimuli-responsive, pentapeptide, nanofiber hydrogel for tissue engineering. *Journal of the American Chemical Society* **2019,** *141* (12), 4886-4899.
162. Basak, S.; Nanda, J.; Banerjee, A., Multi-stimuli responsive self-healing metallo-hydrogels: tuning of the gel recovery property. *Chemical communications* **2014,** *50* (18), 2356-2359.
163. Shundo, A.; Hoshino, Y.; Higuchi, T.; Matsumoto, Y.; Penaloza Jr, D. P.; Matsumoto, K.; Ohno, M.; Miyaji, K.; Goto, M.; Tanaka, K., Facile microcapsule fabrication by spray deposition of a supramolecular hydrogel. *RSC advances* **2014,** *4* (68), 36097-36100.
164. Kumari, A.; Ahmad, B., The physical basis of fabrication of amyloid-based hydrogels by lysozyme. *RSC Advances* **2019,** *9* (64), 37424-37435.
165. Hu, B.; Shen, Y.; Adamcik, J.; Fischer, P.; Schneider, M.; Loessner, M. J.; Mezzenga, R., Polyphenol-binding amyloid fibrils self-assemble into reversible hydrogels with antibacterial activity. *ACS nano* **2018,** *12* (4), 3385-3396.
166. Vegners, R.; Shestakova, I.; Kalvinsh, I.; Ezzell, R. M.; Janmey, P. A., Use of a gel-forming dipeptide derivative as a carrier for antigen presentation. *Journal of peptide science: an official publication of the European Peptide Society* **1995,** *1* (6), 371-378.
167. Zhang, Y.; Gu, H.; Yang, Z.; Xu, B., Supramolecular hydrogels respond to ligand− receptor interaction. *Journal of the American Chemical Society* **2003,** *125* (45), 13680-13681.
168. Rajbhandary, A.; Nilsson, B. L., Investigating the effects of peptoid substitutions in self-assembly of Fmoc-diphenylalanine derivatives. *Peptide Science* **2017,** *108* (2), e22994.
169. Abbas, M.; Xing, R.; Zhang, N.; Zou, Q.; Yan, X., Antitumor photodynamic therapy based on dipeptide fibrous hydrogels with incorporation of photosensitive drugs. *ACS Biomaterials Science & Engineering* **2017,** *4* (6), 2046-2052.

170. Arakawa, H.; Takeda, K.; Higashi, S. L.; Shibata, A.; Kitamura, Y.; Ikeda, M., Self-assembly and hydrogel formation ability of Fmoc-dipeptides comprising α-methyl-L-phenylalanine. *Polymer Journal* **2020,** *52* (8), 923-930.
171. Mahler, A.; Reches, M.; Rechter, M.; Cohen, S.; Gazit, E., Rigid, self-assembled hydrogel composed of a modified aromatic dipeptide. *Advanced Materials* **2006,** *18* (11), 1365-1370.
172. Tao, K.; Levin, A.; Adler-Abramovich, L.; Gazit, E., Fmoc-modified amino acids and short peptides: simple bio-inspired building blocks for the fabrication of functional materials. *Chemical Society Reviews* **2016,** *45* (14), 3935-3953.
173. Cheng, G.; Castelletto, V.; Moulton, C.; Newby, G.; Hamley, I., Hydrogelation and self-assembly of Fmoc-tripeptides: unexpected influence of sequence on self-assembled fibril structure, and hydrogel modulus and anisotropy. *Langmuir* **2010,** *26* (7), 4990-4998.
174. Criado-Gonzalez, M.; Wagner, D.; Rodon Fores, J.; Blanck, C.; Schmutz, M.; Chaumont, A.; Rabineau, M.; Schlenoff, J. B.; Fleith, G.; Combet, J., Supramolecular Hydrogel Induced by Electrostatic Interactions between Polycation and Phosphorylated-Fmoc-Tripeptide. *Chemistry of Materials* **2020,** *32* (5), 1946-1956.
175. Criado-Gonzalez, M.; Iqbal, M. H.; Carvalho, A.; Schmutz, M.; Jierry, L.; Schaaf, P.; Boulmedais, F., Surface Triggered Self-Assembly of Fmoc-Tripeptide as an Antibacterial Coating. *Frontiers in bioengineering and biotechnology* **2020,** *8*, 938.
176. Castelletto, V.; Moulton, C. M.; Cheng, G.; Hamley, I. W.; Hicks, M. R.; Rodger, A.; López-Pérez, D. E.; Revilla-López, G.; Alemán, C., Self-assembly of Fmoc-tetrapeptides based on the RGDS cell adhesion motif. *Soft Matter* **2011,** *7* (24), 11405-11415.
177. Sedman, V.; Chen, X.; Allen, S.; Roberts, C.; Korolkov, V.; Tendler, S., Tuning the mechanical properties of self-assembled mixed-peptide tubes. *Journal of microscopy* **2013,** *249* (3), 165-172.
178. Adler-Abramovich, L.; Kol, N.; Yanai, I.; Barlam, D.; Shneck, R. Z.; Gazit, E.; Rousso, I., Inside Cover: Self-Assembled Organic Nanostructures with Metallic-Like Stiffness (Angew. Chem. Int. Ed. 51/2010). *Angewandte Chemie International Edition* **2010,** *49* (51), 9788-9788.
179. Azuri, I.; Adler-Abramovich, L.; Gazit, E.; Hod, O.; Kronik, L., Why are diphenylalanine-based peptide nanostructures so rigid? Insights from first principles calculations. *Journal of the American Chemical Society* **2014,** *136* (3), 963-969.
180. Basavalingappa, V.; Bera, S.; Xue, B.; O'Donnell, J.; Guerin, S.; Cazade, P.-A.; Yuan, H.; Haq, E. u.; Silien, C.; Tao, K., Diphenylalanine-derivative peptide assemblies with increased aromaticity exhibit metal-like rigidity and high piezoelectricity. *ACS nano* **2020,** *14* (6), 7025-7037.
181. Migliore, A.; Polizzi, N. F.; Therien, M. J.; Beratan, D. N., Biochemistry and theory of proton-coupled electron transfer. *Chemical reviews* **2014,** *114* (7), 3381-3465.
182. Amit, M.; Appel, S.; Cohen, R.; Cheng, G.; Hamley, I. W.; Ashkenasy, N., Hybrid proton and electron transport in peptide fibrils. *Advanced Functional Materials* **2014,** *24* (37), 5873-5880.
183. Creasey, R. C.; Shingaya, Y.; Nakayama, T., Improved electrical conductance through self-assembly of bioinspired peptides into nanoscale fibers. *Materials Chemistry and Physics* **2015,** *158*, 52-59.
184. Yardeni, J. L.; Amit, M.; Ashkenasy, G.; Ashkenasy, N., Sequence dependent proton conduction in self-assembled peptide nanostructures. *Nanoscale* **2016,** *8* (4), 2358-2366.
185. Knowles, T. P.; Buehler, M. J., Nanomechanics of functional and pathological amyloid materials. *Nature nanotechnology* **2011,** *6* (8), 469-479.
186. Erwin, S. C.; Zu, L.; Haftel, M. I.; Efros, A. L.; Kennedy, T. A.; Norris, D. J., Doping semiconductor nanocrystals. *Nature* **2005,** *436* (7047), 91-94.
187. Tao, K.; O'Donnell, J.; Yuan, H.; Haq, E. U.; Guerin, S.; Shimon, L. J.; Xue, B.; Silien, C.; Cao, Y.; Thompson, D., Accelerated charge transfer in water-layered peptide assemblies. *Energy & environmental science* **2020,** *13* (1), 96-101.

188. Amdursky, N.; Molotskii, M.; Gazit, E.; Rosenman, G., Self-assembled bioinspired quantum dots: optical properties. *Applied Physics Letters* **2009,** *94* (26), 261907.
189. Adler-Abramovich, L.; Gazit, E., The physical properties of supramolecular peptide assemblies: from building block association to technological applications. *Chemical Society Reviews* **2014,** *43* (20), 6881-6893.
190. Tarabout, C.; Roux, S.; Gobeaux, F.; Fay, N.; Pouget, E.; Meriadec, C.; Ligeti, M.; Thomas, D.; IJsselstijn, M.; Besselievre, F., Control of peptide nanotube diameter by chemical modifications of an aromatic residue involved in a single close contact. *Proceedings of the National Academy of Sciences* **2011,** *108* (19), 7679-7684.
191. Alivisatos, A. P., Semiconductor clusters, nanocrystals, and quantum dots. *science* **1996,** *271* (5251), 933-937.
192. Harrison, P., *Quantum wells, wires and dots*. Wiley Online Library: 2016.
193. Wang, J.; Liu, K.; Xing, R.; Yan, X., Peptide self-assembly: thermodynamics and kinetics. *Chemical Society Reviews* **2016,** *45* (20), 5589-5604.
194. Martins, T. D.; de Souza, M. I.; Cunha, B. B.; Takahashi, P. M.; Ferreira, F. F.; Souza, J. A.; Fileti, E. E.; Alves, W. A., Influence of pH and pyrenyl on the structural and morphological control of peptide nanotubes. *The Journal of Physical Chemistry C* **2011,** *115* (16), 7906-7913.
195. Pandey, G.; Morla, S.; Nemade, H. B.; Kumar, S.; Ramakrishnan, V., Modulation of aggregation with an electric field; scientific roadmap for a potential non-invasive therapy against tauopathies. *RSC advances* **2019,** *9* (9), 4744-4750.
196. Saikia, J.; Pandey, G.; Sasidharan, S.; Antony, F.; Nemade, H. B.; Kumar, S.; Chaudhary, N.; Ramakrishnan, V., Electric field disruption of amyloid aggregation: potential noninvasive therapy for Alzheimer's disease. *ACS chemical neuroscience* **2019,** *10* (5), 2250-2262.
197. Pandey, G.; Saikia, J.; Sasidharan, S.; Joshi, D. C.; Thota, S.; Nemade, H. B.; Chaudhary, N.; Ramakrishnan, V., Modulation of peptide based nano-assemblies with electric and magnetic fields. *Scientific reports* **2017,** *7* (1), 1-9.
198. Ciani, B.; Hutchinson, E. G.; Sessions, R. B.; Woolfson, D. N., A designed system for assessing how sequence affects α to β conformational transitions in proteins. *Journal of Biological Chemistry* **2002,** *277* (12), 10150-10155.
199. Burley, S.; Petsko, G. A., Aromatic-aromatic interaction: a mechanism of protein structure stabilization. *Science* **1985,** *229* (4708), 23-28.
200. Hill, R. B.; DeGrado, W. F., Solution structure of α2D, a nativelike de novo designed protein. *Journal of the American Chemical Society* **1998,** *120* (6), 1138-1145.
201. Wheeler, S. E., Local nature of substituent effects in stacking interactions. *Journal of the American Chemical Society* **2011,** *133* (26), 10262-10274.
202. Thakuria, R.; Nath, N. K.; Saha, B. K., The nature and applications of π–π interactions: a perspective. *Crystal Growth & Design* **2019,** *19* (2), 523-528.
203. Samanta, U.; Pal, D.; Chakrabarti, P., Packing of aromatic rings against tryptophan residues in proteins. *Acta Crystallographica Section D: Biological Crystallography* **1999,** *55* (8), 1421-1427.
204. Mahalakshmi, R.; Sengupta, A.; Raghothama, S.; Shamala, N.; Balaram, P., Tryptophan-containing peptide helices: interactions involving the indole side chain. *The Journal of peptide research* **2005,** *66* (5), 277-296.
205. Görbitz, C. H., Nanotube formation by hydrophobic dipeptides. *Chemistry–A European Journal* **2001,** *7* (23), 5153-5159.
206. Zhang, H.; Lou, S.; Yu, Z., Polar− π Interactions Promote Self-assembly of Dipeptides into Laminated Nanofibers. *Langmuir* **2019,** *35* (13), 4710-4717.

207. Sasidharan, S.; Shyni, P.; Chaudhary, N.; Ramakrishnan, V., Single crystal organic nanoflowers. *Scientific reports* **2017,** *7* (1), 1-8.
208. Guo, C.; Luo, Y.; Zhou, R.; Wei, G., Triphenylalanine peptides self-assemble into nanospheres and nanorods that are different from the nanovesicles and nanotubes formed by diphenylalanine peptides. *Nanoscale* **2014,** *6* (5), 2800-2811.
209. Bartocci, S.; Berrocal, J. A.; Guarracino, P.; Grillaud, M.; Franco, L.; Mba, M., Peptide-Driven Charge-Transfer Organogels Built from Synergetic Hydrogen Bonding and Pyrene–Naphthalenediimide Donor–Acceptor Interactions. *Chemistry–A European Journal* **2018,** *24* (12), 2920-2928.
210. Kim, J.; Han, T. H.; Kim, Y. I.; Park, J. S.; Choi, J.; Churchill, D. G.; Kim, S. O.; Ihee, H., Role of water in directing diphenylalanine assembly into nanotubes and nanowires. *Advanced Materials* **2010,** *22* (5), 583-587.
211. Li, Q.; Jia, Y.; Dai, L.; Yang, Y.; Li, J., Controlled rod nanostructured assembly of diphenylalanine and their optical waveguide properties. *ACS nano* **2015,** *9* (3), 2689-2695.
212. Ziserman, L.; Lee, H.-Y.; Raghavan, S. R.; Mor, A.; Danino, D., Unraveling the mechanism of nanotube formation by chiral self-assembly of amphiphiles. *Journal of the American Chemical Society* **2011,** *133* (8), 2511-2517.
213. Paramonov, S. E.; Jun, H.-W.; Hartgerink, J. D., Self-assembly of peptide− amphiphile nanofibers: the roles of hydrogen bonding and amphiphilic packing. *Journal of the American Chemical Society* **2006,** *128* (22), 7291-7298.
214. Xu, H.; Wang, Y.; Ge, X.; Han, S.; Wang, S.; Zhou, P.; Shan, H.; Zhao, X.; Lu, J. R., Twisted nanotubes formed from ultrashort amphiphilic peptide I3K and their templating for the fabrication of silica nanotubes. *Chemistry of Materials* **2010,** *22* (18), 5165-5173.
215. Tsonchev, S.; Niece, K. L.; Schatz, G. C.; Ratner, M. A.; Stupp, S. I., Phase diagram for assembly of biologically-active peptide amphiphiles. *The Journal of Physical Chemistry B* **2008,** *112* (2), 441-447.
216. Hu, X.; Liao, M.; Gong, H.; Zhang, L.; Cox, H.; Waigh, T. A.; Lu, J. R., Recent advances in short peptide self-assembly: from rational design to novel applications. *Current Opinion in Colloid & Interface Science* **2020,** *45*, 1-13.
217. Kundu, B.; Eltohamy, M.; Yadavalli, V. K.; Kundu, S. C.; Kim, H.-W., Biomimetic designing of functional silk nanotopography using self-assembly. *ACS applied materials & interfaces* **2016,** *8* (42), 28458-28467.
218. Faul, C. F.; Antonietti, M., Ionic self-assembly: Facile synthesis of supramolecular materials. *Advanced Materials* **2003,** *15* (9), 673-683.
219. Voyer, N.; Roby, J.; Deschênes, D.; Bernier, J., Design, synthesis, and supramolecular properties of bis-crown ether modified peptides. *Supramolecular Chemistry* **1995,** *5* (1), 61-69.
220. Wang, J.; Zhao, X.; Li, J.; Kuang, X.; Fan, Y.; Wei, G.; Su, Z., Electrostatic assembly of peptide nanofiber–biomimetic silver nanowires onto graphene for electrochemical sensors. *ACS Macro Letters* **2014,** *3* (6), 529-533.
221. Sun, H.; Zhang, X.; Miao, L.; Zhao, L.; Luo, Q.; Xu, J.; Liu, J., Micelle-induced self-assembling protein nanowires: versatile supramolecular scaffolds for designing the light-harvesting system. *ACS nano* **2016,** *10* (1), 421-428.
222. Tahara, K.; Lei, S.; Adisoejoso, J.; De Feyter, S.; Tobe, Y., Supramolecular surface-confined architectures created by self-assembly of triangular phenylene–ethynylene macrocycles via van der Waals interaction. *Chemical communications* **2010,** *46* (45), 8507-8525.
223. Caplan, M. R.; Moore, P. N.; Zhang, S.; Kamm, R. D.; Lauffenburger, D. A., Self-assembly of a β-sheet protein governed by relief of electrostatic repulsion relative to van der Waals attraction. *Biomacromolecules* **2000,** *1* (4), 627-631.

224. Shen, C. L.; Murphy, R. M., Solvent effects on self-assembly of beta-amyloid peptide. *Biophys J* **1995,** *69* (2), 640-651.
225. Hamley, I. W.; Nutt, D. R.; Brown, G. D.; Miravet, J.; Escuder, B.; Rodríguez-Llansola, F., Influence of the solvent on the self-assembly of a modified amyloid beta peptide fragment. II. NMR and computer simulation investigation. *The Journal of Physical Chemistry B* **2010,** *114* (2), 940-951.
226. Huang, R.; Qi, W.; Su, R.; Zhao, J.; He, Z., Solvent and surface controlled self-assembly of diphenylalanine peptide: from microtubes to nanofibers. *Soft Matter* **2011,** *7* (14), 6418-6421.
227. Jain, R.; Roy, S., Tuning the gelation behavior of short laminin derived peptides via solvent mediated self-assembly. *Materials Science and Engineering: C* **2020,** *108*, 110483.
228. Liu, X.; Fei, J.; Wang, A.; Cui, W.; Zhu, P.; Li, J., Transformation of Dipeptide-Based Organogels into Chiral Crystals by Cryogenic Treatment. *Angewandte Chemie International Edition* **2017,** *56* (10), 2660-2663.
229. Panda, J. J.; Chauhan, V. S., Short peptide based self-assembled nanostructures: implications in drug delivery and tissue engineering. *Polymer chemistry* **2014,** *5* (15), 4418-4436.
230. D'Andrea, L. D.; Iaccarino, G.; Fattorusso, R.; Sorriento, D.; Carannante, C.; Capasso, D.; Trimarco, B.; Pedone, C., Targeting angiogenesis: structural characterization and biological properties of a de novo engineered VEGF mimicking peptide. *Proceedings of the National Academy of Sciences* **2005,** *102* (40), 14215-14220.
231. Kumar, V. A.; Taylor, N. L.; Shi, S.; Wang, B. K.; Jalan, A. A.; Kang, M. K.; Wickremasinghe, N. C.; Hartgerink, J. D., Highly angiogenic peptide nanofibers. *ACS nano* **2015,** *9* (1), 860-868.
232. Rubert Pérez, C. M.; Álvarez, Z.; Chen, F.; Aytun, T.; Stupp, S. I., Mimicking the bioactivity of fibroblast growth factor-2 using supramolecular nanoribbons. *ACS biomaterials science & engineering* **2017,** *3* (9), 2166-2175.
233. Niyonsaba, F.; Madera, L.; Afacan, N.; Okumura, K.; Ogawa, H.; Hancock, R. E., The innate defense regulator peptides IDR-HH2, IDR-1002, and IDR-1018 modulate human neutrophil functions. *Journal of leukocyte biology* **2013,** *94* (1), 159-170.
234. Shin, H.; Jo, S.; Mikos, A. G., Biomimetic materials for tissue engineering. *Biomaterials* **2003,** *24* (24), 4353-4364.
235. Islam, M. M.; Ravichandran, R.; Olsen, D.; Ljunggren, M.; Fagerholm, P.; Lee, C.-J.; Griffith, M.; Phopase, J., Self-assembled collagen-like-peptide implants as alternatives to human donor corneal transplantation. *RSC advances* **2016,** *6* (61), 55745-55749.
236. Luo, Z.; Dai, Y.; Gao, H., Development and application of hyaluronic acid in tumor targeting drug delivery. *Acta Pharmaceutica Sinica B* **2019,** *9* (6), 1099-1112.
237. Kebebe, D.; Liu, Y.; Wu, Y.; Vilakhamxay, M.; Liu, Z.; Li, J., Tumor-targeting delivery of herb-based drugs with cell-penetrating/tumor-targeting peptide-modified nanocarriers. *International journal of nanomedicine* **2018,** *13*, 1425.
238. Raza, A.; Rasheed, T.; Nabeel, F.; Hayat, U.; Bilal, M.; Iqbal, H., Endogenous and exogenous stimuli-responsive drug delivery systems for programmed site-specific release. *Molecules* **2019,** *24* (6), 1117.
239. Meng, N.; Ren, X.; Santagiuliana, G.; Ventura, L.; Zhang, H.; Wu, J.; Yan, H.; Reece, M. J.; Bilotti, E., Ultrahigh β-phase content poly (vinylidene fluoride) with relaxor-like ferroelectricity for high energy density capacitors. *Nature communications* **2019,** *10* (1), 1-9.
240. Moorcroft, S. C.; Roach, L.; Jayne, D. G.; Ong, Z. Y.; Evans, S. D., Nanoparticle-loaded hydrogel for the light-activated release and photothermal enhancement of antimicrobial peptides. *ACS applied materials & interfaces* **2020,** *12* (22), 24544-24554.
241. Atefyekta, S.; Blomstrand, E.; Rajasekharan, A. K.; Svensson, S.; Trobos, M.; Hong, J.; Webster, T. J.; Thomsen, P.; Andersson, M., Antimicrobial Peptide-Functionalized Mesoporous Hydrogels. *ACS biomaterials science & engineering* **2021,** *7* (4), 1693-1702.

242. Tsao, C. T.; Chang, C. H.; Lin, Y. Y.; Wu, M. F.; Wang, J.-L.; Han, J. L.; Hsieh, K. H., Antibacterial activity and biocompatibility of a chitosan–γ-poly (glutamic acid) polyelectrolyte complex hydrogel. *Carbohydrate Research* **2010,** *345* (12), 1774-1780.
243. Gadepalli, R.; Dhawan, B.; Sreenivas, V.; Kapil, A.; Ammini, A.; Chaudhry, R., A clinico-microbiological study of diabetic foot ulcers in an Indian tertiary care hospital. *Diabetes care* **2006,** *29* (8), 1727-1732.
244. Xiao, Y.; Reis, L. A.; Feric, N.; Knee, E. J.; Gu, J.; Cao, S.; Laschinger, C.; Londono, C.; Antolovich, J.; McGuigan, A. P., Diabetic wound regeneration using peptide-modified hydrogels to target re-epithelialization. *Proceedings of the National Academy of Sciences* **2016,** *113* (40), E5792-E5801.
245. Grek, C. L.; Prasad, G.; Viswanathan, V.; Armstrong, D. G.; Gourdie, R. G.; Ghatnekar, G. S., Topical administration of a connexin43-based peptide augments healing of chronic neuropathic diabetic foot ulcers: a multicenter, randomized trial. *Wound Repair and Regeneration* **2015,** *23* (2), 203-212.
246. Carrejo, N. C.; Moore, A. N.; Lopez Silva, T. L.; Leach, D. G.; Li, I.-C.; Walker, D. R.; Hartgerink, J. D., Multidomain peptide hydrogel accelerates healing of full-thickness wounds in diabetic mice. *ACS biomaterials science & engineering* **2018,** *4* (4), 1386-1396.
247. Gawande, P. V.; Leung, K. P.; Madhyastha, S., Antibiofilm and antimicrobial efficacy of DispersinB®-KSL-W peptide-based wound gel against chronic wound infection associated bacteria. *Current microbiology* **2014,** *68* (5), 635-641.
248. Wei, S.; Xu, P.; Yao, Z.; Cui, X.; Lei, X.; Li, L.; Dong, Y.; Zhu, W.; Guo, R.; Cheng, B., A composite hydrogel with co-delivery of antimicrobial peptides and platelet-rich plasma to enhance healing of infected wounds in diabetes. *Acta Biomaterialia* **2021,** *124*, 205-218.
249. Yang, X.; Guo, J.-L.; Han, J.; Si, R.-J.; Liu, P.-P.; Zhang, Z.-R.; Wang, A.-M.; Zhang, J., Chitosan hydrogel encapsulated with LL-37 peptide promotes deep tissue injury healing in a mouse model. *Military Medical Research* **2020,** *7*, 1-10.
250. Zhao, Y.; Du, X.; Jiang, L.; Luo, H.; Wang, F.; Wang, J.; Qiu, L.; Liu, L.; Liu, X.; Wang, X., Glucose oxidase-loaded antimicrobial peptide Hydrogels: potential dressings for diabetic wound. *Journal of nanoscience and nanotechnology* **2020,** *20* (4), 2087-2094.
251. Liu, Q.; Wang, J.; Boyd, B. J., Peptide-based biosensors. *Talanta* **2015,** *136*, 114-127.
252. Hasanzadeh, M.; Shadjou, N., (Nano)-materials and methods of signal enhancement for genosensing of p53 tumor suppressor protein: Novel research overview. *Materials Science and Engineering: C* **2017,** *76*, 1424-1439.
253. He, Y.; Xie, S.; Yang, X.; Yuan, R.; Chai, Y., Electrochemical peptide biosensor based on in situ silver deposition for detection of prostate specific antigen. *ACS applied materials & interfaces* **2015,** *7* (24), 13360-13366.
254. Colherinhas, G.; Malaspina, T.; Fileti, E. E., Storing energy in biodegradable electrochemical supercapacitors. *ACS omega* **2018,** *3* (10), 13869-13875.
255. Liu, X.; Sun, X.; Liang, G., Peptide-based supramolecular hydrogels for bioimaging applications. *Biomaterials Science* **2020**.
256. Sakala, G. P.; Reches, M., Peptide-based approaches to fight biofouling. *Advanced Materials Interfaces* **2018,** *5* (18), 1800073.
257. Schnitzer, T.; Paenurk, E.; Trapp, N.; Gershoni-Poranne, R.; Wennemers, H., Peptide–Metal Frameworks with Metal Strings Guided by Dispersion Interactions. *Journal of the American Chemical Society* **2021,** *143* (2), 644-648.
258. Chen, Y.; Wu, J. J.; Huang, L., Nanoparticles targeted with NGR motif deliver c-myc siRNA and doxorubicin for anticancer therapy. *Molecular therapy* **2010,** *18* (4), 828-834.
259. Sasidharan, S.; P. C, S.; Chaudhary, N.; Ramakrishnan, V., Single Crystal Organic Nanoflowers. *Scientific Reports* **2017,** *7* (1), 17335.

260. Novotny, M.; Kleywegt, G. J., A Survey of Left-handed Helices in Protein Structures. *Journal of Molecular Biology* **2005,** *347* (2), 231-241.
261. Kumar, A.; Ramakrishnan, V., Creating novel protein scripts beyond natural alphabets. *Systems and Synthetic Biology* **2010,** *4* (4), 247-256.
262. Coppedge, J. F., *Evolution: Possible Or Impossible?: Molecular Biology and the Laws of Chance in Nontechnical Language; a New Approach to the Subject, Based on Exciting Recent Discoveries Involving Proteins and DNA, the "golden Molecule" of Heredity*. Zondervan: 1973.
263. Durani, S., Protein Design with l- and d-α-Amino Acid Structures as the Alphabet. *Accounts of Chemical Research* **2008,** *41* (10), 1301-1308.
264. Hazam, P. K.; Jerath, G.; Kumar, A.; Chaudhary, N.; Ramakrishnan, V., Effect of tacticity-derived topological constraints in bactericidal peptides. *Biochimica et Biophysica Acta (BBA) - Biomembranes* **2017,** *1859* (8), 1388-1395.
265. Bada, J. L., Origins of homochirality. *Nature* **1995,** *374* (6523), 594-595.
266. Flory, P. J.; Volkenstein, M., Statistical mechanics of chain molecules. *Biopolymers* **1969,** *8* (5), 699-700.
267. Brant, D. A.; Flory, P. J., The Configuration of Random Polypeptide Chains. II. Theory. *Journal of the American Chemical Society* **1965,** *87* (13), 2791-2800.
268. Gordon, M., Statistical mechanics of chain molecules. P. J. Flory, pp. xix + 432, 1969. New York: Interscience. 164s. *British Polymer Journal* **1970,** *2* (5), 302-303.
269. Ramakrishnan, V.; Ranbhor, R.; Durani, S., Simulated folding in polypeptides of diversified molecular tacticity: Implications for protein folding and de novo design. *Biopolymers* **2005,** *78* (2), 96-105.
270. Davis, L. K., Intelligent Design of 14-3-3 Docking Proteins Utilizing Synthetic Evolution Artificial Intelligence (SYN-AI). *ACS Omega* **2019,** *4* (21), 18948-18960.
271. Huang, P.-S.; Boyken, S. E.; Baker, D., The coming of age of de novo protein design. *Nature* **2016,** *537* (7620), 320-327.
272. Hosseinzadeh, P.; Bhardwaj, G.; Mulligan, V. K.; Shortridge, M. D.; Craven, T. W.; Pardo-Avila, F.; Rettie, S. A.; Kim, D. E.; Silva, D.-A.; Ibrahim, Y. M.; Webb, I. K.; Cort, J. R.; Adkins, J. N.; Varani, G.; Baker, D., Comprehensive computational design of ordered peptide macrocycles. *Science (New York, N.Y.)* **2017,** *358* (6369), 1461-1466.
273. Dou, J.; Vorobieva, A. A.; Sheffler, W.; Doyle, L. A.; Park, H.; Bick, M. J.; Mao, B.; Foight, G. W.; Lee, M. Y.; Gagnon, L. A.; Carter, L.; Sankaran, B.; Ovchinnikov, S.; Marcos, E.; Huang, P.-S.; Vaughan, J. C.; Stoddard, B. L.; Baker, D., De novo design of a fluorescence-activating β-barrel. *Nature* **2018,** *561* (7724), 485-491.
274. Neidigh, J. W.; Fesinmeyer, R. M.; Andersen, N. H., Designing a 20-residue protein. *Nature Structural Biology* **2002,** *9*, 425.
275. Juraszek, J.; Bolhuis, P. G., Sampling the multiple folding mechanisms of Trp-cage in explicit solvent. *Proceedings of the National Academy of Sciences* **2006,** *103* (43), 15859-15864.
276. Zheng, W.; Gallicchio, E.; Deng, N.; Andrec, M.; Levy, R. M., Kinetic Network Study of the Diversity and Temperature Dependence of Trp-Cage Folding Pathways: Combining Transition Path Theory with Stochastic Simulations. *The Journal of Physical Chemistry B* **2011,** *115* (6), 1512-1523.
277. Lakowicz, J. R., *Principles of fluorescence spectroscopy*. Springer Science & Business Media: 2013.
278. R. Callis, P., *Binding phenomena and fluorescence quenching. II: Photophysics of aromatic residues and dependence of fluorescence spectra on protein conformation*. 2014; Vol. 1077, p 22-29.
279. Shao, J.; Korendovych, I. V.; Broos, J., Biosynthetic incorporation of the azulene moiety in proteins with high efficiency. *Amino Acids* **2015,** *47* (1), 213-216.

280. Loidl, G.; Musiol, H. J.; Budisa, N.; Huber, R.; Poirot, S.; Fourmy, D.; Moroder, L., Synthesis of β-(1-azulenyl)-L-alanine as a potential blue-colored fluorescent tryptophan analog and its use in peptide synthesis. *Journal of Peptide Science* **2000,** *6* (3), 139-144.
281. Budisa, N.; Paramita Pal, P., Designing novel spectral classes of proteins with a tryptophan-expanded genetic code. In *Biological Chemistry*, 2004; Vol. 385, p 893.
282. Creasey, R. C. G.; Mostert, A. B.; Solemanifar, A.; Nguyen, T. A. H.; Virdis, B.; Freguia, S.; Laycock, B., Biomimetic Peptide Nanowires Designed for Conductivity. *ACS Omega* **2019,** *4* (1), 1748-1756.
283. Zanna, N.; Focaroli, S.; Merlettini, A.; Gentilucci, L.; Teti, G.; Falconi, M.; Tomasini, C., Thixotropic Peptide-Based Physical Hydrogels Applied to Three-Dimensional Cell Culture. *ACS Omega* **2017,** *2* (5), 2374-2381.
284. Ranbhor, R.; Kumar, A.; Patel, K.; Ramakrishnan, V.; Durani, S., Automated design evolution of stereochemically randomized protein foldamers. *Physical biology* **2018,** *15* (3), 036001.
285. Ranbhor, R.; Kumar, A.; Tendulkar, A.; Patel, K.; Ramakrishnan, V.; Durani, S., IDeAS: automated design tool for hetero-chiral protein folds. *Physical Biology* **2018,** *15* (6), 066005.
286. Alston, R. W.; Lasagna, M.; Grimsley, G. R.; Scholtz, J. M.; Reinhart, G. D.; Pace, C. N., Peptide sequence and conformation strongly influence tryptophan fluorescence. *Biophys J* **2008,** *94* (6), 2280-2287.
287. Moroz, Y. S.; Binder, W.; Nygren, P.; Caputo, G. A.; Korendovych, I. V., Painting proteins blue: [small beta]-(1-azulenyl)-l-alanine as a probe for studying protein-protein interactions. *Chemical Communications* **2013,** *49* (5), 490-492.
288. Dhar, A.; Girdhar, K.; Singh, D.; Gelman, H.; Ebbinghaus, S.; Gruebele, M., Protein stability and folding kinetics in the nucleus and endoplasmic reticulum of eucaryotic cells. *Biophys J* **2011,** *101* (2), 421-430.
289. Cooper, A., Protein heat capacity: An anomaly that maybe never was. *The Journal of Physical Chemistry Letters* **2010,** *1* (22), 3298-3304.
290. Durowoju, I. B.; Bhandal, K. S.; Hu, J.; Carpick, B.; Kirkitadze, M., Differential scanning calorimetry—a method for assessing the thermal stability and conformation of protein antigen. *JoVE (Journal of Visualized Experiments)* **2017,** (121), e55262.
291. Culik, R. M.; Serrano, A. L.; Bunagan, M. R.; Gai, F., Achieving secondary structural resolution in kinetic measurements of protein folding: a case study of the folding mechanism of Trp-cage. *Angew Chem Int Ed Engl* **2011,** *50* (46), 10884-10887.
292. Chakrabartty, A.; Kortemme, T.; Padmanabhan, S.; Baldwin, R. L., Aromatic side-chain contribution to far-ultraviolet circular dichroism of helical peptides and its effect on measurement of helix propensities. *Biochemistry* **1993,** *32* (21), 5560-5565.
293. Diez-García, F.; Pantoja-Uceda, D.; Jiménez, M.; Chakrabartty, A.; Laurents, D. V., Structure of a simplified β-hairpin and its ATP complex. *Archives of biochemistry and biophysics* **2013,** *537* (1), 62-71.
294. Hauser, K.; Engelhard, M.; Friedman, N.; Sheves, M.; Siebert, F., Interpretation of Amide I Difference Bands Observed during Protein Reactions Using Site-Directed Isotopically Labeled Bacteriorhodopsin as a Model System. *The Journal of Physical Chemistry A* **2002,** *106* (14), 3553-3559.
295. Barth, A., Infrared spectroscopy of proteins. *Biochimica et Biophysica Acta (BBA) - Bioenergetics* **2007,** *1767* (9), 1073-1101.
296. Haris, P. I.; Chapman, D., Does Fourier-transform infrared spectroscopy provide useful information on protein structures? *Trends in Biochemical Sciences* **1992,** *17* (9), 328-333.
297. Hauser, C. A. E.; Zhang, S., Peptides as biological semiconductors. *Nature* **2010,** *468* (7323), 516-517.
298. Dey, S.; Swargiary, D.; Dasgupta, D.; Bordoloi, D.; Saikia, R.; Neog, D.; Shimray, S.; Paul, S.; Brahma, K.; Dey, J., The confinement energy of quantum dots. *arXiv preprint arXiv:1212.2318* **2012**.

299. Cahay, M. In *Quantum confinement VI: nanostructured materials and devices: proceedings of the international symposium*, The Electrochemical Society: 2001.
300. Haug, H.; Koch, S. W., *Quantum theory of the optical and electronic properties of semiconductors: fivth edition*. World Scientific Publishing Company: 2009.
301. Zirak, M.; Moyen, E.; Alehdaghi, H.; Kanwat, A.; Choi, W.-C.; Jang, J., Anion-and cation-codoped all-inorganic blue-emitting perovskite quantum dots for light-emitting diodes. *ACS Applied Nano Materials* **2019,** *2* (9), 5655-5662.
302. Shi, M.; Dong, L.; Zheng, S.; Hou, P.; Cai, L.; Zhao, M.; Zhang, X.; Wang, Q.; Li, J.; Xu, K., "Bottom-up" preparation of MoS2 quantum dots for tumor imaging and their in vivo behavior study. *Biochemical and biophysical research communications* **2019,** *516* (4), 1090-1096.
303. Katz, H. E.; Huang, J., Thin-Film Organic Electronic Devices. *Annual Review of Materials Research* **2009,** *39* (1), 71-92.
304. Zhou, M.; Ghosh, I., Quantum dots and peptides: a bright future together. *Peptide Science: Original Research on Biomolecules* **2007,** *88* (3), 325-339.
305. Zhang, M.-Z.; Yu, R.-N.; Chen, J.; Ma, Z.-Y.; Zhao, Y.-D., Targeted quantum dots fluorescence probes functionalized with aptamer and peptide for transferrin receptor on tumor cells. *Nanotechnology* **2012,** *23* (48), 485104.
306. Choi, M.-J.; Pierson, R.; Chang, Y.; Guo, H.; Kang, I.-K., Enhanced Intracellular Uptake of CdTe Quantum Dots by Conjugation of Oligopeptides. *Journal of Nanomaterials* **2013,** *2013*, 291020.
307. Aswathy, R. G.; Sivakumar, B.; Brahatheeswaran, D.; Fukuda, T.; Yoshida, Y.; Maekawa, T.; Kumar, D. S., Biocompatible fluorescent zein nanoparticles for simultaneous bioimaging and drug delivery application. *Advances in Natural Sciences: Nanoscience and Nanotechnology* **2012,** *3* (2), 025006.
308. Zhou, M.; Nakatani, E.; Gronenberg, L. S.; Tokimoto, T.; Wirth, M. J.; Hruby, V. J.; Roberts, A.; Lynch, R. M.; Ghosh, I., Peptide-Labeled Quantum Dots for Imaging GPCRs in Whole Cells and as Single Molecules. *Bioconjugate Chemistry* **2007,** *18* (2), 323-332.
309. Hild, W.; Breunig, M.; Göpferich, A., Quantum dots–nano-sized probes for the exploration of cellular and intracellular targeting. *European Journal of Pharmaceutics and Biopharmaceutics* **2008,** *68* (2), 153-168.
310. Tao, K.; Makam, P.; Aizen, R.; Gazit, E., Self-assembling peptide semiconductors. *Science* **2017,** *358* (6365), eaam9756.
311. Lee, J. S.; Yoon, I.; Kim, J.; Ihee, H.; Kim, B.; Park, C. B., Self-assembly of semiconducting photoluminescent peptide nanowires in the vapor phase. *Angewandte Chemie International Edition* **2011,** *50* (5), 1164-1167.
312. Amdursky, N.; Gazit, E.; Rosenman, G., Quantum Confinement in Self-Assembled Bioinspired Peptide Hydrogels. *Advanced Materials* **2010,** *22* (21), 2311-2315.
313. Hartgerink, J. D.; Granja, J. R.; Milligan, R. A.; Ghadiri, M. R., Self-assembling peptide nanotubes. *Journal of the American Chemical Society* **1996,** *118* (1), 43-50.
314. Yang, H.; Yang, S.; Kong, J.; Dong, A.; Yu, S., Obtaining information about protein secondary structures in aqueous solution using Fourier transform IR spectroscopy. *Nature protocols* **2015,** *10* (3), 382-96.
315. Ji, Y.; Yang, X.; Ji, Z.; Zhu, L.; Ma, N.; Chen, D.; Jia, X.; Tang, J.; Cao, Y., DFT-Calculated IR Spectrum Amide I, II, and III Band Contributions of N-Methylacetamide Fine Components. *ACS Omega* **2020,** *5* (15), 8572-8578.
316. Yang, M.; Xing, R.; Shen, G.; Yuan, C.; Yan, X., A versatile cyclic dipeptide hydrogelator: Self-assembly and rheology in various physiological conditions. *Colloids and Surfaces A: Physicochemical and Engineering Aspects* **2019,** *572*, 259-265.

317. Alig, R.; Bloom, S. l., Electron-hole-pair creation energies in semiconductors. *Physical review letters* **1975,** *35* (22), 1522.
318. Shur, M., 6 - Semiconductors. In *The Electrical Engineering Handbook*, Chen, W.-K., Ed. Academic Press: Burlington, 2005; pp 153-162.
319. Schubert, E.; Göbel, E.; Horikoshi, Y.; Ploog, K.; Queisser, H., Alloy broadening in photoluminescence spectra of Al x Ga 1− x As. *Physical Review B* **1984,** *30* (2), 813.
320. Kaye, G. W. C.; Laby, T. H., *Tables of physical and chemical constants and some mathematical functions*. Longmans, Green and Company: 1911.
321. Ridley, B. K., *Quantum processes in semiconductors*. Oxford University Press: 2013.
322. Sánchez-Carrera, R. S.; Coropceanu, V.; Kim, E.-G.; Brédas, J.-L., Charge-transport properties of the 1, 4-diiodobenzene crystal: A quantum-mechanical study. *Chemistry of Materials* **2008,** *20* (18), 5832-5838.
323. Kim, J. H.; Morikis, D.; Ozkan, M., Adaptation of inorganic quantum dots for stable molecular beacons. *Sensors and Actuators B: Chemical* **2004,** *102* (2), 315-319.
324. Zhang, S.; Marini, D. M.; Hwang, W.; Santoso, S., Design of nanostructured biological materials through self-assembly of peptides and proteins. *Current opinion in chemical biology* **2002,** *6* (6), 865-71.
325. Dasgupta, A., Exploring architectures at the nanoscale: the interplay between hydrophobic twin lipid chains and head groups of designer peptide amphiphiles in the self-assembly process and application. *Soft Matter* **2016,** *12* (19), 4352-4360.
326. Garifullin, R.; Guler, M. O., Supramolecular chirality in self-assembled peptide amphiphile nanostructures. *Chemical Communications* **2015,** *51* (62), 12470-12473.
327. Niyogi, S.; Hamon, M. A.; Hu, H.; Zhao, B.; Bhowmik, P.; Sen, R.; Itkis, M. E.; Haddon, R. C., Chemistry of Single-Walled Carbon Nanotubes. *Accounts of Chemical Research* **2002,** *35* (12), 1105-1113.
328. Zhang, S., Fabrication of novel biomaterials through molecular self-assembly. *Nature biotechnology* **2003,** *21* (10), 1171-1178.
329. Li, R.; Horgan, C. C.; Long, B.; Rodriguez, A. L.; Mather, L.; Barrow, C. J.; Nisbet, D. R.; Williams, R. J., Tuning the mechanical and morphological properties of self-assembled peptide hydrogels via control over the gelation mechanism through regulation of ionic strength and the rate of pH change. *RSC advances* **2015,** *5* (1), 301-307.
330. Yang, K.; Han, Q.; Chen, B.; Zheng, Y.; Zhang, K.; Li, Q.; Wang, J., Antimicrobial hydrogels: promising materials for medical application. *International journal of nanomedicine* **2018,** *13*, 2217.
331. Caliari, S. R.; Burdick, J. A., A practical guide to hydrogels for cell culture. *Nature methods* **2016,** *13* (5), 405-414.
332. Protopapa, E.; Maude, S.; Aggeli, A.; Nelson, A., Interaction of self-assembling β-sheet peptides with phospholipid monolayers: the role of aggregation state, polarity, charge and applied field. *Langmuir* **2009,** *25* (5), 3289-3296.
333. Nielsen, J. E.; König, N.; Yang, S.; Skoda, M. W.; Maestro, A.; Dong, H.; Cárdenas, M.; Lund, R., Lipid membrane interactions of self-assembling antimicrobial nanofibers: effect of PEGylation. *RSC Advances* **2020,** *10* (58), 35329-35340.
334. Irwansyah, I.; Li, Y. Q.; Shi, W.; Qi, D.; Leow, W. R.; Tang, M. B.; Li, S.; Chen, X., Gram-positive antimicrobial activity of amino acid-based hydrogels. *Advanced Materials* **2015,** *27* (4), 648-654.
335. Frisch, H.; Besenius, P., pH-Switchable self-assembled materials. *Macromolecular rapid communications* **2015,** *36* (4), 346-363.
336. Jenssen, H.; Aspmo, S. I., Serum stability of peptides. In *Peptide-based drug design*, Springer: 2008; pp 177-186.
337. Saikia, K.; Chaudhary, N., Antimicrobial peptides from C-terminal amphipathic region of E. coli FtsA. *Biochimica et Biophysica Acta (BBA)-Biomembranes* **2018,** *1860* (12), 2506-2514.

338. Saikia, K.; Chaudhary, N., Interaction of MreB-derived antimicrobial peptides with membranes. *Biochemical and biophysical research communications* **2018,** *498* (1), 58-63.
339. Aggeli, b. A.; Bell, M.; Boden, N.; Keen, J.; Knowles, P.; McLeish, T.; Pitkeathly, M.; Radford, S., Responsive gels formed by the spontaneous self-assembly of peptides into polymeric β-sheet tapes. *Nature* **1997,** *386* (6622), 259-262.
340. Kurbasic, M.; Garcia, A. M.; Viada, S.; Marchesan, S., Tripeptide Self-Assembly into Bioactive Hydrogels: Effects of Terminus Modification on Biocatalysis. *Molecules* **2021,** *26* (1), 173.
341. Xue, C.; Lin, T. Y.; Chang, D.; Guo, Z., Thioflavin T as an amyloid dye: fibril quantification, optimal concentration and effect on aggregation. *Royal Society open science* **2017,** *4* (1), 160696.
342. Wu, C.; Biancalana, M.; Koide, S.; Shea, J.-E., Binding modes of thioflavin-T to the single-layer β-sheet of the peptide self-assembly mimics. *Journal of molecular biology* **2009,** *394* (4), 627-633.
343. Johnson, E. K.; Adams, D. J.; Cameron, P. J., Peptide based low molecular weight gelators. *Journal of Materials Chemistry* **2011,** *21* (7), 2024-2027.
344. Tang, C.; Smith, A. M.; Collins, R. F.; Ulijn, R. V.; Saiani, A., Fmoc-diphenylalanine self-assembly mechanism induces apparent p K a shifts. *Langmuir* **2009,** *25* (16), 9447-9453.
345. Li, Y.; Zhang, Y.; Shi, F.; Tao, L.; Wei, Y.; Wang, X., Modulus-regulated 3D-cell proliferation in an injectable self-healing hydrogel. *Colloids and Surfaces B: Biointerfaces* **2017,** *149*, 168-173.
346. Georges, P. C.; Janmey, P. A., Cell type-specific response to growth on soft materials. *Journal of applied physiology* **2005,** *98* (4), 1547-1553.
347. Wells, R. G., The role of matrix stiffness in hepatic stellate cell activation and liver fibrosis. *Journal of clinical gastroenterology* **2005,** *39* (4), S158-S161.
348. Paszek, M. J.; Zahir, N.; Johnson, K. R.; Lakins, J. N.; Rozenberg, G. I.; Gefen, A.; Reinhart-King, C. A.; Margulies, S. S.; Dembo, M.; Boettiger, D., Tensional homeostasis and the malignant phenotype. *Cancer cell* **2005,** *8* (3), 241-254.
349. Wingate, K.; Floren, M.; Tan, Y.; Tseng, P. O. N.; Tan, W., Synergism of matrix stiffness and vascular endothelial growth factor on mesenchymal stem cells for vascular endothelial regeneration. *Tissue Engineering Part A* **2014,** *20* (17-18), 2503-2512.
350. Singh, H.; Gahane, A.; Singh, V.; Ghosh, S.; Thakur, A., Antibiofilm activity of Fmoc-phenylalanine against Gram-positive and Gram-negative bacterial biofilms. *The Journal of Antibiotics* **2021,** *74* (6), 407-416.
351. Paiva, C. N.; Bozza, M. T., Are reactive oxygen species always detrimental to pathogens? *Antioxidants & redox signaling* **2014,** *20* (6), 1000-1037.
352. Schnaider, L.; Brahmachari, S.; Schmidt, N. W.; Mensa, B.; Shaham-Niv, S.; Bychenko, D.; Adler-Abramovich, L.; Shimon, L. J.; Kolusheva, S.; DeGrado, W. F., Self-assembling dipeptide antibacterial nanostructures with membrane disrupting activity. *Nature communications* **2017,** *8* (1), 1-10.
353. Haldar, J.; Kondaiah, P.; Bhattacharya, S., Synthesis and antibacterial properties of novel hydrolyzable cationic amphiphiles. Incorporation of multiple head groups leads to impressive antibacterial activity. *Journal of medicinal chemistry* **2005,** *48* (11), 3823-3831.
354. Bem, H.; Gallorini, M.; Rizzio, E.; Krzeminska, M., Comparative studies on the concentrations of some elements in the urban air particulate matter in Lodz City of Poland and in Milan, Italy. *Environment international* **2003,** *29* (4), 423-8.
355. Xu, C.; Qiu, B.; Gu, H.; Yang, X.; Wei, H.; Huang, X.; Wang, Y.; Rutman, D.; Cao, D.; Bhana, S., Synergistic interactions between activated carbon fabrics and toxic hexavalent chromium. *ECS Journal of Solid State Science and Technology* **2013,** *3* (3), M1.
356. Qiu, B.; Gu, H.; Yan, X.; Guo, J.; Wang, Y.; Sun, D.; Wang, Q.; Khan, M.; Zhang, X.; Weeks, B. L., Cellulose derived magnetic mesoporous carbon nanocomposites with enhanced hexavalent chromium removal. *Journal of Materials Chemistry A* **2014,** *2* (41), 17454-17462.

357. Owlad, M.; Aroua, M. K.; Daud, W. A. W.; Baroutian, S., Removal of Hexavalent Chromium-Contaminated Water and Wastewater: A Review. *Water, Air, and Soil Pollution* **2009,** *200* (1), 59-77.
358. Fu, F.; Wang, Q., Removal of heavy metal ions from wastewaters: A review. *Journal of Environmental Management* **2011,** *92* (3), 407-418.
359. López-Maldonado, E. A.; Oropeza-Guzman, M. T.; Jurado-Baizaval, J. L.; Ochoa-Terán, A., Coagulation–flocculation mechanisms in wastewater treatment plants through zeta potential measurements. *Journal of hazardous materials* **2014,** *279*, 1-10.
360. Choong, T. S. Y.; Chuah, T. G.; Robiah, Y.; Gregory Koay, F. L.; Azni, I., Arsenic toxicity, health hazards and removal techniques from water: an overview. *Desalination* **2007,** *217* (1), 139-166.
361. Babel, S.; Kurniawan, T. A., Cr(VI) removal from synthetic wastewater using coconut shell charcoal and commercial activated carbon modified with oxidizing agents and/or chitosan. *Chemosphere* **2004,** *54* (7), 951-67.
362. Abdel-Tawwab, M.; El-Sayed, G. O.; Shady, S. H. H., Capability of some agricultural wastes for removing some heavy metals from polluted water stocked in combination with Nile tilapia, Oreochromis niloticus (L.). *International Aquatic Research* **2017,** *9* (2), 153-160.
363. Taamneh, Y.; Sharadqah, S., The removal of heavy metals from aqueous solution using natural Jordanian zeolite. *Applied Water Science* **2017,** *7* (4), 2021-2028.
364. Kostal, J.; Mulchandani, A.; Chen, W., Tunable Biopolymers for Heavy Metal Removal. *Macromolecules* **2001,** *34* (7), 2257-2261.
365. Wu, W.; He, Q.; Jiang, C., Magnetic iron oxide nanoparticles: synthesis and surface functionalization strategies. *Nanoscale research letters* **2008,** *3* (11), 397-415.
366. Ingole, D. N.; Burghate, S., *Adsorption of Oil from Waste Water by Using Human Hair*. 2014; Vol. 3, p 207-2017.
367. Mondal, N. K.; Basu, S., Potentiality of waste human hair towards removal of chromium (VI) from solution: kinetic and equilibrium studies. *Applied Water Science* **2019,** *9* (3), 1-8.
368. Nakamura, A.; Arimoto, M.; Takeuchi, K.; Fujii, T., A rapid extraction procedure of human hair proteins and identification of phosphorylated species. *Biological & pharmaceutical bulletin* **2002,** *25* (5), 569-72.
369. da Rosa Chagas, A. G.; Spinelli, E.; Fiaux, S. B.; da Silva Barreto, A.; Rodrigues, S. V., Particle-size distribution (PSD) of pulverized hair: A quantitative approach of milling efficiency and its correlation with drug extraction efficiency. *Forensic science international* **2017,** *277*, 188-196.
370. Langmuir, I., The adsorption of gases on plane surfaces of glass, mica and platinum. *Journal of the American Chemical society* **1918,** *40* (9), 1361-1403.
371. Mahapatra, A.; Mishra, B.; Hota, G., Studies on Electrospun Alumina Nanofibers for the Removal of Chromium(VI) and Fluoride Toxic Ions from an Aqueous System. *Industrial & Engineering Chemistry Research* **2013,** *52*, 1554–1561.
372. Gupta, V. K.; Rastogi, A.; Nayak, A., Adsorption studies on the removal of hexavalent chromium from aqueous solution using a low cost fertilizer industry waste material. *Journal of Colloid and Interface Science* **2010,** *342* (1), 135-141.
373. Freundlich, H., Over the adsorption in solution. *J. Phys. chem* **1906,** *57* (385471), 1100-1107.
374. Garg, U. K.; Kaur, M. P.; Garg, V. K.; Sud, D., Removal of hexavalent chromium from aqueous solution by agricultural waste biomass. *Journal of hazardous materials* **2007,** *140* (1), 60-68.
375. Shahnaz, T.; Patra, C.; Sharma, V.; Selvaraju, N., A comparative study of raw, acid-modified and EDTA-complexed Acacia auriculiformis biomass for the removal of hexavalent chromium. *Chemistry and Ecology* **2020,** *36* (4), 360-381.

376. Nagaraj, A.; Munusamy, M. A.; Al-Arfaj, A. A.; Rajan, M., Functional Ionic Liquid-Capped Graphene Quantum Dots for Chromium Removal from Chromium Contaminated Water. *Journal of Chemical & Engineering Data* **2019,** *64* (2), 651-667.
377. Gomberg, M., AN INSTANCE OF TRIVALENT CARBON: TRIPHENYLMETHYL. *Journal of the American Chemical Society* **1900,** *22* (11), 757-771.
378. He, Y. T.; Traina, S. J., Cr (VI) reduction and immobilization by magnetite under alkaline pH conditions: the role of passivation. *Environmental science & technology* **2005,** *39* (12), 4499-4504.
379. Pan, Z.; Zhu, X.; Satpathy, A.; Li, W.; Fortner, J. D.; Giammar, D. E., Cr(VI) Adsorption on Engineered Iron Oxide Nanoparticles: Exploring Complexation Processes and Water Chemistry. *Environmental Science & Technology* **2019,** *53* (20), 11913-11921.
380. Eary, L. E.; Rai, D., Chromate removal from aqueous wastes by reduction with ferrous ion. *Environmental Science & Technology* **1988,** *22* (8), 972-977.
381. Pan, C.; Troyer, L. D.; Catalano, J. G.; Giammar, D. E., Dynamics of Chromium(VI) Removal from Drinking Water by Iron Electrocoagulation. *Environmental Science & Technology* **2016,** *50* (24), 13502-13510.
382. Peterson, M. L.; Brown, G. E.; Parks, G. A., Direct XAFS evidence for heterogeneous redox reaction at the aqueous chromium/magnetite interface. *Colloids and Surfaces A: Physicochemical and Engineering Aspects* **1996,** *107*, 77-88.
383. Meena, A. H.; Arai, Y., Effects of common groundwater ions on chromate removal by magnetite: Importance of chromate adsorption. *Geochemical transactions* **2016,** *17* (1), 1-13.
384. Patra, C.; Shahnaz, T.; Subbiah, S.; Narayanasamy, S., Comparative assessment of raw and acid-activated preparations of novel Pongamia pinnata shells for adsorption of hexavalent chromium from simulated wastewater. *Environmental Science and Pollution Research* **2020**, 1-16.
385. Pienpinijtham, P.; Thammacharoen, C.; Naranitad, S.; Ekgasit, S., Analysis of cosmetic residues on a single human hair by ATR FT-IR microspectroscopy. *Spectrochimica Acta Part A: Molecular and Biomolecular Spectroscopy* **2018,** *197*, 230-236.
386. Hamadi, N. K.; Chen, X. D.; Farid, M. M.; Lu, M. G. Q., Adsorption kinetics for the removal of chromium(VI) from aqueous solution by adsorbents derived from used tyres and sawdust. *Chemical Engineering Journal* **2001,** *84* (2), 95-105.
387. Mohamed, A.; Nasser, W. S.; Osman, T. A.; Toprak, M. S.; Muhammed, M.; Uheida, A., Removal of chromium (VI) from aqueous solutions using surface modified composite nanofibers. *Journal of Colloid and Interface Science* **2017,** *505*, 682-691.
388. Albadarin, A. B.; Mangwandi, C.; Ala'a, H.; Walker, G. M.; Allen, S. J.; Ahmad, M. N., Kinetic and thermodynamics of chromium ions adsorption onto low-cost dolomite adsorbent. *Chemical engineering journal* **2012,** *179*, 193-202.
389. Ghasemi, M.; Naushad, M.; Ghasemi, N.; Khosravi-Fard, Y., Adsorption of Pb (II) from aqueous solution using new adsorbents prepared from agricultural waste: adsorption isotherm and kinetic studies. *Journal of Industrial and Engineering Chemistry* **2014,** *20* (4), 2193-2199.
390. Zhang, J.; Shang, T.; Jin, X.; Gao, J.; Zhao, Q., Study of chromium(vi) removal from aqueous solution using nitrogen-enriched activated carbon based bamboo processing residues. *RSC Advances* **2015,** *5* (1), 784-790.
391. Sadaf, S.; Bhatti, H., Evaluation of peanut husk as a novel, low cost biosorbent for the removal of Indosol Orange RSN dye from aqueous solutions: Batch and fixed bed studies. *Clean Technologies and Environmental Policy* **2014,** *16*.
392. Gonzalez, M. H.; Araújo, G. C.; Pelizaro, C. B.; Menezes, E. A.; Lemos, S. G.; De Sousa, G. B.; Nogueira, A. R. A., Coconut coir as biosorbent for Cr (VI) removal from laboratory wastewater. *Journal of Hazardous Materials* **2008,** *159* (2-3), 252-256.

393. Jain, M.; Garg, V.; Kadirvelu, K., Chromium (VI) removal from aqueous system using Helianthus annuus (sunflower) stem waste. *Journal of hazardous materials* **2009,** *162* (1), 365-372.
394. Parlayici, Ş.; Pehlivan, E., Comparative study of Cr (VI) removal by bio-waste adsorbents: equilibrium, kinetics, and thermodynamic. *Journal of Analytical Science and Technology* **2019,** *10* (1), 1-8.
395. Karthikeyan, T.; Rajgopal, S.; Miranda, L. R., Chromium (VI) adsorption from aqueous solution by Hevea Brasilinesis sawdust activated carbon. *Journal of hazardous materials* **2005,** *124* (1-3), 192-199.
396. Alomá, I. d. l. C.; Rodriguez, I.; Calero, M.; Blazquez, G., Biosorption of Cr6+ from aqueous solution by sugarcane bagasse. *Desalination and Water Treatment* **2014,** *52* (31-33), 5912-5922.
397. Elangovan, R.; Philip, L.; Chandraraj, K., Biosorption of chromium species by aquatic weeds: kinetics and mechanism studies. *Journal of Hazardous materials* **2008,** *152* (1), 100-112.

Appendices

Appendix # 1

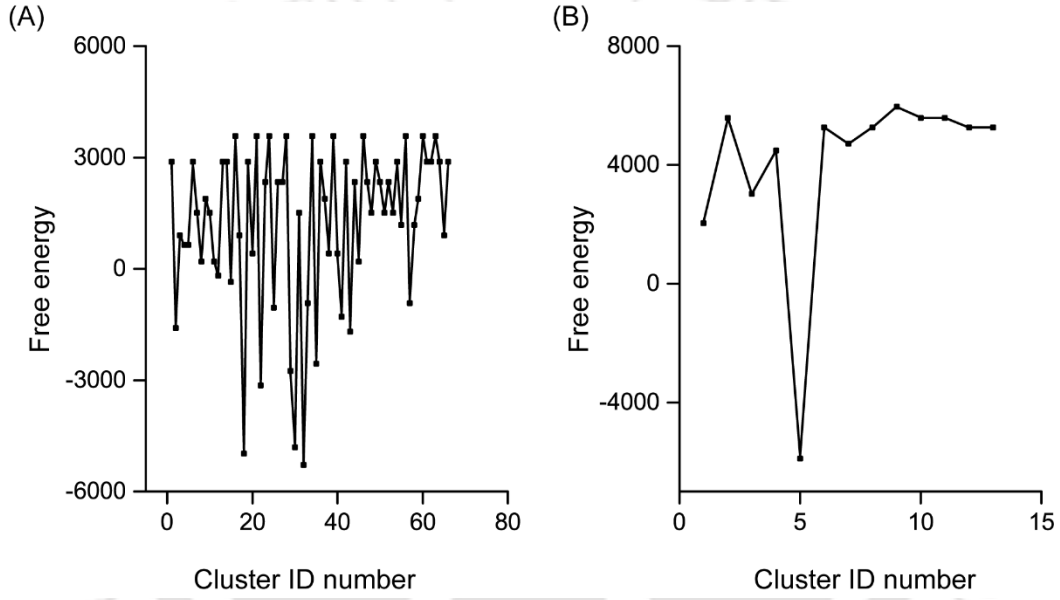

Figure A1. Gibbs free energy landscape, calculated based on the cluster population, obtained from a 10 ns MD simulation run of (A) $(FF)_3$ peptide, (B) $(Ff)_3$ peptide

Appendix # 2

Table A1. Comparison of bio-adsorption capacity of PH against already reported bio-adsorbent

S.No	Bioadsorbent	Bioadsorption capacity (mg/g)	References
1	Coconut Coir	26.8	[392]
2	Boiled sunflower head	7.9	[393]
3	Cranberry kernel shell	10.42	[394]
4	Hevea Brasilinesis	44.05	[395]
5	Sugarcane bagasse	1.76	[396]
6	Water lily	8.44	[397]
7	Pulverized Hair	15.14	Present study

Appendix # 3

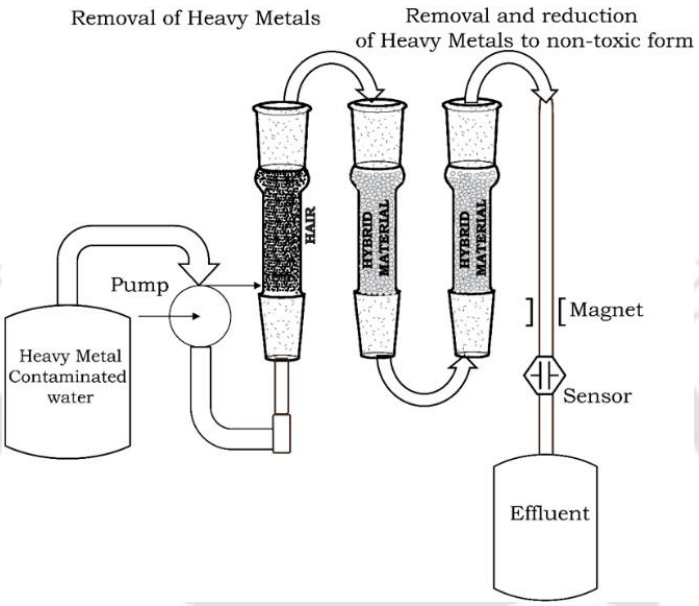

Figure A2. Prototype of a possible device for chromium removal

List of Publications

Patents

- Vibin Ramakrishnan, Gaurav Pandey and Vivek Prakash. Peptide based modulators for amyloidogenic diseases. Patent No. TEMP/E-1/36478/2019-KOL Dated 27.08.2019
- Ultrashort antimicrobial peptide hydrogels for topical applications. (Under filing)

Journal articles

- **Vivek Prakash**, Ranjit Ranbhor, and Vibin Ramakrishnan.* De Novo Designed Heterochiral Blue Fluorescent Protein. **ACS omega**. (2020), doi: 10.1021/acsomega.0c02574
- **Vivek Prakash**, Mukesh B, Sajitha Sasidharan, Amay Sanjay Redkar, Abhishek Roy, R. Anandalakshmi, and Vibin Ramakrishnan.* Quantum confinement in a Peptide Organogel. **European Biophysics Journal.** (under review).
- **Vivek Prakash**, Amay Sanjay Redkar, Yvonne Christian, Abhishek Roy, R. Anandalakshmi, and Vibin Ramakrishnan.* Ultra-short antimicrobial peptide hydrogels (Manuscript under preparation)
- **Vivek Prakash**, K. Dharmalingam, R. Anandalakshmi, and Vibin Ramakrishnan.* Biodegradable alternatives for heavy metal sequestration (Manuscript under preparation)

Book Chapter

- Bioinspired Functional Molecular Constructs (Publisher: Elsevier, Accepted)

Conference proceedings

- Vivek Prakash, Vibin Ramakrishnan.* Electric Field Modulated Peptide Nano-Assembly. Biophys J. 2021;120(3):271a.**Biophysical Journal**.(2021), doi:10.1016/j.bpj.2020.11.1730

Conferences

- Poster presentation at 65th Annual Biophysical Society meeting, 2021. Title: Electric field modulated peptide nano-assembly. (International conference)

- Oral presentation at 45th FEBS Annual Congress, 2021. Title: De novo designed minimal blue fluorescent protein. (International conference)
- Poster presentation at 14th International Conference on Eco-materials, 2020. Title: Metal Impregnated Nano-assemblies for Heavy Metal Removal from Wastewater. (International conference)
- Awarded 'Third prize in Poster Presentation' during 'Research Conclave 2019' organized by IIT Guwahati.

Workshop

- 'Recent advances on bioinspired nanomaterials for environmental applications' 2019, organized by Center for the Environment, IIT Guwahati.